2015-09-28

Synthesis of Silver Nano wires and their Polymer Nanocomposite

Abbasi Moud, Aref

UNIVERSITY OF CALGARY

Synthesis of Silver Nanowires and Their Polymer Nanocomposite

by

Aref Abbasi Moud

A THESIS

SUBMITTED TO THE FACULTY OF GRADUATE STUDIES

IN PARTIAL FULFILMENT OF THE REQUIREMENTS FOR THE

DEGREE OF Master of Science

GRADUATE PROGRAM IN CHEMICAL AND PETROLEUM ENGINEERING

CALGARY, ALBERTA

SEPTEMBER, 2015

Abstract

Polymers and polymer engineering have been revolutionized using nano inclusions such as MWCNT and metal nanowires. In this study due to its amazing properties silver nanowire was singled out for embedding in polymers and produced using an efficient electrochemical process. Silver nanowires (AgNWs) were synthesized by the AC electrodeposition of Ag into porous aluminum oxide templates. AgNWs were embedded into polystyrene with a solution processing technique to create a nanocomposite. For comparison, carbon nanotube (CNT)/polystyrene nanocomposites were identically generated. TEM and XRD analyses showed that synthesized AgNWs had an average diameter and length of 25nm and 5.6±1.4 μm, respectively. TEM images also revealed that at molding temperature (240ºC), AgNWs transformed into a chain of nanospheres (fragmentation phenomenon). At low filler loadings (concentration < 1 vol %), the AgNW/polystyrene nanocomposites presented inferior electrical properties compared to CNT/polystyrene nanocomposites due to lower aspect ratio, fragmentation phenomenon and poorer conductive network for AgNWs. However, at high filler loadings (concentration > 1 vol %), the electrical properties of the AgNW/polystyrene nanocomposites significantly surpassed those of their CNT counterparts. It seems that at high filler loadings, the conductive network was well-established for both types of nanocomposites and thus, higher innate conductivity of AgNWs played a dominant role in presenting superior electrical properties.

In another study, the time dependence of EMI shielding of AgNWs/PS was measured after 3 months and the result showed that EMI shielding of the nanocomposite declined with time. This remarkable result was attributed to changes in surface chemistry of AgNWs while they were encased inside the polymer matrix.

In the final study, broadband EMI shielding properties of nanocomposites were studied and we showed that AgNWs has comparable charge storage capabilities compared to other nano inclusion such as graphene and CNT.

In a nutshell, this study is aimed at attaining high EMI shielding effectiveness for silver nanowire/polymer nanocomposite and finding a correlation between deteriorating effect of surface oxidation and EMI shielding efficacy. To the best of our knowledge, to date, no one has studied the effect of change in silver surface chemistry and subsequent changes in conductivity, on EMI shielding effectiveness. The novelty of this study is using silver nanowire in EMI shielding related applications of nanocomposites. The goal was set to achieve a level of EMI shielding higher than 30 dB over X-band regime (8.5-13 GHz) as this level of EMI shielding efficacy corresponds to 99.9% attenuation of incoming electromagnetic waves.

Acknowledgment

I would like to thank Professor Sundararaj for his vigilant supervision during my master studies. Also I would like to take this opportunity to thank all my friends in my research group. I would like to thank Ivonne Otero and Mohammad Arjmand for their help and many useful discussions. I would like to thank Yan Li for her support during making nanowires and making nanocomposite samples. I thank Kyle Leinweber for his research assistance and also I would like to thank Maryam Khajehpour, Ali Sarvi and Soheil Sadeghi for their great company. I would like to acknowledge Dr. Michael Schoel for operation of SEM and Dr. Tobias Fürstenhaupt and Dr. Wei-Xiang Dong for TEM images taken. Finally, I really appreciate the support from my parents and my siblings, for their support and understanding.

Table of Contents

List of figures

List of Symbols and Abbreviations

Abbreviations

AC	Alternating current
CNT	Carbon nanotube
CPC	Conductive filler/polymer composites
CuNW	Copper nanowire
AgNW	Silver nanowire
DC	Direct current
DMF	N,N-Dimethylformamide
EMI	Electromagnetic interference
ESD	Electrostatic discharge
hr	Hour
MeOH	Methanol
Min	Minute
MWCNT	Multi-walled carbon nanotube
MWS	Maxwell-Wagner-Sillars
NIR	Near-infrared
PAO	Porous aluminum oxide
PPG	Polymer Processing Group
PVDF	Poly(vinylidene fluoride)
PS	Polystyrene
SE	Shielding effectiveness
SEM	Scanning electron microscopy
SWCNT	Single-walled carbon nanotube
TEM	Transmission electron microscopy

VNA	Vector network analyzer
XRD	X-ray diffraction
3-D	Three dimensional
AFM	Atomic force microscopy
RF	Radio frequency
ICP	Intrinsically conductive polymer
RMS	Root mean square
FCC	Face centered cubic
EM	Electromagnetic wave

Greek Letters

γ	Propagation constant
δ	Skin depth
ε'	Dielectric (real) permittivity
ε''	Dielectric loss (Imaginary permittivity)
ε_0	Dielectric permittivity of free space
ε_r	Relative dielectric permittivity
η	Intrinsic Impedance of shielding materials
η_0	Intrinsic impedance EM wave in free space
μ	Magnetic permeability
μ_0	Magnetic permeability of free space
μ_r	Relative magnetic permeability
ρ_0	Volume resistivity of conductive filler
ρ_s	Surface resistivity
ρ_v	Volume resistivity
σ	Electrical conductivity
σ_r	Relative electrical conductivity
τ	Time constant
Ω	Ohm (unit of resistance)
ω	Angular frequency
λ	Wave length of the radiated wave
f	Frequency of the radiated wave
Z	Impedance
V	AC voltage
C_0	Capacitance of free space
ω	Frequency
I_R	Resistive current

I_C Capacitive current

Chapter 1: Application and integration of AgNWs in CPCs (Conductive Polymer Composites)

Polymer composites can be called as the oldest and newest of materials. The first record of polymer composite materials can be traced back to Genesis and Exodus in the Bible as being used by the people of Babylonia and Mesopotamia around 4000-2000 B.C [1, 2]. Polymers are a vital part of our lives today and everything that surrounds us—from the basic building blocks of construction, commercial products such as automobiles and airplanes and medical products for the human body are made of polymers [3, 4]. Most of these materials are composed of a combination of one or more materials, i.e. polymer composites.

As the usage of computer parts and communication equipment in the world of electronics increases, interference among aforementioned equipment, such as cellphones, laptops and other electronic devices increases and the performance of these devices will degrade over time. Degradation of super-sensitive electronic devices is not the only issue arising from EM waves (electromagnetic waves) as EM waves also put human health in jeopardy over time. Shielding electromagnetic radiation is one state-of-the-art technique to mitigate the harm from EM waves prevalent in the world today. The destructive effects of EM waves can be minimized using novel materials including metal coated polymers, ICPs (intrinsically conductive polymers) and conductive filler/polymer composites (CPCs).

CPCs stand out among the rest as they do not have drawbacks such as delamination of metal, poor adhesion and poor stability. CPCs filled with metals are effective materials for EMI shielding. Using metals nanowires is attractive due to metal characteristics, such as accessibility, reproducibility, and easy methods of production. Metals are superior to other well-known inclusions such as carbon nanotubes (CNT) and graphene but they are prone to corrosion and their performance degrades over the course of time even when they are encased deep within polymer layers. This problem arises from the active unwanted gas molecules in the ambient air usually found in industrial environments. For example, copper is the nanowire that has been mainly contemplated for EMI shielding; however it gets readily oxidized even under atmospheric

conditions. This problem will be mitigated if the exposure time of freshly synthesized nanowires to air is minimized but effects of gradual diffusion of small active gas molecules through polymer cannot be stopped totally. The high vulnerability of copper to active gas molecules put forth the idea of using silver (Ag) nanowires as they have higher electrical conductivity than copper ($6.3\times10^{+5}$ $S\cdot cm^{-1}$ versus $5.9\times10^{+5}$ $S\cdot cm^{-1}$) along with greater immunity to oxidation. One should bear in mind that although silver is fairly unreactive as it does not react with oxygen in the air even at high temperature, its surface tarnishes due to formation of silver sulfide over time. Additionally, also it is susceptible to ozone molecules present in the air and it forms silver oxide (Ag_2O). Though metal oxides are less conductive than metals, silver oxides are comparatively more conductive than copper oxide.

Corrosion of Ag with reduced sulfur compounds in the air at atmospheric condition is known to be started by sulfur compounds as well as free sulfur. For instance, Elechiguerra et al. [5] found that silver sulfide (Ag_2S) started to form on the surface of the nanowires after three weeks, and corrosion became even worse after six months, leading to the discontinuity of nanowires. Fortunately, none of the sulfur species are abundant in the atmosphere. For the case of ozone, Chen et al. studied the influence of atmospheric corrosion on bare silver. Their result showed that presence of ozone and UV radiation through photo dissociation generates reactive atomic oxygen which reacts with Ag rapidly to form Ag_2O. Other silver corrosion by products such as AgCl and Ag_2CO_3 are not formed on the surface of nanowires as their precursors are not abundant in the atmosphere [6].

Although in this study measures were taken to minimize amount of exposure time to the air of nanowires but due to the nature of polymer, these gases can still diffuse through the polymer and chemically react with the silver nanowire surface. Both ozone and reduced silver compounds are very small in size and can diffuse readily through polymers. It should be noted that silver oxide and silver sulfide are both semi-conductive and both will affect conductivity and related EMI shielding of nanocomposite made of AgNWs.

Unfortunately shielding effectiveness (*SE*), the ability of shields to attenuate EM waves, can be severely affected by semi conductive nature of silver oxide and silver sulfide created on the surface of nanowires due to the loss of total charge as a result of change in silver surface chemistry. Therefore, further steps must be taken to make CPCs made of AgNWs more robust. For instance,

results published in literature shows that there are two new methods to address the problem associated with surface chemistry degradation: (1) developing new materials with low permeability to gas and (2) encapsulation of the silver nanowires with higher corrosion and oxidation resistance materials. Considering these two methods to mitigate effects of change in surface chemistry, measures should be taken to improve and keep *SE* level close to 30dB, corresponding to 99.9% attenuation of incident EM waves, which is sufficient for many practical engineering applications.

This study is aimed at attaining high EMI shielding effectiveness for silver nanowire/polymer nanocomposite and finding a correlation between deteriorating effect of surface oxidation and EMI shielding efficacy. To the best of our knowledge, to date, no one has studied effect of change in silver surface chemistry and subsequent changes in conductivity, on EMI shielding effectiveness.

1.2 Antistatic protection

Customarily the risk involved in using hazardous or potentially hazardous substances has to be minimized. A static electric charge is created whenever two surfaces contact and separate, when at least one of the surfaces has a high resistance to electric current. Antistatic protection is crucial in areas where relative motion between dissimilar objects takes place in applications such as crucial application like conveyor belts and airplane tires. Static charges on the surface of these materials build up over time which poses hazards to adjacent flammable materials. Antistatic protection is useful in areas where static electricity is generated over time since it reduces the amount of charge created and lets it discharge in a controlled manner.

1.3 Knowledge required for understanding EMI shielding

EMI shielding in definition is the practice of reducing electromagnetic field in a space by blocking the field with barriers made of conductive or magnetic materials. Electromagnetic radiation mainly consists of coupled electric and magnetic fields. The electric field implements forces on the charge carriers (i.e., electrons) within the conductor. In a nutshell applied electric field induces a current inside the conductor which leads to displacements of the charges, at which point the current stops. Unfortunately many computer parts due to movements of electrons within them automatically emit electromagnetic waves which either interfere with

the operation of other nearby electronic devices or pose health hazards to the surrounding humans. For instance, radars usually perform at radio frequencies (RF) between 300 MHz and 15 GHz. Depending on source frequency, generated RF fields are known to interact differently with human body. RF fields below 10 GHz (to 1 MHz) penetrate exposed tissues and produce heating due to energy absorption and eventually cause the tissue temperature to go up. The depth of wave's penetration depends on the frequency of the field and is greater for lower frequencies.

Most applications require EMI shielding effectiveness (EMI SE) of at least 30 dB, which corresponds to shielding of 99.9% of incident radiation, i.e., 0.1% is transmitted is considered as a sufficient level of shielding for many applications [33, 35]. Pure metals, the most commonly used materials for EMI shielding, have drawbacks such as lack of guarantee for seamless finish, delamination, and expensive recyclability. These problems put CPCs in the pole position due to tunable electrical properties and extra light weight.

1.4 Understanding the concept

When designing a CPC, understanding mechanism and roots of EMI shielding is vital as it has many positive consequences such as knowing the exact amount of filler to design a shield which averts both under shielding and over shielding.

Based on the distance between source of EM generation and shield, the radiation can be classified as near-field and far-field. There is no formal definition for the near-field as it depends on types of application and the antenna. However, the most agreed upon existing definition describes the near-field as less than one wavelength from the antenna. Wave length in meter is given by following formula:

$$\lambda = 300/f(MHz) \qquad (1\text{-}1)$$

In this relation λ is wave length and f is frequency of the radiated wave. One readily understands the critical distance for near-field can also be calculated from following

$$Distance = \lambda/2\pi \ = \ 0.159\lambda \qquad (1\text{-}2)$$

The EMI shielding devices used in our lab operate at far-field, so all following discussions and interpretation of results will be based on far-field theories. Application-wise, in the far-field, EM wave is a plane wave, in which both electric fields and magnetic fields are in each other's company, and they are perpendicular to each other. In the near field however, simple definitions, such as the above, cannot be applied, as the fields are more complex. Lorentz's force law predicts the actual response of a charge carrier inside the shield as it stands against the propagation of an EM wave.

$$\vec{F} = q\vec{E} + q\vec{v} \times \mu_0\vec{H} \qquad (1\text{-}3)$$

Where q is the charge of each particle of velocity,$\vec{v}$; μ_0 is the magnetic permeability of free space equal to $4\pi\times10^{-7}$ H·m $^{-1}$; and, $\vec{E}$ and $\vec{H}$ are the electric and magnetic fields, respectively.

The charge carrier stops propagation of the incident EM waves in two ways: (1) energy gets dissipated when charge carriers change their locations as result of electric fields, (2) mobile charge carriers induce a field, which decreases the power of the transmitted EM wave.

A shield can block EM waves in three different ways: reflection, absorption, and multiple reflection [16, 33, 40-42]. When an EM wave strikes a conductive material, a fraction of the wave is reflected from the shield due to interaction with surface charges and a fraction is transmitted through the shield, with its energy dissipated via absorption. The amplitude of the wave that penetrates through the conductive material is attenuated by a factor of $e^{\frac{-z}{\delta}}$, where z is the distance the EM wave penetrates into the shield, and δ is the skin depth of the conductive material. The skin depth δ of a substance is the distance within the conductive material in which electromagnetic radiation penetrates [43].

1.5 EMI Shielding of CPCs

CPCs display a complex EMI shielding behavior, as they possess components with different electrical conductivities. Shielding effectiveness typically depends on factors such as conductivity of filler and polymeric matrix, dispersion of conductive filler, and total nomadic charge present in the nano composite [7-12]. The knowledge required for investigation of the effects of these parameters can only be obtained through rigorous comprehensive, theoretical and experimental studies.

Generally most polymeric matrices, due to lack of nomadic charges, are unable to interact with incoming EM waves [13]. Therefore, in a CPC the whole EMI shielding ability is centered around the role of the conductor and its morphology, and its ability to interact with EM waves.

EMI shielding and filler concentration are correlated through two mechanisms - Ohmic loss and polarization loss. Individual fillers with insulative polymeric layers between them can simply be considered capacitors [14]. Therefore, visualizing a CPC with numerous nanocapacitors can easily be used as a tool to correlate EMI shielding to concentration. Higher concentration means a greater number of nomadic charges, which attenuates EM waves much more efficiently. For instance, in a study reported by Arjmand et al. [15] ascending trend in EMI shielding of MWNT with concentration over X-band regime were found. In another systematic study, ascending trend of EMI SE in SBR composites, with variation of carbon black content from 10 phr to 60 phr, were reported [14].

Overall, EMI shielding in CPCs invloves three mechanisms - reflection, absorption and multiple reflection. Multiple reflection efficacy, as a mechanism for overall EMI shielding, is hidden in values reported by reflection and absorption. A shield with reflection must have a mobile charge carrier (either electrons or holes) to engage with EM waves. The second most important mechanism is absorption, which depends on the thickness of the sample. Multiple reflection also represents the internal reflection within filler or between closely spaced fillers, which increases total reflection of the system.

EMI SE is the logarithm of the ratio of incident power to transmitted power. When there is no shielding, transmitted power of EM waves simply is equal to the incident power. Using an overall

balance, Al Saleh et al. [16] used net term to account for the effect of the multiple reflection mechanism inside the reflection and absorption mechanisms.

$$Overall\ SE = \quad (1\text{-}4)$$
$$SE_R + SE_A =$$
$$10\ log(I/(I-R)) + 10\ log((I-R)/T)$$

Where SE_R is the shielding is effectiveness related to reflection, SE_A is the shielding effectiveness related to absorption, I is the incident power, R is the reflected power and T is the transmitted power. Reflection and absorption both increase with total nomadic charges present in the system. Therefore using a filler with higher innate conductivity, or using a greater concentration of filler, leads to an increase in shielding ability. Reflection is purely related to the total nomadic charges present in the system, while absorption is much more complex in CPCs. It is related to Ohmic loss and polarization loss.

Imaginary permittivity, as a representation of energy dissipated in the system, is indirectly related to real permittivity through polarization loss. Real permittivity in CPCs is related to the formation of a large number of nanocapacitors and insulative layers separating them [17-21]. Increasing filler concentration results in an increase in the number of nanocapacitors, leading to higher real permittivity [22]. Additionally, the higher the concentration, the closer the gaps between nanoelectrodes, which enhances electronic polarization of the polymeric layer. Therefore, a direct relationship between concentration and polarization loss as a major contributor to imaginary permittivity is expected. On the other hand, higher real permittivity of CPCs causes greater momentum in electrons, which dissipates electrical energy even more. By mapping the above information, one recognizes the complexity of the mechanisms involved in describing EMI shielding behavior of a system.

1.6 Dielectric Material

A material is classified as “dielectric” if it has the ability to store energy when an external electric field is applied. Dissipation of electrical energy is usually in the form of heat, and generally the lower the *dielectric loss* (the proportion of energy lost as heat), the more effective a dielectric material is. If a DC voltage V is applied to such a capacitor, where the plates are separated by the distance d, the electric field between the plates is uniform and equal to E=V/d. This electric field leads to charge polarization within the dielectric material, i.e. separation of positive and negative charges. In other words, dielectric material increases the storage capacity of capacitors by neutralizing charges at the electrodes (see Figure 1-1).

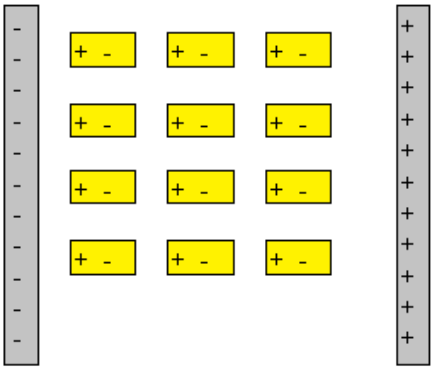

Figure 1-1: Charges on a parallel plate capacitor with a dielectric between plates

When the dielectric material is free space, the charges per area stored on the surface of plates is equal to $Q=\varepsilon_0 E$, where ε_0 is real permittivity of free space. However, if free space is replaced with a dielectric material, an extra charge is stored on the surface of the capacitor, originating from higher polarisability of dielectric material relative to free space. For instance, the dielectric constant of SiO_2, the material utilized in microchips, is approximately 4 which is the permittivity of SiO_2 divided by permittivity of vacuum, $\varepsilon_{SiO2}/\varepsilon_0$,where $\varepsilon_0 = 8.854\times10^{-6}$ pF/μm. The higher the real permittivity of a dielectric material and the greater the applied electric field, the higher the stored energy on the surface of a capacitor.

1.7 Dielectric Mechanisms

A dielectric material (dielectric for short) is an *insulator* that can be *polarized* by an induced *electric field*. The definition of dielectric constant is related to the permittivity of the material. The permittivity indicates the ability of the material to polarize in response to an applied electric field. Generally, the greater polarization that is developed within the material, the greater the dielectric constant will become. Physically speaking, in polarized materials in an applied electric field, electrons are not distributed evenly around the core, as a cloud of electrons is displaced under the effect of the electric field. In a CPC, there are several mechanisms that can enhance real permittivity in a system, such as interfacial, dipolar, atomic and electronic polarization [46-48]: (1) Electronic polarization – slight displacement of electrons with respect to the core (2) Atomic polarization – displacement of atoms in a molecule or lattice; and (3) Orientational polarization for polar molecules such as water-containing materials.

There is a tendency for molecular dipole to align by the electric field to give a net polarization in that direction. There is another polarization that occurs in the inner dielectric boundary layers or on a macroscopic scale at the external electrode sample interface, which is also referred to by Maxwell-Wagner-Sillars (MWS). The first study for this mechanism was performed by Maxwell [51] and was extended to AC electric fields by Wagner-Sillars [52-54]. Interfacial polarization occurs because of accumulation of mobile charges at the interface of dissimilar phases with different electrical properties (conductivity and permittivity). Interfacial polarization, as its name suggests, requires a heterogeneous system with different phases. For instance, blends of polymers with different levels of conductivities and CPCs with myriad types of fillers can be mentioned [45, 49, 50].

Polymers, based on their molecular structure, can either be polar or non-polar. Examples of polar polymers are PMMA, PVC, and PA, while non-polar polymers are simple PTFE, PE, PP and PS. At low frequencies, the dipoles buried deep within polymers find enough time to align along the imposed electric field, while at high frequency the dipole finds it difficult to align harmoniously with the changing AC field. For electronic polarization and atomic polarization, frequency has a slight impact on its net value; therefore, it is instantaneous at whatever frequency. Ergo, polar polymers at low frequencies and high frequencies, such as PVDF, have non-changing dielectric constants. The friction between the molecules as result of million times changes in orientation in

a microwave oven can be used to generate heat at the molecular level. Additional information about dielectric mechanisms can be found elsewhere [15].

Finally, in high electric fields, a material that is normally an electrical insulator may begin to conduct electricity, which means it ceases to act as a dielectric. This phenomenon is known as dielectric breakdown. The mechanism describing dielectric breakdown can be understood using band theory. This peculiar phenomenon is used in cigarette lighters to create a spark to ignite a flammable material. A charge is piled up on the electrodes on either side of the tip of the cigarette lighter until the strength of the field across them exceeds the dielectric strength of the air.

1.8 Conductivity and Percolation Theory

Electrical conductivity is the degree to which a specified material conducts electricity, calculated as the ratio of the current density in the material to the electric field that causes the flow of current. In band theory, the definition for Fermi level is the top available electron energy levels at low temperatures. The position of conduction band relative to Fermi level determines the electrical properties [23]. Metals are good conductors, since molecules in them are so packed that electrons can move freely through them. In most metals, Fermi level is below the conduction band and electrons can dissociate from their parent atoms and contribute to overall conductivity. However, in insulators, the conduction band lies below the Fermi level, and there is no carrier for the current. For instance, polymers contain a very low concentration of free charge carriers and are therefore generally good electrical insulators [24]. In conductive polymer composites (CPCs), investigations have been confined almost entirely to measurements of electrical conductivity of a material where one component has electron conduction ability while the other is nonconducting [25].

The most general approach for describing the charge transport in conducting polymeric composites in relation to the content of conducting filler is offered by the percolation theory [26]. According to percolation theory, at percolation threshold a condensed network of nanofiller starts to partially span the 3D space of the polymer. At percolation threshold, first a conductive path forms and

transforms CPCs from insulating into conductive. Physical contacts between neighboring nanofillers, in combination with tunneling and hopping, are the main mechanisms for the transference of electrons in CPCs [27, 28]. When concentrations are below this point, CPCs behave as if nothing has been added to the polymer, as the conductivity level remains almost the same as pure polymer. When the concentration goes beyond the percolation threshold, material shows graphitic conductivity corresponding to the conduction network becoming continuous. Although all filler, of all shapes and sizes, eventually reach percolation threshold, theoretically and experimentally, fillers with a higher aspect ratio have a greater chance of forming a more compact percolating network. For instance, CNT and nanowires, due to their elongated geometry, match the mentioned criteria and reach percolation threshold much faster than lower aspect ratio filers. In a study reported by Ma et al. it was experimentally verified that higher aspect ratio fillers offer lower percolation thresholds. For instance for MWCNT with 500 and 200 aspect ratios, percolation thresholds with 0.06 and 0.19vol% were reported respectively [29]. Generally, factors that have influence over conductivity of CPCs are innate conductivity of filler, aspect ratio, filler geometry, chemical affinity toward polymer and distribution-dispersion. In the literature, many insightful reviews have been published so far on correlation of macroscopic properties with microscopic and nanoscopic parameters, which assists in explaining electrical data obtained through experiments [30-32].

1.9 Factors Affecting Distribution and Dispersion of Fillers or Conductivity

To obtain acceptable levels of conductivity, manipulation of dispersion and distribution is of prime importance [33-35]. These two parameters can be judged based on final morphology of the filler in a polymer matrix and are critical in determining percolation threshold. Generally, preferential distribution and good dispersion will enhance the probability for the individual filler to attach to other fillers and form a connective network. Regarding distribution, one may also speculate that homogenous distribution of a filler will lead to an array of macroscopic properties, such as different levels of conductivity and mechanical strength. From a thermodynamic point of view, some dispersions can be unstable and they can be only kinetically stable over a period of time, which determines their shelf life. In these systems, spatial positions of nanofillers are highly dependent

on time; therefore, macroscopic properties such as electrical conductivity and EMI shielding may also change. So, in these systems, the effect of these changes with respect to time should be taken into account

1. 10 Physical and Thermal Dynamic Factors

In the preparation of filled polymers, the action of uniformly distributing fillers and breaking down of filler agglomeration or physical association provides the final morphology of filler inside a polymeric matrix [36]. Polymer and filler surface tension is yet another critical factor affecting distribution and dispersion of filler. The surface tension between these two components will determine the affinity of these materials towards each other. Greater harmony in terms of chemistry between filler and polymeric matrix will allow researchers to achieve lower percolation threshold and, consequently, better electrical properties. For instance, after many years of research, the full potential of CNTs as a reinforcement agent has not been fully realized. It is limited because of the difficulties associated with dispersion of entangled CNT during processing [37].

1.11 Effects of Filler (MWCNT versus AgNW) on Electrical Properties of CPCs

Fillers are particles added to polymers to lower the consumption of more expensive material or to add better properties to the composite. Various parameters are considered before adding them to the polymer, such as final properties of the finished products, the amount of filler, and economic parameters [38]. For instance, the intrinsic conductivity of filler type has an important impact on final electrical properties, as filler with a higher electrical conductivity leads to CPCs with better electrical properties. For CPCs, high electrical conductivity is achievable at a very low filler content for advanced applications in electronics. Percolation is a point where individual fillers weave into each other and produce a 3D network inside the polymer. As factors such as composite price, and properties such as optical properties hinge on achieving percolation at lowest possible filler content, aspect ratio also comes into play. As the aspect ratio of the filler increases, the

probability of the fillers reaching the percolation threshold at lower filler content also increases [29, 30, 39].

With continual usage of electronics and micromechanical devices, materials that conduct electrons and dissipate heat efficiently without structural damage have received considerable attention. The rigid sp^3 bonds in diamonds make them one of the best thermal conductors in today's demanding industry [40]. A high thermal conductivity can also be expected from carbon nanotubes, with a rigid backbone and atomically flawless cylindrical structure [41-43]. For instance, in a study by Berber et al. [44], it was reported that the thermal conductivity of MWCNT can reach values as high as a staggering 6600 W/m.K at room temperature. In summary, many factors need to be considered before selection of the filler, which ultimately hinges on the composite's desired properties. As the focus of this study is on achieving good electrical properties, MWCNT and AgNWs were selected as the desirable fillers. MWCNT is a commercial filler with excellent electrical properties, such as high aspect ratio and unique adjustable molecular structure. As MWCNT electrical properties were limited, we opted to use AgNWs which have better intrinsic electrical conductivity.

1.12. References

[1] Bhattacharya S, Chaklader A. Review on metal-filled plastics. Part1. Electrical conductivity. Polymer-Plastics Technology and Engineering. 1982;19(1):21-51.

[2] Arjmand M, Sundararaj U. Broadband dielectric properties of multiwalled carbon nanotube/polystyrene composites. Polymer Engineering & Science. 2015;55(1):173-9.

[3] Carraher Jr CE. Introduction to polymer chemistry: CRC press; 2011.

[4] Arjmand M, Mahmoodi M, Gelves GA, Park S, Sundararaj U. Electrical and electromagnetic interference shielding properties of flow-induced oriented carbon nanotubes in polycarbonate. Carbon. 2011;49(11):3430-40.

[5] Elechiguerra JL, Larios-Lopez L, Liu C, Garcia-Gutierrez D, Camacho-Bragado A, Yacaman MJ. Corrosion at the nanoscale: the case of silver nanowires and nanoparticles. Chemistry of Materials. 2005;17(24):6042-52.

[6] Graedel T. Corrosion mechanisms for silver exposed to the atmosphere. Journal of the Electrochemical Society. 1992;139(7):1963-70.

[7] Bagwell RM, McManaman JM, Wetherhold RC. Short shaped copper fibers in an epoxy matrix: their role in a multifunctional composite. Composites science and technology. 2006;66(3):522-30.

[8] Arjmand M, Apperley T, Okoniewski M, Sundararaj U. Comparative study of electromagnetic interference shielding properties of injection molded versus compression molded multi-walled carbon nanotube/polystyrene composites. Carbon. 2012;50(14):5126-34.

[9] Yang YL, Gupta MC, Dudley KL, Lawrence RW. A comparative study of EMI shielding properties of carbon nanofiber and multi-walled carbon nanotube filled polymer composites. Journal of Nanoscience and Nanotechnology. 2005;5(6):927-31.

[10] Jou W-S, Cheng H-Z, Hsu C-F. A carbon nanotube polymer-based composite with high electromagnetic shielding. Journal of electronic materials. 2006;35(3):462-70.
[11] Janda NB, Keith JM, King JA, Perger WF, Oxby TJ. Shielding-effectiveness modeling of carbon-fiber/nylon-6, 6 composites. Journal of applied polymer science. 2005;96(1):62-9.
[12] Che R, Peng LM, Duan XF, Chen Q, Liang X. Microwave absorption enhancement and complex permittivity and permeability of Fe encapsulated within carbon nanotubes. Advanced Materials. 2004;16(5):401-5.
[13] Dhawan S, Singh N, Venkatachalam S. Shielding behaviour of conducting polymer-coated fabrics in X-band, W-band and radio frequency range. Synthetic Metals. 2002;129(3):261-7.
[14] Mohanraj G, Chaki T, Chakraborty A, Khastgir D. AC impedance analysis and EMI shielding effectiveness of conductive SBR composites. Polymer Engineering & Science. 2006;46(10):1342-9.
[15] Arjmand M. Electrical Conductivity, Electromagnetic Interference Shielding and Dielectric Properties of Multi-walled Carbon Nanotube/Polymer Composites. University of Calgary, PhD, 2014.
[16] Al-Saleh MH, Sundararaj U. Electromagnetic interference shielding mechanisms of CNT/polymer composites. Carbon. 2009;47(7):1738-46.
[17] Jiang M-J, Dang Z-M, Bozlar M, Miomandre F, Bai J. Broad-frequency dielectric behaviors in multiwalled carbon nanotube/rubber nanocomposites. Journal of Applied Physics. 2009;106(8):084902.
[18] Dang Z-M, Yuan J-K, Zha J-W, Zhou T, Li S-T, Hu G-H. Fundamentals, processes and applications of high-permittivity polymer–matrix composites. Progress in Materials Science. 2012;57(4):660-723.
[19] Zetsche A, Kremer F, Jung W, Schulze H. Dielectric study on the miscibility of binary polymer blends. Polymer. 1990;31(10):1883-7.
[20] Shen Y, Lin Y, Li M, Nan CW. High dielectric performance of polymer composite films induced by a percolating interparticle barrier layer. Advanced Materials. 2007;19(10):1418-22.
[21] Lee CY, Song HG, Jang KS, Oh EJ, Epstein AJ, Joo J. Electromagnetic interference shielding efficiency of polyaniline mixtures and multilayer films. Synthetic Metals. 1999;102(1-3):1346-9.
[22] Pramanik P, Khastgir D, De S, Saha T. Pressure-sensitive electrically conductive nitrile rubber composites filled with particulate carbon black and short carbon fibre. Journal of Materials Science. 1990;25(9):3848-53.
[23] Kim KK, Bae JJ, Park HK, Kim SM, Geng H-Z, Park KA, et al. Fermi level engineering of single-walled carbon nanotubes by AuCl3 doping. Journal of the American Chemical Society. 2008;130(38):12757-61.
[24] Barrau S, Demont P, Peigney A, Laurent C, Lacabanne C. DC and AC conductivity of carbon nanotubes-polyepoxy composites. Macromolecules. 2003;36(14):5187-94.
[25] Bergman DJ, Imry Y. Critical behavior of the complex dielectric constant near the percolation threshold of a heterogeneous material. Physical Review Letters. 1977;39(19):1222.
[26] Vilčáková J, Sáha P, Quadrat O. Electrical conductivity of carbon fibres/polyester resin composites in the percolation threshold region. European Polymer Journal. 2002;38(12):2343-7.
[27] Balberg I. TUNNELING AND NONUNIVERSAL CONDUCTIVITY IN COMPOSITE-MATERIALS. Physical Review Letters. 1987;59(12):1305-8.
[28] Sichel EK, Gittleman JI, Sheng P. TRANSPORT PROPERTIES OF THE COMPOSITE-MATERIAL CARBON-POLY(VINYL CHLORIDE). Physical Review B. 1978;18(10):5712-6.
[29] Li J, Ma PC, Chow WS, To CK, Tang BZ, Kim JK. Correlations between percolation threshold, dispersion state, and aspect ratio of carbon nanotubes. Advanced Functional Materials. 2007;17(16):3207-15.
[30] Bauhofer W, Kovacs JZ. A review and analysis of electrical percolation in carbon nanotube polymer composites. Composites Science and Technology. 2009;69(10):1486-98.
[31] Thostenson ET, Ren Z, Chou T-W. Advances in the science and technology of carbon nanotubes and their composites: a review. Composites science and technology. 2001;61(13):1899-912.
[32] Spitalsky Z, Tasis D, Papagelis K, Galiotis C. Carbon nanotube–polymer composites: chemistry, processing, mechanical and electrical properties. Progress in polymer science. 2010;35(3):357-401.

[33] Spinks GM, Shin SR, Wallace GG, Whitten PG, Kim SI, Kim SJ. Mechanical properties of chitosan/CNT microfibers obtained with improved dispersion. Sensors and Actuators B: Chemical. 2006;115(2):678-84.
[34] Singh K, Ohlan A, Saini P, Dhawan SK. Poly(3,4-ethylenedioxythiophene) gamma-Fe2O3 polymer composite-super paramagnetic behavior and variable range hopping 1D conduction mechanism-synthesis and characterization. Polymers for Advanced Technologies. 2008;19(3):229-36.
[35] Rubianes MD, Rivas GA. Dispersion of multi-wall carbon nanotubes in polyethylenimine: A new alternative for preparing electrochemical sensors. Electrochemistry communications. 2007;9(3):480-4.
[36] Mukherjee S, Schroers J, Johnson W, Rhim W-K. Influence of kinetic and thermodynamic factors on the glass-forming ability of zirconium-based bulk amorphous alloys. Physical review letters. 2005;94(24):245501.
[37] Ma P-C, Siddiqui NA, Marom G, Kim J-K. Dispersion and functionalization of carbon nanotubes for polymer-based nanocomposites: a review. Composites Part A: Applied Science and Manufacturing. 2010;41(10):1345-67.
[38] Shenoy AV. Rheology of filled polymer systems: Springer Science & Business Media; 1999.
[39] Behnam A, Guo J, Ural A. Effects of nanotube alignment and measurement direction on percolation resistivity in single-walled carbon nanotube films. Journal of Applied Physics. 2007;102(4):044313.
[40] Wei L, Kuo P, Thomas R, Anthony T, Banholzer W. Thermal conductivity of isotopically modified single crystal diamond. Physical Review Letters. 1993;70(24):3764.
[41] Paz AP, García-Lastra JM, Markussen T, Thygesen KS, Rubio A. Carbon nanotubes as heat dissipaters in microelectronics. The European Physical Journal B. 2013;86(5):1-14.
[42] Park J, Bifano MF, Prakash V. Sensitivity of thermal conductivity of carbon nanotubes to defect concentrations and heat-treatment. Journal of applied physics. 2013;113(3):034312.
[43] Micheli L, Sarmah N, Luo X, Reddy K, Mallick TK. Opportunities and challenges in micro-and nano-technologies for concentrating photovoltaic cooling: A review. Renewable and Sustainable Energy Reviews. 2013;20:595-610.
[44] Berber S, Kwon Y-K, Tomanek D. Unusually high thermal conductivity of carbon nanotubes. Physical review letters. 2000;84(20):4613.

Chapter 2: Experimental section

2.1 Introduction

Silver nanowire (AgNWs) is a 1D structure nanomaterial. In recent years, various preparation methods of Ag nanowires have been put forth by myriad of researchers. Each process typically due to its unique processing environment leads to different morphological and structural features. For instance, Kim et al. [1, 2] used polyol process to synthesize silver nanowires. In their chemically driven process KBr was initially added to the solution and then required amount of $AgNO_3$ were added. As result of reduction among silver ions, silver nanowires formed in the system. Although for initiation seeds like NaCl were needed, for initiation if high seed concentration is used with respect to Ag^+ ions, nanoparticles fromed instead of nanowires.

Although many techniques [3-8] are available to generate AgNWs, the most widely used method for generating metallic nanowires with less than 50 nm diameter is still template-directed synthesis, which involves either chemical or electrochemical deposition [9]. Aluminum plates (5cm × 11cm) 1mm thickness were used as primary templates. The aluminum plates were anodized in parallel by immersing in a large tank filled with 0.3M H_2SO_4 at 2°C. Counter-electrodes were stainless steel plates with the same dimensions as the aluminum plates. Growth of the porous aluminum oxide (alumina) templates was performed in two steps: in the first step, the plates were immersed in a 0.3M H_2SO_4 solution for 2 hr under 25.0V to create initial porous structure. Afterwards, the plates were placed in a 1:1 mixture of 0.2M H_2CrO_4 and 0.6M H_3PO_4 at 60°C for 30min to make the already formed porous structure more uniform. In the next step, the plates were reimmersed in the 0.3M H_2SO_4 solution for 8hr, and then the applied voltage was reduced incrementally to reduce the alumina barrier layer at the pore bottom. Thinning the alumina barrier is a crucial part of the process since it keeps the end of the porous structure electrically conductive for the electrodeposition process. The protocol to decrease the voltage was initiated by a reduction rate of 2V/min from 25V to 15V; then it was followed by 1V/min rate to 9V, and eventually after 5min keeping at 9V, the voltage was dropped to zero. These synthesis steps generated cylindrical pores arranged hexagonally [10].

AC electrodeposition of Ag into the hexagonal-shaped pores was accomplished by insulating the edges of the electrodes by applying nail polish, and then immersing the plates for 5min in an electrolyte solution of silver sulfate (Ag_2SO_4, 8.5g/L), diammonium hydrogen citrate ($(NH_4)_2HC_6H_5O_7$, 200 g/L), and potassium thiocyanate (KSCN, 105 g/L). Square wave voltage pulses were applied between the Al plates and two pure Ag counter-electrodes to push the Ag ions toward the end of the pores. The voltage pulses were applied at 100Hz frequency and ±8.0V peaks (pulsed every 400ms) for 1.5hr.

Liberation of the nanowires was started by physically removing bulk-deposited Ag from the surface of the Al plates, and then Ag nanowires were liberated from porous alumina in a beaker filled with 1.0M NaOH(aq) at room temperature. NaOH(aq) dissolved the surrounding alumina sheath so that we could recover the individual nanowires. After the liberation, floating fragments (bundled nanowires) were collected into a 1:1 mixture of 0.1M NaOH(aq) and MeOH, and sonicated for 10min. Immediately afterwards, collected AgNWs were purified through filter paper (Whatman with less than 1μm pore size), rinsed with MeOH, and then transferred to a beaker containing 100mL of MeOH. Additionally concise description of the synthesis of the AgNWs can be found elsewhere [8].

2.2 Experiment

2.2.1 Manufacturing of the template

The original aluminum plates purchased from Alfa Aesar, (99.99+%, 1mm thickness) were cut into the required dimensions (10 cm width, 25 cm length) and then were plunged in the 1M NaOH solution to remove the formed oxide layer. The PAO templates used in this study have been produced by a two-step anodization method. Initially, a 0.3 M H_2SO_4 electrolyte solution is used for the anodization with in-house installed agitators which efficiently regulate the temperature to increase the heat transfer between the cooling system and the solution, helping the solution temperature to stay between 0 – 4 ºC [8]. In the anodization system, immersed stainless steel plates placed in parallel to aluminium plates served as the cathode. The first anodizations were performed

for 2 h at 25.0 V. The initial PAO film was dissolved in a 1:1 mixture of 0.2 M H_2CrO_4 and 0.6 M H_3PO_4 at 60 °C for 30 min, and the generated PAO was reanodized under identical conditions for 8 hr. Reactions that occur while voltage was applied between anode and cathode are followings. During these reactions, hydrogen was generated upon stainless steel plates and anode became porous.

$$2H^+ + 2e^- \rightarrow H_2\uparrow \qquad (2\text{-}1)$$

$$2Al + 3O^{2-} - 6e^- \rightarrow 2Al_2O_3 \qquad (2\text{-}2)$$

At the end of the anodization, the DC voltage dropped from 25 V to 15 V, by 2 volt reductions per minute, then decreased from 15 V to 9 V by 1 volt per minute, and is finally held at 9 V for five minutes. In this way, the barrier layer at the bottom of the pores remains sufficiently electrically conductive for subsequent part of AgNWs generation process.

2.2.2 Filling using AC electrodeposition

As mentioned in previous step, pore bottom is the bottleneck of AgNWs generation as it has to get thin enough. It's highly important as the growth of nanowires starts at the pore ending and then it continues to fully fill the alumina made corridor [11]. The capacitance of the electrically insulating alumina barrier layer at the base of the pores (between the Al metal and the solution) prevents electrodeposition of materials using DC voltage or current signals. Apparently Al is a valve metal which demonstrates rectification by preferentially passing current in the cathodic direction. This inherent rectifying property of the barrier layer allows the reduction of ions in pores during cathodic half-cycles, without allowing re-oxidation during the anodic half-cycles [12]. Although AC method was chosen here, DC method also can be applied under certain conditions. In a nutshell, several steps are required to enable DC electro deposition in polymer or alumina membranes. First, one side of the membrane is coated with an electrical contact by evaporation of a metal, usually Au or Ag (Ag is preferable), then a metal contact is electrodeposited to facilitate contact to and manipulation of the electrode, and finally, the electrode is immersed in an electrolyte and DC electrodeposition is applied. AC electro deposition on the other hand is not that

complicated and requires no additional steps. Moreover this technique consumes less amount of Al with higher nanowire purity.

Edges of plates are also preferential spots for AgNWs deposition so before electrodeposition, the edges of the aluminum plates are insulated with nail polish to prevent preferential deposition of silver on the edges. The electrodeposition occurs in a 4 L beaker filled with aqueous solution of 0.5 mol/L $CuSO_4 \cdot 5H_2O$ (99%, Alfa Aesar) and 0.285 mol/L H_3BO_3 (99.5% min., EMD Millipore). Each time a single aluminum plate is immersed into the solution, with one silver plate (99.999%, Alfa Aesar) parallel at each side. The AC voltage get applied for 90 mins.

Prior to application of voltage for 90 min, templates were immersed in the electrodeposition solution for 5 minutes to let the solution and plates reach equilibrium and also remaining trapped air bubbles get released into the solution. Immediately afterwards, 200 Hz of continuous sinusoidal AC current of 10 V_{rms} was applied to fill the hollow interiors. Figure 2-1 shows electrodeposition stage of the process.

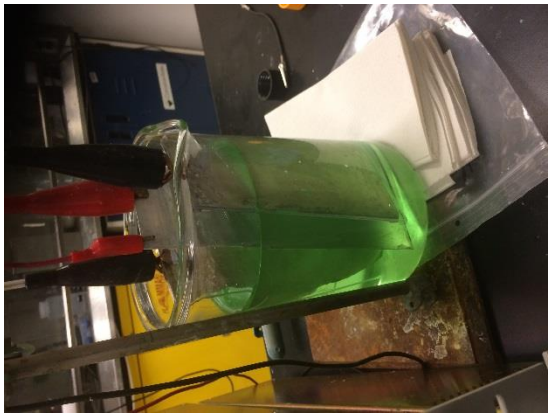

Figure 2-1: Electrodeposition step of synthesis of AgNWs

2.2.3 Liberation of AgNWs

Liberation of the nanowires was started by physically removing of bulk-deposited Ag from the surface of the Al plates, and then Ag nanowires were liberated from porous alumina in a beaker filled with 1.0M NaOH(aq) at room temperature. NaOH(aq) dissolved the surrounding alumina

sheath so that we could recover the individual nanowires. After the liberation, floating fragments (bundled nanowires) were collected into a 1:1 mixture of 0.1M NaOH(aq) and MeOH, and sonicated for 10min. Immediately afterwards, collected AgNWs were purified through filter paper (Whatman, with less than 1µm pore size), rinsed with MeOH, and then transferred to a beaker containing 100mL of MeOH. Figure 2-2 shows the overview of the process. Additionally details on the synthesis of the AgNWs can be found elsewhere [8].

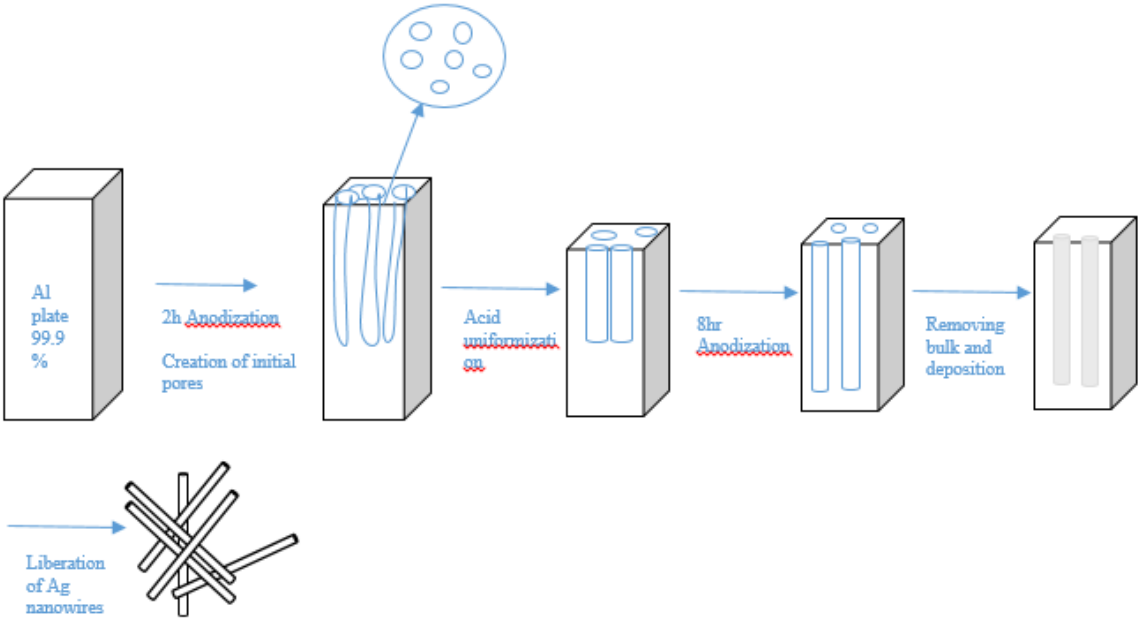

Figure 2-2: overview of generation process of Ag nanowires

Produced nanowires had following length and diameter distribution. Average length was 5.6 µm±1.4 and average diameter 25 nm.

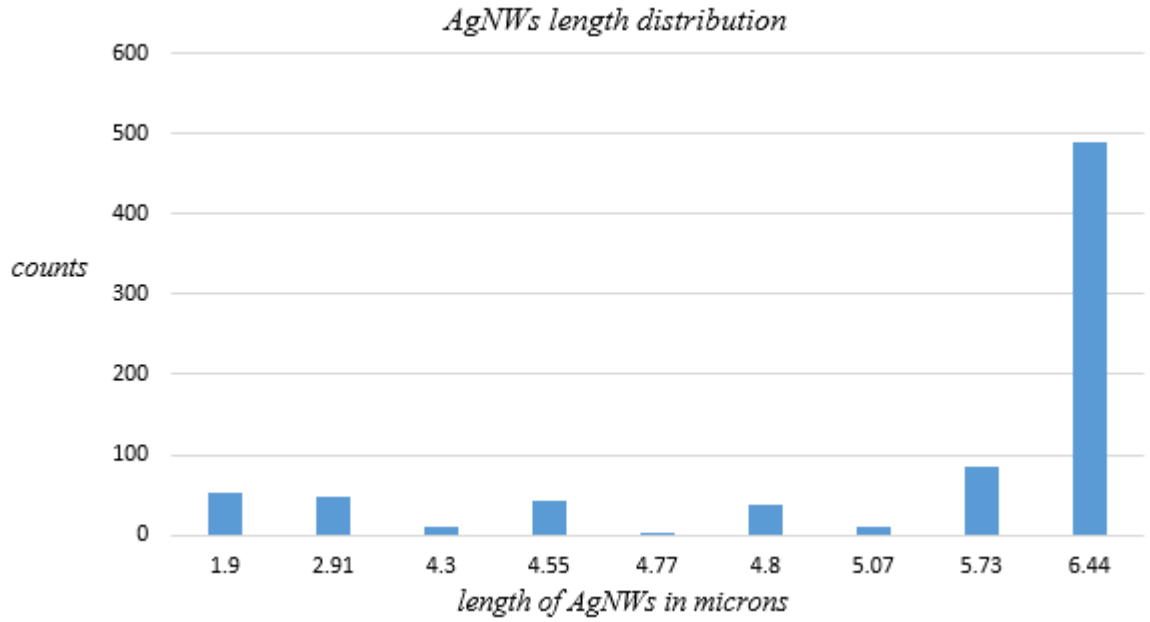

Figure 2-3: Length distribution of liberated Ag nanowires

2.3 Materials properties

Multiwall Carbon Nanotube (MWCNT): The MWCNTs (NanocylTM NC7000) were obtained from Nanocyl S.A. (Sambreville, Belgium). Details published for NC7000 are:

- Average diameter: 9.5 nm
- Average length: 1.5 μm
- Surface area: 250-300 m^2/g
- Specific gravity: 1.3-2.0 g/cm^3
- Electrical conductivity: 10^4-10^5 S/cm

Polystyrene (PS): PS used in this study was supplied by America styrenics Styron 666D, and specifications are as follow:

- M.I : 7.5
- M_w : 200,000 g/mol
- T_g : 100˚C

- Melting point: 200 ˚C
- Specific gravity: 1.04 g/cm^3

2.4. AgNW and MWCNT nanocomposites preparation

Nanocomposites were prepared by the miscible solvent mixing and precipitation (MSMP) technique. The nanocomposites with different concentrations of AgNWs were produced by mixing different volumes of 3.3mg/ml AgNW/MeOH suspension with 20mg/ml PS (Styron® 615 APR, Americas Styrenics LLC)/methylene chloride solution. Each mixture was treated in ultrasound bath for 30min, and then stirred for 10min prior to mixing. The suspension was then filtered and placed in an evaporation dish for 16h in a fume hood. The residue was further dried in a vacuum oven at 50°C for 24hr to obtain nanocomposite nuggets. The polymer nanocomposite nuggets were then molded into a rectangular cavity, with the dimensions of 22.9×10.2×0.8mm, at 240°C and 38MPa for 15min. For the sake of comparison, MWCNT/PS nanocomposites were produced at the same volumetric concentrations with the same technique. MWCNTs (Nanocyl™ NC7000) were obtained from Nanocyl S.A. (Sambreville, Belgium). The size of the produced samples are as follow: Thickness 0.87 mm and 10.16×22.86 mm lateral dimensions.

2.5. Materials characterization

The TEM analyses of the nanofillers and nanocomposites were carried out on a Tecnai TF20 G2 FEG-TEM (FEI, Hillsboro, Oregon, USA) at 200kV acceleration voltage with a standard single-tilt holder. The images were taken with a Gatan UltraScan 4000 CCD (Gatan, Pleasanton, California, USA) at 2048×2048 pixels. For the TEM analysis of the nanofillers, the droplets of AgNW and MWCNT suspensions were placed on a holey carbon-coated Cu TEM grid, and dried at room conditions. For the TEM analysis of the nanocomposites, the molded nanocomposites were ultramicrotomed to achieve 70nm thick sections.

Both the molded nanocomposites and powdery liberated AgNWs were analyzed by X-ray diffraction (XRD). The XRD analysis was performed using a Rigaku ULTIMA III X-ray diffractometer with Cu K-alpha radiation as the X-ray source. The scan was carried out in the range

2θ=30–90 degrees using a 0.02 degree step and a counting time of 1 degree per minute at 40kV and 44mA to obtain the full diffractogram for the materials.

The electrical conductivity measurements were carried out on the molded rectangular samples. All the samples' surfaces were wiped with ethanol to remove impurities prior to the measurements. For nanocomposites with electrical conductivities more than 10^{-4} $S \cdot cm^{-1}$, we carried out the measurements according to ASTM 257-75 using a Loresta GP resistivity meter (MCPT610 model, Mitsubishi Chemical Co., Japan). A standard four-pin probe was used to reduce the effect of contact resistance. For an electrical conductivity less than 10^{-4} $S \cdot cm^{-1}$, a Keithley 6517A electrometer connected to Keithley 8009 test fixture (Keithley Instruments, USA) was used.

The EMI shielding measurements were carried out over the X-band (8.2–12.4GHz) frequency range using an E5071C network analyzer (ENA series 300KHz – 20GHz). The samples under the test were squeezed between two flanges connecting the waveguides of the network analyzer. The network analyzer sent a signal down the waveguide incident to the sample, and then the scattering parameters (S-parameters) of each sample were recorded, and used to calculate *SE*. The dielectric properties of the generated nanocomposites were also obtained via conversion of the measurements using Reflection/Transmission Mu and Epsilon Nicolson-Ross Model.

In this thesis for dielectric measurements, the broadband dielectric spectroscopy of CPCs was performed with impedance / gain-phase analyzer (Solartron SI 1260) in the frequency range of $10^{-1} – 10^{+6}$ Hz. Holding samples were carried out using 12962A sample holder with electrode diameter of 10 mm. Before measurement commencement, electrode surface were painted with silver paste to minimize resistance between samples and sample holder electrodes. The impedance analyzer applied a voltage over a wide frequency range, and then measured in-phase and out-of phase currents. The obtained data were used to finally calculate impedance and dielectric properties.

For each measurement including EMI shielding measurement and electrical conductivity for both carbon nanotube and silver nanowire loaded specimens, three samples for each concentration were prepared. To ensure further reliability of measured data each of sample's properties were measured three times and result were reported as total average of all measurements.

2.6. References

[1] Kim T, Canlier A, Kim GH, Choi J, Park M, Han SM. Electrostatic spray deposition of highly transparent silver nanowire electrode on flexible substrate. ACS applied materials & interfaces. 2013;5(3):788-94.
[2] Calderwood JH. FIELD AND WAVE ELECTROMAGNETICS - CHENG,DK. Iee Proceedings-a-Science Measurement and Technology. 1984;131(8):660-.
[3] Fleischer R, Price P, Walker R. Method of forming fine holes of near atomic dimensions. Review of Scientific Instruments. 1963;34(5):510-2.
[4] Murphy CJ, Sau TK, Gole AM, Orendorff CJ, Gao J, Gou L, et al. Anisotropic metal nanoparticles: synthesis, assembly, and optical applications. The Journal of Physical Chemistry B. 2005;109(29):13857-70.
[5] Xia Y, Yang P, Sun Y, Wu Y, Mayers B, Gates B, et al. One-dimensional nanostructures: synthesis, characterization, and applications. Advanced materials. 2003;15(5):353-89.
[6] Kline TR, Tian M, Wang J, Sen A, Chan MW, Mallouk TE. Template-grown metal nanowires. Inorganic chemistry. 2006;45(19):7555-65.
[7] Possin GE. A method for forming very small diameter wires. Review of Scientific Instruments. 1970;41(5):772-4.
[8] Gelves GA, Lin B, Sundararaj U, Haber JA. Low electrical percolation threshold of silver and copper nanowires in polystyrene composites. Advanced Functional Materials. 2006;16(18):2423-30.
[9] Sun Y, Yin Y, Mayers BT, Herricks T, Xia Y. Uniform silver nanowires synthesis by reducing AgNO3 with ethylene glycol in the presence of seeds and poly (vinyl pyrrolidone). Chemistry of Materials. 2002;14(11):4736-45.
[10] Gelves GA, Al-Saleh MH, Sundararaj U. Highly electrically conductive and high performance EMI shielding nanowire/polymer nanocomposites by miscible mixing and precipitation. Journal of Materials Chemistry. 2011;21(3):829-36.
[11] El-Sayed MA. Some interesting properties of metals confined in time and nanometer space of different shapes. Accounts of chemical research. 2001;34(4):257-64.
[12] Gerein NJ, Haber JA. Effect of ac electrodeposition conditions on the growth of high aspect ratio copper nanowires in porous aluminum oxide templates. The Journal of Physical Chemistry B. 2005;109(37):17372-85.

Chapter 3: Outstanding Electromagnetic Interference Shielding of Silver Nanowire: Comparison with MWCNT

Presentation of the Article: This article can be divided into two general sections as followings

- ✓ Interpretation of the electrical properties of MWCNT/PS and AgNW/PS composites as functions of filler loading, i.e., electrical conductivity and EMI shielding
- ✓ Effect of fragmentation on electrical propeties of AgNW/PS composites

This work has been done with the help of Dr. Mohammad Arjmand and Yan Li who assisted me in making the samples, and getting some of the characterizations and interpretation of results.

Aref Abbasi Moud, Mohammad Arjmand, Yan Li, Uttandaraman Sundararaj*

Department of Chemical and Petroleum Engineering, University of Calgary, Calgary, Canada

Keywords: Silver nanowires (AgNWs); Carbon nanotubes (CNTs); Nanocomposites; Electrical conductivity; Electromagnetic interference shielding; Imaginary permittivity; percolation; fragmentation; morphology; Nano capacitors

Abstract

Silver nanowires (AgNWs) were synthesized by the AC electrodeposition of Ag into porous aluminum oxide templates. AgNWs were embedded into polystyrene with a solution processing technique to create a nanocomposite. For comparison, carbon nanotube (CNT)/polystyrene nanocomposites were generated identically. TEM and XRD analyses showed that synthesized of AgNWs had an average diameter and length of 25nm and 5.6±1.4 μm, respectively. The actual measurement of more than 100 AgNWs showed that AgNWs individual wires length and diameter

were so close to average values as distribution of silver nanowires due to their identical genesis were narrow. TEM images also revealed that at molding temperature (240ºC), AgNWs transformed into a chain of nanospheres (fragmentation phenomenon). At low filler loadings, the AgNW/polystyrene nanocomposites presented inferior electrical properties compared to CNT/polystyrene nanocomposites. This was attributed to lower aspect ratio, fragmentation phenomenon and poorer conductive network for AgNWs. However, at high filler loadings, the electrical properties of the AgNW/polystyrene nanocomposites significantly surpassed those of their CNT counterparts. It seems that at high filler loadings, the conductive network was well-established for the both types of nanocomposites and thus, higher innate conductivity of AgNWs played a dominant role in presenting superior electrical properties.

3.1 Introduction

The increase in using electronic devices for telecommunication and computation has heightened the need to resolve the issue of electromagnetic interference (EMI). Emitted electromagnetic (EM) waves from electronics bring up a serious concern in society as they are potentially hazardous for health, human body and efficacy of devices [1, 2].

The performance of shields to attenuate EM waves is assessed by shielding effectiveness (*SE*). The *SE* of a material is defined as the logarithm of the ratio of incident power to transmitted power and its unit is expressed in dB:

$$SE = 10 \log\left(\frac{P_i}{P_o}\right) \tag{3-1}$$

where P_i is the incident power and P_0 is the transmitted power. Time-averaged power is proportional to the root mean square (rms) of the electric field strength; therefore Equation 1 can also be rewritten as:

$$SE = 20 \log\left(\frac{E_i}{E_o}\right) \tag{3-2}$$

where E_0 and E_i are the incident and transmitted electric field strengths, respectively [3]. Commercially, 99.9% attenuation of incident EM waves, corresponding to *SE* of 30 dB, is considered sufficient for many practical engineering applications [4-7].

In order to minimize the undesirable effects of EM waves, several novel materials have been developed [8, 9], among which, metal coated polymers, ICPs (intrinsically conductive polymers) and conductive filler/polymer composites (CPCs) are the most common. Metal coated polymers exhibit drawbacks such as delamination of metal, poor adhesion between layers and environmental hazards. The commercialization of ICPs is also very limited due to poor long-term stability and lack of industrial processing methods. The aforementioned problems give CPCs an edge to be employed as futuristic shielding materials. CPCs benefit from inherent properties of polymers, such as light weight, low cost, easy processability and corrosion resistance, coupled with adjustable electrical properties originating from controlling the level of conductive network formation [10].

Designing a CPC with a high EMI shielding capability should be performed considering processing and economic parameters. Overloading fillers well over percolation threshold makes nanocomposites expensive and heavy, while underloading makes the system and its environment vulnerable to EM waves. EMI shielding capability of a CPC relies on two main factors: (1) intrinsic properties of filler, such as filler's innate electrical conductivity, diameter and aspect ratio [11, 12], and (2) processing-related factors such as dispersion, distribution and orientation of fillers [13].

It is has been proved both theoretically and experimentally that conductive shields comprising fillers with higher aspect ratio (higher length and lower diameter) provide lower percolation threshold, and higher electrical conductivity and EMI shielding [14-18]. It is well known that the surface area of a unit mass of a filler has an inverse relationship with its diameter, and fillers with higher length also have more probability to come close to, or contact, each other. For example, Al-Saleh and Sundararaj [19] compared the EMI shielding of high structured nano-sized carbon black and multi-walled carbon nanotube (MWCNT) in the X-band frequency range, and showed that at 7.5vol%, the EMI shielding of MWCNT was almost double of carbon black (35 dB versus 18 dB). In another study, Huang et al. [18] studied the effect of aspect ratio on percolation threshold and EMI shielding by comparing long and short MWCNTs. Their result showed longer MWCNTs offered lower percolation threshold and higher shielding.

The impacts of processing parameters on the electrical properties of CPCs were well reviewed in the literature [20-22]. Arjmand et al. [23] observed a huge effect of orientation of MWCNTs on the conductivity and EMI shielding. It was shown that, orientation affects the level of conductive network formation, and therefore changes the attenuation ability of CPCs. Im et al. [13] studied carbon black/polyaniline system, and enhanced the affinity of carbon black toward polyaniline by using fluorination. Their result showed that enhanced adhesion between the host matrix and filler led to a better dispersion and therefore higher conductivity and EMI shielding.

For efficient shielding, shields must possess mobile charge carriers and/or electric/magnetic dipoles to interact with electric/magnetic vectors of an incident EM wave [24, 25]. This amplifies the importance of the inherent properties of fillers embedded in CPCs. Regarding the choice of fillers, MWCNTs are proposed as promising candidates due to their huge surface area, high electrical conductivity, significant corrosion resistance and industrial growth. Moreover,

MWCNTs have long mean-free-paths and extremely high current densities, which are both vital to shielding. These properties commend MWCNTs as excellent fillers for EMI shielding applications [26].

Despite the fascinating properties of MWCNTs, their lower electrical conductivity limits their use in advanced applications. Accordingly, metal nanowires, as a new class of nanofillers, with superior electrical conductivity have been introduced to fill the aforementioned gap. Copper is the main metallic nanowire used for EMI shielding; however, it is readily oxidized under atmospheric condition [27]. This brings up the idea of using silver (Ag) nanowires as they have higher electrical conductivity than copper ($6.3\times10^{+5}$ $S\cdot cm^{-1}$ versus $5.9\times10^{+5}$ $S\cdot cm^{-1}$) along with greater resistance to oxidation [28, 29]. Silver oxidation in oxygen rich environment is not kinematically favorable but it's thermodynamically favorable. Kinematic of silver oxidation is so slow that we can rule the oxidation of silver out altogether. Although Ag, unlike some other metals, does not naturally form surface oxides [30, 31], however, exposure time of Ag nanowires should still be minimized due to potential corrosion arising from reduced sulfur gases present in the air. Corrosion of Ag at atmospheric condition is well-known to be instigated by sulfur compounds as well as free sulfur [32]. For instance, Elechiguerra et al. [32] reported that AgNWs were corroded with reduced sulfur gases in the air. They found that silver sulfide (Ag_2S) started to cover the surface of the nanowires after three weeks, and corrosion became even worse after six months, leading to the discontinuity of nanowires. Fortunately, none of the sulfur species are abundant in the atmosphere [33].

This paper describes the synthesis and EMI shielding of Ag nanowire (AgNW)/polymer nanocomposites. The EMI shielding of MWCNT/polymer nanocomposites are also presented as a matter of comparison. Comparing the EMI shielding of AgNW and MWCNT also verifies a tight correlation between EMI shielding performance and level of conductive network formation.

3.2 Experimental

3.2.1 Materials and composites preparation

3.2.1.1 Synthesis of AgNWs

The most widely used method for generating metallic nanowires less than 50 nm diameter is still template-directed synthesis, which involves either chemical or electrochemical deposition

[29]. Aluminum plates (5cm × 11cm) 1mm thickness were used as primary templates. The aluminum plates were anodized in parallel by immersing in a large tank filled with 0.3M H_2SO_4 at 2°C. Counter-electrodes were stainless steel plates with the same dimensions as the aluminum plates. Growth of the porous aluminum oxide (alumina) templates was performed in two steps: in the first step, the plates were immersed in a 0.3M H_2SO_4 solution for 2 hr under 25.0V to create initial porous structure. Afterwards, the plates were placed in a 1:1 mixture of 0.2M H_2CrO_4 and 0.6M H_3PO_4 at 60°C for 30min to make the already formed porous structure more uniform. In the next step, the plates were reimmersed in the 0.3M H_2SO_4 solution for 8hr, and then the applied voltage was reduced incrementally to reduce the alumina barrier layer at the pore bottom. Thinning the alumina barrier is a crucial part of the process since it keeps the end of the porous structure electrically conductive for the electrodeposition process. The protocol to decrease the voltage was initiated by a reduction rate of 2V/min from 25V to 15V; then it was followed by 1V/min rate to 9V, and eventually after 5min keeping at 9V, the voltage was dropped to zero. These synthesis steps generated cylindrical pores with hexagonal cross sections [34].

AC electrodeposition of Ag into the hexagonal-shaped pores was accomplished by insulating the edges of the electrodes by applying nail polish, and then immersing the plates for 5min in an electrolyte solution of silver sulfate (Ag_2SO_4, 8.5g/L), diammonium hydrogen citrate ($(NH_4)_2HC_6H_5O_7$, 200 g/L), and potassium thiocyanate (KSCN, 105 g/L). Square wave voltage pulses were applied between the Al plates and two pure Ag counter-electrodes to push the Ag ions toward the end of the pores. The voltage pulses were applied at 100Hz frequency and ±8.0V peaks (pulsed every 400ms) for 1.5hr.

Liberation of the nanowires was started by physically removing of bulk-deposited Ag from the surface of the Al plates, and then Ag nanowires were liberated from porous alumina in a beaker filled with 1.0M NaOH(aq) at room temperature. NaOH(aq) dissolved the surrounding alumina sheath so that we could recover the individual nanowires. After the liberation, floating fragments (bundled nanowires) were collected into a 1:1 mixture of 0.1M NaOH(aq) and MeOH, and sonicated for 10min. Immediately afterwards, collected AgNWs were purified through filter paper (Whatman with less than 1μm pore size), rinsed with MeOH, and then transferred to a beaker containing 100mL of MeOH. Additionally details on the synthesis of the AgNWs can be found elsewhere [35].

3.2.2. AgNW and MWCNT nanocomposites preparation

Nanocomposites were prepared by the miscible solvent mixing and precipitation (MSMP) technique [34]. The nanocomposites with different concentrations of AgNWs were produced by mixing different volumes of 3.3mg/ml AgNW/MeOH suspension with 20mg/ml PS (Styron® 615 APR, Americas Styrenics LLC)/methylene chloride solution. Each mixture was treated in ultrasound bath for 30min, and then stirred for 10min prior to mixing. The suspension was then filtered and placed in an evaporation dish for 16h in a fume hood. The residue was further dried in a vacuum oven at 50°C for 24hr to obtain nanocomposite nuggets. The polymer nanocomposite nuggets were then molded into a rectangular cavity, with the dimensions of 22.9×10.2×0.8mm, at 240°C and 38MPa for 15min. For the sake of comparison, MWCNT/PS nanocomposites were produced at the same volumetric concentrations with the same technique. MWCNTs (Nanocyl™ NC7000) were obtained from Nanocyl S.A. (Sambreville, Belgium).

3.3. Materials characterization

The TEM analyses of the nanofillers and nanocomposites were carried out on a Tecnai TF20 G2 FEG-TEM (FEI, Hillsboro, Oregon, USA) at 200kV acceleration voltage with a standard single-tilt holder. The images were taken with a Gatan UltraScan 4000 CCD (Gatan, Pleasanton, California, USA) at 2048×2048 pixels. For the TEM analysis of the nanofillers, the droplets of AgNW and MWCNT suspensions were placed on a holey carbon-coated Cu TEM grid, and dried at room conditions. For the TEM analysis of the nanocomposites, the molded nanocomposites were ultramicrotomed to achieve 70nm thick sections.

Both the molded nanocomposites and powdery liberated AgNWs were analyzed by X-ray diffraction (XRD). The XRD analysis was performed using a Rigaku ULTIMA III X-ray diffractometer with Cu K-alpha radiation as the X-ray source. The scan was carried out in the range 2θ=30–90 degrees using a 0.02 degree step and a counting time of 1 degree per minute at 40kV and 44mA to obtain the full diffractogram for the materials.

The electrical conductivity measurements were carried out on the molded rectangular samples. All the samples' surfaces were wiped with ethanol to remove impurities prior to the measurements. For nanocomposites with electrical conductivities more than 10^{-4} $S \cdot cm^{-1}$, we carried out the measurements according to ASTM 257-75 utsing a Loresta GP resistivity meter (MCPT610 model, Mitsubishi Chemical Co., Japan). A standard four-pin probe was used to reduce the effect of contact resistance. For an electrical conductivity less than 10^{-4} $S \cdot cm^{-1}$, a Keithley 6517A electrometer connected to Keithley 8009 test fixture (Keithley Instruments, USA) was used.

The EMI shielding measurements were carried out over the X-band (8.2–12.4GHz) frequency range using an E5071C network analyzer (ENA series 300KHz – 20GHz). The samples under the test were squeezed between two flanges connecting the waveguides of the network analyzer. The network analyzer sent a signal down the waveguide incident to the sample, and then the scattering parameters (S-parameters) of each sample were recorded, and used to calculate *SE*. The dielectric properties of the generated nanocomposites were also obtained via conversion of the measurements using Reflection/Transmission Mu and Epsilon Nicolson-Ross Model.

3.4. Results and Discussion

3.4.1. Morphology

In order to obtain essential information about the morphology of AgNWs, the TEM images of AgNWs were captured before and after processing. Figure 3-1(a) displays the bundles of pristine AgNWs with uniform length before processing, demonstrating the ability of the synthesis method to produce AgNWs with uniform dimensions. The statistical analysis of over 100 AgNWs indicated that AgNWs had average diameter and length of 25 nm and 5.6±1.4 μm, respectively. As depicted in Figure 3-1(b), despite the long sonication time, some portions of AgNWs are still bundled in the PS matrix. This can be ascribed to large surface area and huge van der Waals forces between AgNWs, and this agglomeration can adversely affect the electrical properties. Gelves et al. [35] also showed the irreversible agglomeration of clean nanowires after liberation. Figure 3-1(c) shows that MWCNTs were relatively well dispersed and distributed in the PS matrix, promising enhanced electrical properties.

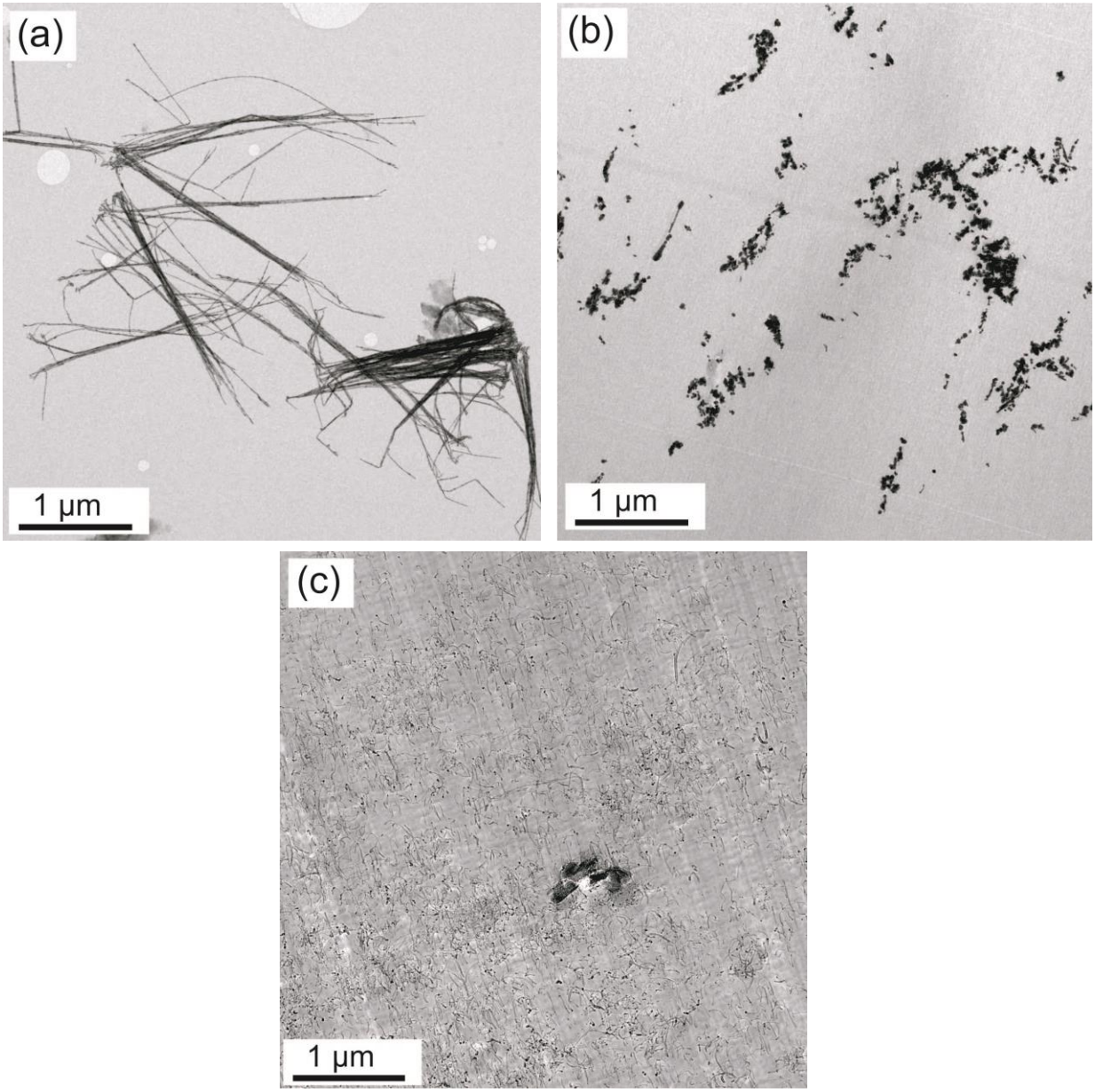

Figure 3-1: (a) TEM micrographs of (a) pristine AgNWs, (b) 1.5vol% AgNW/PS nanocomposite, and (c) 1.5vol% MWCNT/PS nanocomposite.

TEM images of AgNWs after processing revealed that during the mixing process, AgNWs became unstable and surprisingly lost their original shape and aspect ratio breaking into short cylinders with bulbous ends or into spheres (Figure 3-1(b)). Deformation of AgNWs during the mixing process at high temperature can be ascribed to fragmentation phenomenon, which has been

reported in the literature [36]. This observation is quite significant due to the significant impact of the filler's aspect ratio on the final electrical properties of CPCs.

The fragmentation phenomenon is believed to change the shape of nanowires from a cylinder to a linear row of nanospheres at high temperatures, where atomic movements by diffusion become fairly important [37-41]. Karim et al. [38] observed fragmentation for gold nanowires at 600 ° C, and believe that the fragmentation arises from thickness undulation along the axis of the nanowires followed by spheroidization. In another study, Li et al. [36] ascribed the fragmentation of nanowires, which were annealed at high temperatures 220 ° C , to a crystalline phase transition from less stable body-centered tetragonal (BCT) to a more stable face-centered cubic (FCC) of colloidal AgNWs. They also proved that long AgNWs exhibit an inhomogeneous core-shell structure with highly strained cores and less strained sheath due to the existence of the fivefold twinning crystal structure. They claimed that, the strains in the AgNWs cores distort the common FCC crystalline lattice to BCT lattice symmetry. At elevated temperatures, the energy required for the diffusion of Ag atoms on the surface of AgNWs becomes sufficiently high to surpasses the required activation energy, and thus the crystalline phase transition occurs.

In order to achieve a more vivid picture of the fragmentation phenomenon, the AgNW/PS nanocomposites were suspended in CH_2Cl_2 to extract AgNWs from the nanocomposites (Figure 3-2). As evident in Figure 3-2, the fragmentation is at its early stages for our samples since most of the nanowires retained their original cylindrical geometries. However, for some nanowires the shape transformation from cylindrical to linear row of nanospheres is observable. Although the crystalline phase transition might be the main driving force for the fragmentation, other factors such as corrosion with sulfur gases in the air might also play a role in making the nanowires discontinuous. For instance, Franey et al. [33] and Khaligh et al. [42] reported that that exposing nanowires to elevated temperatures resulted in considerable increase in the amount of sulfur on the surface. White parts in TEM images are the holes in the carbon grids used for holding sample suspensions.

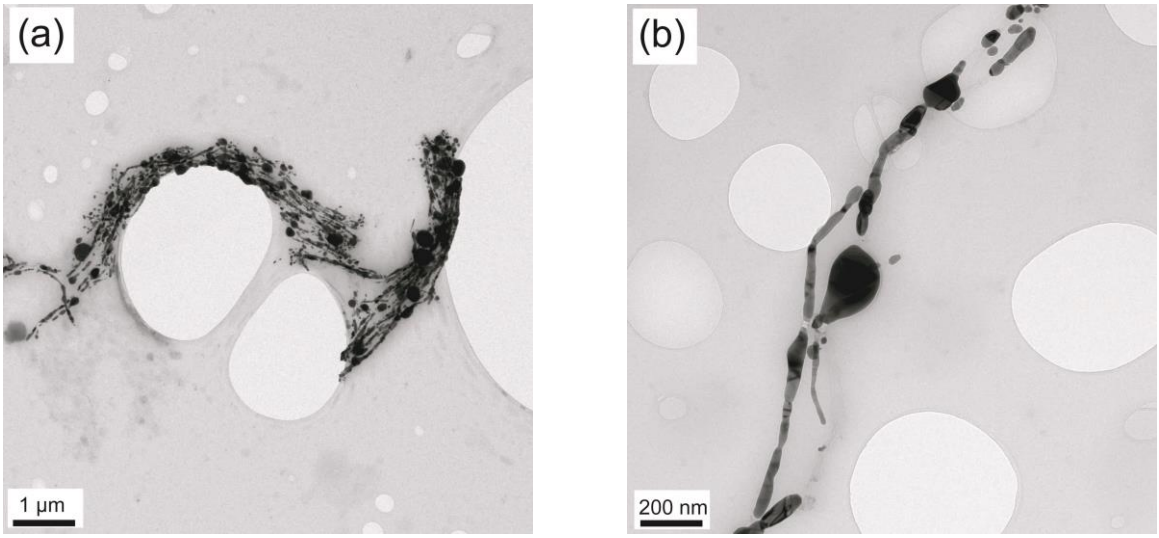

Figure 3-2: Fragmentation in AgNW/PS nanocomposites at two various magnifications. AgNWs were extracted from 2.5vol% AgNW/PS nanocomposites employing CH2Cl2 (a) low magnification (b) high magnification

In order to detect traces of silver oxide and silver crystalline structure, X-ray diffraction (XRD) analysis was carried out for pristine AgNWs and AgNW/PS nanocomposites. Figure 3-3 shows the X-ray diffractograms of AgNWs powder and AgNW/PS nanocomposites with 2.5vol% loading. Five strong characteristic peaks of silver at 2θ equal to 38.1°, 44.2°, 64.4°, 77.3° and 81.9° are clearly observable. These peaks correspond to the crystal faces of (111), (200), (220), (311) and (222) of silver face-centered cubic (FCC) crystalline structure, respectively. The X-ray diffractograms in conjunction with the TEM images confirm the successful synthesis of AgNWs and presence of AgNWs in the nanocomposites.

In the literature, Sun et al. [43] claimed that when the dry AgNWs are deposited on a substrate, the orientation of all the (110) planes cannot be equally distributed due to the high aspect ratio of the nanowires. Therefore, different relative intensities of major peaks compared with standard powder diffraction pattern are expected. Furthermore, one may notice very strong (111) orientation along AgNWs axial direction, which is due to the fact that specific free energy of silver is minimum on (111) planes of the FCC structure [44]. As shown in Figure 3-3, no trace of crystalline silver oxide or silver sulfide before or after processing was found by XRD. Silver oxidation in oxygen rich environment is not kinematically favorable but it's thermodynamically favorable. Kinematic of silver oxidation is so slow that we can rule the oxidation of silver out altogether. The absence of silver oxide was also reported by other researchers who believe that silver does not form silver oxide naturally [30, 31]. Apprently, since AgNWs were embedded in polymer matrix right after

their synthesis, sulfur components did not find sufficient time to corrode the surface of AgNWs. As silver oxide is semi-conductive with less conductivity than pristine form of silver, the absence of silver oxide is a postive sign for obtaining enhanced electrical properties [45].

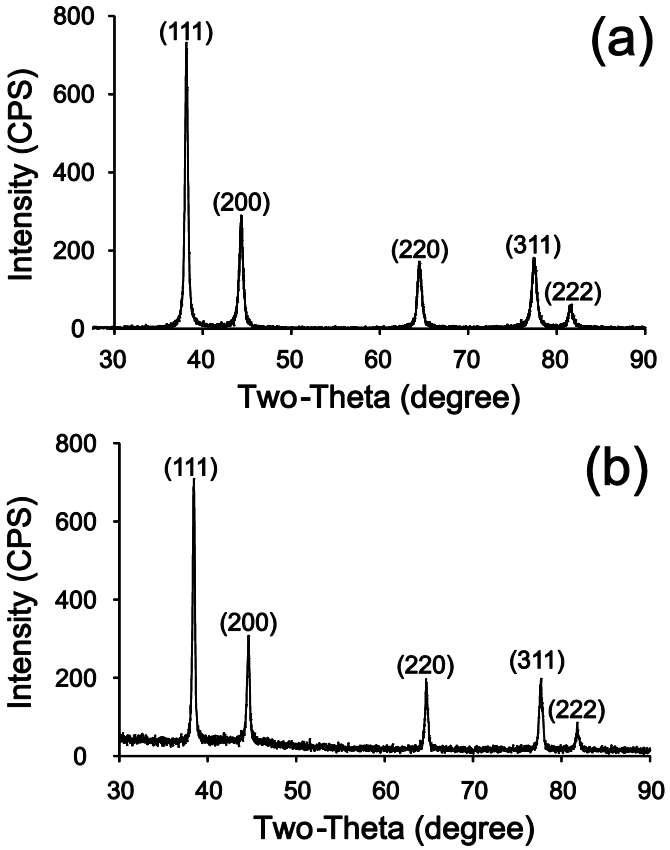

Figure 3-3: XRD pattern of (a) AgNWs powder right after liberation, (b) AgNW/PS nanocomposite having 2.5vol% AgNWs.

3.4.2. Comparison of electrical conductivity of AgNW/PS and MWCNT/PS nanocomposites

Technically, polymers are insulating and need to be filled with conductive fillers to develop lightweight electrically conductive materials. The electrical conductivity of CPCs increases dramatically beyond a concentration called the percolation threshold. In fact, at the percolation threshold, the first conductive path forms, transforming CPCs from insulative into conductive. Physical contacts between neighboring nanofillers in combination with tunneling and hopping are the main mechanisms for the transference of electrons in CPCs [46, 47]. At filler loadings around the percolation threshold, where the conductive network is not well-established, all the

aforementioned mechanisms contribute significantly to electron transference; however, at filler loadings far above the percolation threshold, the conductivity is primarily due to physical contacts between nanofillers.

Figure 3-4 depicts the percolation curves of the AgNW/PS and MWCNT/PS nanocomposites. The results showed that for the both types of nanocomposites adding 2.5vol% conductive nanofiller into the PS matrix led to about 16 orders of magnitude enhancement in the electrical conductivity. The percolation threshold, obtained from the percolation theory, for the MWCNT/PS nanocomposites was 0.04vol%, while the AgNW/PS nanocomposites presented a percolation threshold noticeably higher and equal to 1.2vol%. Several factors could account for higher percolation threshold in the AgNW/PS nanocomposites, namely (1) lower aspect ratio of AgNWs, (2) fragmentation phenomenon in AgNWs, and (3) inferior dispersion and distribution of AgNWs. It has been proven both theoretically and experimentally that fillers with higher aspect ratio (higher length and lower diameter) present lower percolation threshold [18]. In fact, the higher the aspect ratio of conductive fillers, the more their likelihood to neighbor or contact each other. It should be considered that the discrepancy in the aspect ratio of MWCNTs and AgNWs was intensified by the fragmentation phenomenon, where AgNWs transformed from cylindrical shapes to linear rows of nanospheres. Furthermore, inferior dispersion and distribution of AgNWs to MWCNTs within the PS matrix, as corroborated by the TEM images, could be another reason for the higher percolation threshold of the AgNW/PS nanocomposites.

Figure 3-4 indicates that at high filler loadings the electrical conductivity of the AgNW/PS nanocomposites is higher than MWCNT/PS nanocomposites. For instance, at 2.5vol%, the electrical conductivity of the AgNW/PS was about twenty times higher than MWCNT/PS nanocomposites (19.2 versus $0.9 S \cdot cm^{-1}$). At filler loadings far above the percolation threshold, due to the formation of a well-established conductive network, the conductivity of CPCs relies significantly on the innate conductivity of nanofillers [35]. This justifies the higher electrical conductivity seen for the AgNW/PS nanocomposites at high filler loadings.

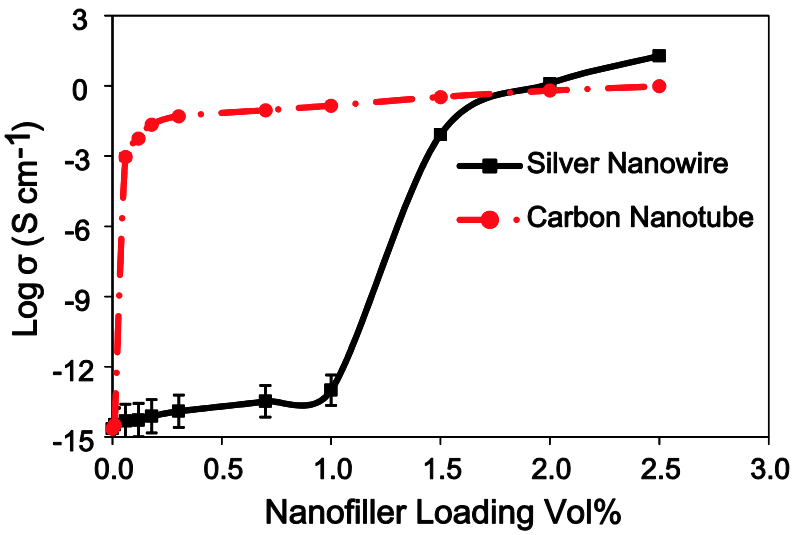

Figure 3-4: Electrical conductivity of AgNW/PS versus MWCNT/PS nanocomposites as a function of nanofiller loading.

Figure 3-4 also depicts a huge difference between the maximum obtained electrical conductivity of the AgNW/PS nanocomposite and Ag bulk (19.2 versus $6.25\times10^{+5}S\cdot cm^{-1}$). This dissimilarity can be attributed to junction resistance and possibly the low diameter of AgNWs. Electrical measurements on individual metallic nanowires have shown that as their diameter decreases, their electrical properties deviate from bulk properties [48, 49]. This phenomenon is attributed to the presence of grain boundaries (*defects*) in the *crystalline* structure of nanowires, where electrons are scattered (either elastically or inelastically) when they try to go through a grain boundary. Nonetheless, the results of a study by Chen et al. [50] demonstrated that Ag nanobeams retain the high conductivity of bulk silver for thicknesses down to ~ 15nm. Sun et al. [29] also measured the conductivity of their in-house silver nanowire (40nm diameter) by aligning them across two gold probe electrodes, and reported conductivity values close to bulk silver conductivity. Given 25nm is the average diameter of our synthesized AgNWs, we are uncertain whether our synthesized AgNWs suffered from the grain boundary scattering effect. This issue is beyond the scope of the current paper, and will be targeted in future studies.

3.4.3. EMI shielding of AgNW/PS versus MWCNT/PS nanocomposites

EMI shielding is performed by a using conductive and/or magnetic barrier to attenuate irradiated EM waves from electronics by using. An EM wave encompasses two components: electric field and magnetic field. The ratio of electric field to magnetic field of a propagating wave is an inherent property of a medium, and named as intrinsic impedance. This ratio is considerably significant in defining the level of shielding and prevailing shielding mechanisms in conductive shields. The intrinsic impedance of a medium is defined as follows [23]:

$$\eta = \sqrt{\frac{j\omega\mu}{\sigma + j\omega\epsilon}} \tag{3-3}$$

where η is intrinsic impedance, ω is angular frequency, μ is magnetic permeability, σ is electrical conductivity and ε is real permittivity. The permittivity and permeability of free space are equal to $8.85\times10^{-12}F\cdot m^{-1}$ and $4\pi\times10^{-7}H\cdot m^{-1}$, respectively. Given the low conductivity of free space, its intrinsic impedance is equal to 377Ω; conductive shields present significantly lower intrinsic impedance [24, 25].

Essentially, there are three mechanisms involved in the EMI shielding of CPCs, i.e. reflection, absorption and multiple-reflection. Reflection occurs due to impedance mismatch between two media. That is to say, a highly reflective shield must possess a low magnetic permeability, high electrical conductivity and/or high real permittivity. The portion of the EM wave that is not reflected infiltrates into conductive shields. As the impedance of a conductive shield is much lower than free space, a large portion of the infiltrated electric field is converted to the magnetic field. Thus, it is very important to attenuate both the electric and magnetic fields inside a shield. The attenuation of the EM wave inside a conductive shield is performed through absorption mechanism, which is composed of Ohmic loss and polarization loss (electric polarization and magnetic polarization loss). The Ohmic loss is due to the interaction of propagating EM wave with nomadic charges, is in phase with the EM wave and quantified by imaginary permittivity. The polarization loss arises from the energy required to reorient electric/magnetic dipoles in each half cycle of the alternating field [51]. The levels of the electric and magnetic polarizations are expressed by real permittivity and magnetic permeability, respectively.

Multiple-reflection is the third shielding mechanism in CPCs, which occurs due to the existence of huge interfacial area. Theoretically, the first reflection from the second interface of a shield is

counted as a part of the reflection mechanism. According to this definition, multiple-reflection adversely impacts the overall EMI shielding due to its augmentation effect on the transmitted waves. It is believed that the multiple-reflection can be ignored if a CPC's thickness is larger than its skin depth or if shielding by absorption is more than 10dB [23]. The skin depth of a conductive shield is defined as the depth inside the shield at which the power of the EM wave drops to 1/e of its incident value. Skin depth is proportional to the root square of electrical conductivity and magnetic permeability [25].

Figure 3-5 compares the average EMI shielding (overall, reflection and absorption) of the generated nanocomposites as a function of nanofiller loading over the X-band frequency range. It should be noted that the effect of multiple-reflection is included within the reported values of shielding by reflection and absorption. It was seen that the MWCNT/PS nanocomposites showed a steady ascending trend of EMI SE with increasing conductive filler loading. The overall EMI SE of the MWCNT/PS nanocomposites rose from 0.01dB for pure PS to 22.14dB for nanocomposites with 2.5vol% MWCNT loading, which is sufficient for commercial applications. Surprisingly it was also observed that the AgNW/PS nanocomposites were transparent to EM waves at low AgNW loadings, and incorporating AgNW up to about 1.0vol% into the AgNW/PS nanocomposites did not enhance the EMI SE (both the reflection and absorption). However, beyond 1.0vol%, the EMI SE of the AgNW/PS nanocomposites drastically increased. For instance, at 2.0 and 2.5vol%, the overall EMI SEs of the AgNW/PS nanocomposites were 22.70 and 31.85dB, respectively, which were significantly higher than those of their MWCNT counterparts.

The clues to understand the strange behavior of the AgNW/PS nanocomposites are in the percolation curves (Figure 3-4). According to the percolation curves, the percolation threshold of the MWCNT/PS and AgNW/PS nanocomposites were 0.04 and 1.20vol% respectively, and beyond these concentrations the number of conductive networks increase. In the literature, it is believed that EMI shielding does not require filler connectivity; however it increases with filler connectivity [7]. This could justify the large difference between the EMI shielding value of the AgNW/PS nanocomposites below and above the percolation threshold. If this is the case, Figure 3-5 denotes that shielding by both reflection and absorption are highly sensitive to the formation of the conductive network.

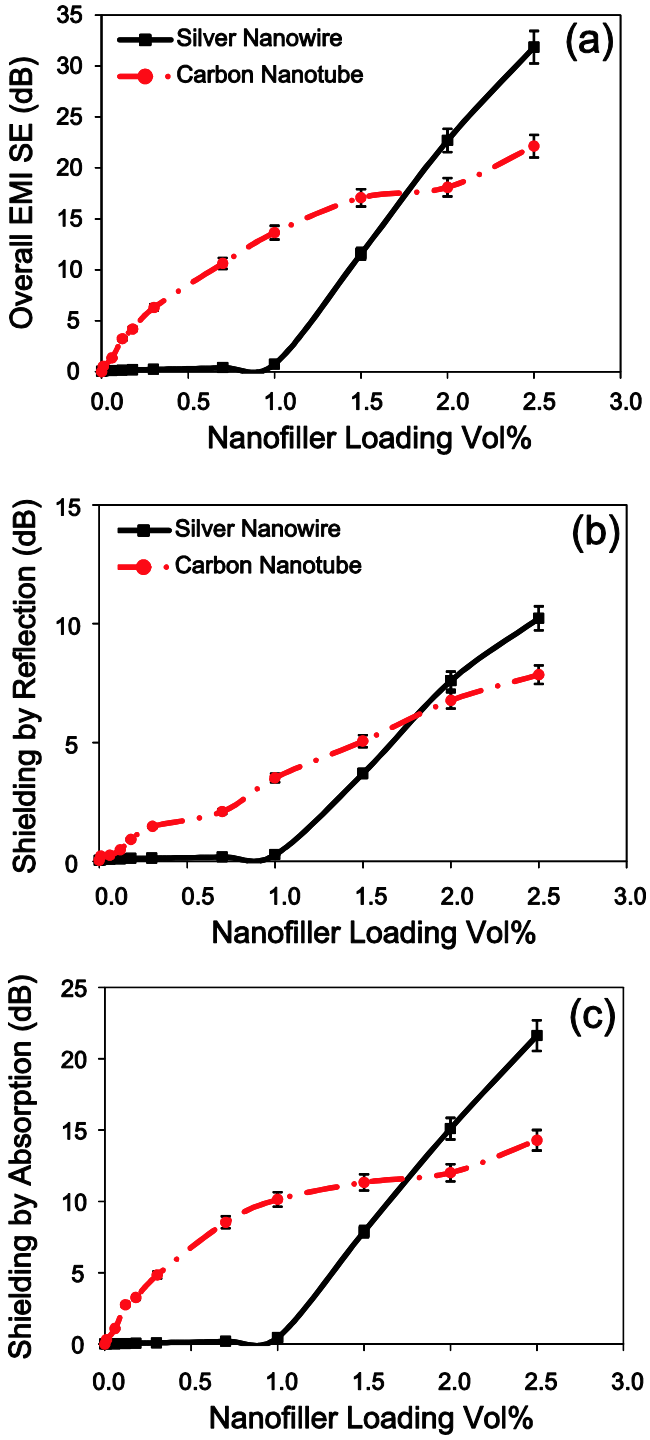

Figure 3-5: EMI SE (overall, reflection and absorption) of AgNW/PS and MWCNT/PS nanocomposites as a function of nanofiller loading.

In order to validate this, we investigated the imaginary permittivity and real permittivity of the generated nanocomposites (Figure 3-6). It is worth mentioning that all the nanocomposites presented a non-magnetic behavior. Imaginary permittivity signifies the amount of energy

dissipated by nomadic charges inside a conductive shield, and is highly sensitive to conductive network formation. It is evident that the imaginary permittivity follows the same trend as EMI SE for the both types of nanocomposites. The imaginary permittivity of the AgNW/PS nanocomposites was close to zero below the percolation threshold, and then it increased pronouncedly above the percolation threshold. Drastic increase in the imaginary permittivity above the percolation threshold stems from the formation of extensive and numerous conductive networks, wherein electrons can find more mean-free-path to go through in each half cycle of alternating field, and can dissipate more electrical energy.

Figure 3-6 also shows that the imaginary permittivity of the AgNW/PS nanocomposites at high loadings is much greater than MWCNT/PS nanocomposites. Technically, several factors play a role in determining the imaginary permittivity including the innate conductivity of nanofiller, nanofillers' available surface area and the level of conductive network formation. At low filler loadings The MWCNT/PS nanocomposites presented higher imaginary permittivity due to enhanced conductive network formation (See figure 3-4) and larger available surface area (10 nm diameter versus 25 nm diameter for AgNWs). Nevertheless, at high filler contents, the innate conductivity of AgNW overcome its lower aspect ratio and inferior conductive network formation, leading to superior electrical properties over MWCNT/PS nanocomposites. Enhanced electrical properties of AgNWs beyond the percolation threshold commend them as futuristic materials for EMI shielding applications. Moreover, the comparison of the electrical properties of MWCNT/PS and AgNW/PS nanocomposites verifies the dominant role of the conductive network formation on EMI shielding and imaginary permittivity.

Figure 3-6(b) compares the real permittivities of the generated nanocomposites, which present the same trend as the imaginary permittivity. It is can be seen that the real permittivity of the MWCNT/PS nanocomposites shows a uniform ascending trend with filler loading, whereas the AgNW/PS nanocomposites experienced a sudden increase in real permittivity just above the percolation threshold. In general, several polarization mechanisms can occur in CPCs depending on the structure and frequency range, i.e. interfacial, dipolar, atomic and electronic polarization [52]. However, in the current study, due to the nonpolar nature of the PS matrix and high frequency range of the X-band, the electronic polarization of the PS matrix and dipolar polarization within the nanofillers are deemed to be the only probable mechanisms in play.

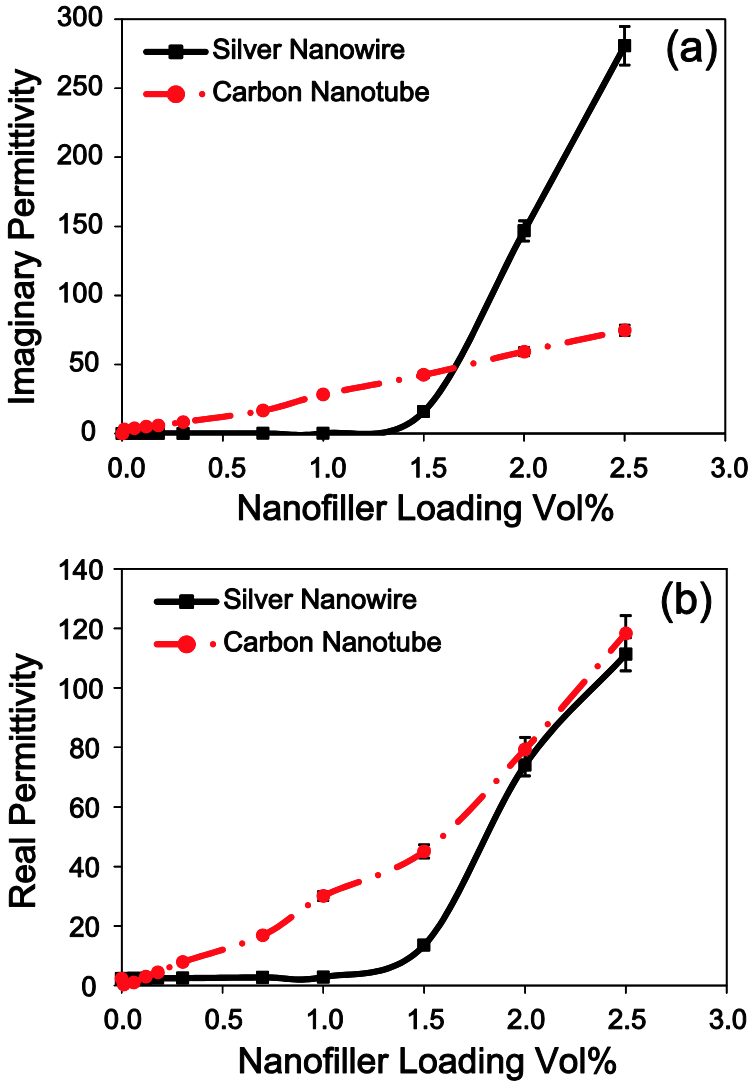

Figure 3-6: (a) Imaginary permittivity, and (b) real permittivity as a function of nanofiller loading.

Electronic polarization in CPCs originates from the concept of nanocapacitors, nanofillers act as nanoelectrodes and polymer matrix between them plays the role of nanodielectric [53, 54]. As conductive filler content approaches the percolation threshold, the thickness of nanodielectric decreases, thus the applied electric field within nanodielectric increases, which leads to enhanced electronic polarization. Hence, the enhancement in the real permittivity of the AgNW/PS nanocomposites above the percolation threshold arises from the formation of a large number of nanocapacitor structures. However, the MWCNT/PS nanocomposites experienced nanocapacitorformation at much lower loadings, i.e. 0.04vol%, and this accounts for their steady ascending trend with MWCNT content. It is possible that if we obtained more points below 0.04 vol % we would see the same type of discontinuity in the curve. Furthermore, the presence of

defects in the crystalline structure of both MWCNT and AgNW could result in dipolar polarization and further increase of the real permittivity [55, 56].

The capacitance of a capacitor is defined as following:

$$C = \frac{\varepsilon A}{d} \tag{3-4}$$

where ε real permittivity, A surface area and d thickness of capacitors. Moreover, the capacitance has a direct relationship with the amount of charges stored on the surface of a capacitor. MWCNTs, due to their high aspect ratio and enhanced conductive network formation, possessed larger A and lower d than AgNWs. However, higher innate electrical conductivity of AgNWs led to more potential charges to be stored on the surface of their nanocapacitors. Thus, there is a competition between higher surface area and enhanced conductive network of MWCNTs and superior electrical conductivity of AgNWs. The outcome of this competition was higher polarization loss of the MWCNT/PS nanocomposites at low filler contents, and comparable polarization loss at high filler loadings.

3.5. Conclusion

Silver nanowires (AgNWs) were synthesized successfully by the AC electrodeposition of Ag into porous aluminum oxide templates. AgNWs were embedded into polystyrene via the miscible solvent mixing and precipitation (MSMP) technique. XRD showed silver FCC crystal structure peaks but no trace of crystalline silver oxide or silver sulfide before or after processing. Absence of silver oxide peaks was related to natural resistance of silver towards oxidation. Peaks related to silver sulfide also were also not observed as AgNWs exposure time to sulfur components in the air was minimal. TEM analysis verified successful synthesis of AgNWs with an average diameter and length of 25nm and 5.6±1.4 μm, respectively. TEM images also revealed that an AgNW at high temperature transformed into chain of nanospheres by fragmentation phenomenon. Crystalline phase transition might be the main driving force for the fragmentation but other factors such as corrosion with sulfur gases in the air might also come into play to break up the nanowires. The latter was ruled out since no noticeable peak related to corrosion was observed in XRD patterns. Moreover, TEM images demonstrated that fragmentation was at its early stages and good level of distribution and dispersion was achieved by sonication. Electrical resistivity measurements

indicate that the percolation thresholds, obtained from the percolation theory, for the MWCNT/PS nanocomposites was 0.04vol%, while the AgNW/PS nanocomposites presented a percolation threshold noticeably higher, equal to 1.2vol%. Several factors could explain higher percolation threshold in the AgNW/PS nanocomposites, namely (1) lower aspect ratio of AgNWs, (2) fragmentation phenomenon in AgNWs, and (3) inferior dispersion and distribution of AgNWs. EMI SE, like electrical conductivity, reduced due to adverse effect of fragmentation in delaying the network formation. Despite negative effect of fragmentation on EMI shielding, EMI SE of AgNW/PS was 31.84 dB, ~10 dB higher than MWCNT/PS at 2.5vol % loading. It seems that at high filler loadings, where the conductive network was well established for both types of nanocomposites, higher innate conductivity of AgNWs played a dominant role. The imaginary permittivity of the AgNW/PS nanocomposites at high loadings is much greater than MWCNT/PS nanocomposites. At low filler loading, the MWCNT/PS nanocomposites presented higher imaginary permittivity due to enhanced conductive network formation and larger available surface area, but at high filler contents, the innate conductivity of AgNW dominated over the effect of lower aspect ratio. Real permittivity experienced the trend as imaginary permittivity. There is an ascending trend for real permittivity of MWCNT/PS nanocomposites from any low concentrations while there is a jump in real permittivity of AgNW/PS nanocomposites at 1.2 vol %. The enhancement in the real permittivity of the AgNW/PS nanocomposites above the percolation threshold originates from the formation of a great number of nanocapacitors; i.e. starting at 0.04vol% for MWCNT/PS nanocomposites and 1.2vol % for AgNW/PS nanocomposites. Additionally, defects in the crystalline structure of both MWCNT and AgNW could result in dipolar polarization; and further enhance of the real permittivity.

These new novel material that has the ability to store energy in a way that they can be recharged in seconds rather than hours, would hold electrical charge timelessly. One day these new nano loaded materials can lead to breakthroughs in hybrid cars and provide energy wells for resources such as solar and wind. Our new capacitors has the ability to store energy in an electric field, has the advantage of being chemical reaction free and they can deliver energy quickly and be able to be charged in matter of seconds. They can bear temperature changes, and physical sudden agitations. In the nutshell, in addition that they are cost effective they are environmental friendly materials as well.

3.6 Acknowledgements

The financial support from the Natural Sciences and Engineering Research Council of Canada (NSERC) is highly appreciated.

3.7 References

[1] Li N, Huang Y, Du F, He XB, Lin X, Gao HJ, et al. Electromagnetic interference (EMI) shielding of single-walled carbon nanotube epoxy composites. Nano Letters. 2006;6(6):1141-5.

[2] Hong YK, Lee CY, Jeong CK, Sim JH, Kim K, Joo J, et al. Electromagnetic interference shielding characteristics of fabric complexes coated with conductive polypyrrole and thermally evaporated Ag. Current Applied Physics. 2001;1(6):439-42.

[3] Colaneri NF, Shacklette LW. EMI SHIELDING MEASUREMENTS OF CONDUCTIVE POLYMER BLENDS. Ieee Transactions on Instrumentation and Measurement. 1992;41(2):291-7.

[4] Markham D. Shielding: quantifying the shielding requirements for portable electronic design and providing new solutions by using a combination of materials and design. Materials & Design. 2000;21(1):45-50.

[5] Yang SY, Lozano K, Lomeli A, Foltz HD, Jones R. Electromagnetic interference shielding effectiveness of carbon nanofiber/LCP composites. Composites Part a-Applied Science and Manufacturing. 2005;36(5):691-7.

[6] Huang JC. EMI SHIELDING PLASTICS - A REVIEW. Advances in Polymer Technology. 1995;14(2):137-50.

[7] Arjmand M, Apperley T, Okoniewski M, Sundararaj U. Comparative study of electromagnetic interference shielding properties of injection molded versus compression molded multi-walled carbon nanotube/polystyrene composites. Carbon. 2012;50(14):5126-34.

[8] Brown RW, Shvartsman SM. Supershielding: Confinement of magnetic fields. Physical Review Letters. 1999;83(10):1946-9.
[9] Takei K, Ishii O, Senda M, Ieee. Application of magnetic metal thin films to EMI noise filter. Ieee 1996 International Symposium on Electromagnetic Compatibility - Emc: Silicon to Systems, Symposium Record. 1996:508-10.
[10] Su L, Gao F, Mao LQ. Electrochemical properties of carbon nanotube (CNT) film electrodes prepared by controllable adsorption of CNTs onto an alkanethiol monolayer self-assembled on gold electrodes. Analytical Chemistry. 2006;78(8):2651-7.
[11] Chung DDL. Electromagnetic interference shielding effectiveness of carbon materials. Carbon. 2001;39(2):279-85.
[12] Joo J, Lee CY. High frequency electromagnetic interference shielding response of mixtures and multilayer films based on conducting polymers. Journal of Applied Physics. 2000;88(1):513-8.
[13] Im JS, Kim JG, Lee YS. Fluorination effects of carbon black additives for electrical properties and EMI shielding efficiency by improved dispersion and adhesion. Carbon. 2009;47(11):2640-7.
[14] Li J, Ma PC, Chow WS, To CK, Tang BZ, Kim JK. Correlations between percolation threshold, dispersion state, and aspect ratio of carbon nanotubes. Advanced Functional Materials. 2007;17(16):3207-15.
[15] Behnam A, Guo J, Ural A. Effects of nanotube alignment and measurement direction on percolation resistivity in single-walled carbon nanotube films. Journal of Applied Physics. 2007;102(4).
[16] Kim DY, Yun YS, Bak H, Cho SY, Jin HJ. Aspect ratio control of acid modified multiwalled carbon nanotubes. Current Applied Physics. 2010;10(4):1046-52.
[17] Arjmand M, Mahmoodi M, Park S, Sundararaj U. An innovative method to reduce the energy loss of conductive filler/polymer composites for charge storage applications. Composites Science and Technology. 2013;78:24-9.
[18] Huang Y, Li N, Ma YF, Feng D, Li FF, He XB, et al. The influence of single-walled carbon nanotube structure on the electromagnetic interference shielding efficiency of its epoxy composites. Carbon. 2007;45(8):1614-21.

[19] Al-Saleh MH, Sundararaj U. X-band EMI shielding mechanisms and shielding effectiveness of high structure carbon black/polypropylene composites. Journal of Physics D: Applied Physics. 2013;46(3):035304.
[20] Spitalsky Z, Tasis D, Papagelis K, Galiotis C. Carbon nanotube-polymer composites: Chemistry, processing, mechanical and electrical properties. Progress in Polymer Science. 2010;35(3):357-401.
[21] Bauhofer W, Kovacs JZ. A review and analysis of electrical percolation in carbon nanotube polymer composites. Composites Science and Technology. 2009;69(10):1486-98.
[22] Thostenson ET, Ren ZF, Chou TW. Advances in the science and technology of carbon nanotubes and their composites: a review. Composites Science and Technology. 2001;61(13):1899-912.
[23] Arjmand M, Mahmoodi M, Gelves GA, Park S, Sundararaj U. Electrical and electromagnetic interference shielding properties of flow-induced oriented carbon nanotubes in polycarbonate. Carbon. 2011;49(11):3430-40.
[24] Chatterton PA, Houlden MA. EMC-Electromagnetic theory to practical design. NASA STI/Recon Technical Report A. 1992;93:17521.
[25] Kaiser KL. Electromagnetic shielding: CRC Press; 2005.
[26] Abbasi Moud A, Javadi A, Nazockdast H, Fathi A, Altstaedt V. Effect of dispersion and selective localization of carbon nanotubes on rheology and electrical conductivity of polyamide 6 (PA6), Polypropylene (PP), and PA6/PP nanocomposites. Journal of Polymer Science Part B: Polymer Physics. 2014.
[27] da Silva AB, Arjmand M, Sundararaj U, Bretas RES. Novel composites of Copper nanowire/PVDF with superior dielectric properties. Polymer. 2014;55(1):226-34.
[28] Sachan R, Ramos V, Malasi A, Yadavali S, Bartley B, Garcia H, et al. Oxidation-Resistant Silver Nanostructures for Ultrastable Plasmonic Applications. Advanced Materials. 2013;25(14):2045-50.
[29] Sun Y, Yin Y, Mayers BT, Herricks T, Xia Y. Uniform silver nanowires synthesis by reducing AgNO3 with ethylene glycol in the presence of seeds and poly (vinyl pyrrolidone). Chemistry of Materials. 2002;14(11):4736-45.

[30] Campbell W, Thomas U. Tarnish Studies The Electrolytic Reduction Method for the Analysis of Films on Metal Surfaces. Transactions of the Electrochemical Society. 1939;76(1):303-28.
[31] Czanderna A. The adsorption of oxygen on silver. The Journal of Physical Chemistry. 1964;68(10):2765-71.
[32] Elechiguerra JL, Larios-Lopez L, Liu C, Garcia-Gutierrez D, Camacho-Bragado A, Yacaman MJ. Corrosion at the nanoscale: the case of silver nanowires and nanoparticles. Chemistry of Materials. 2005;17(24):6042-52.
[33] Franey J, Kammlott G, Graedel T. The corrosion of silver by atmospheric sulfurous gases. Corrosion Science. 1985;25(2):133-43.
[34] Gelves GA, Al-Saleh MH, Sundararaj U. Highly electrically conductive and high performance EMI shielding nanowire/polymer nanocomposites by miscible mixing and precipitation. Journal of Materials Chemistry. 2011;21(3):829-36.
[35] Gelves GA, Lin B, Sundararaj U, Haber JA. Low electrical percolation threshold of silver and copper nanowires in polystyrene composites. Advanced Functional Materials. 2006;16(18):2423-30.
[36] Li Z, Okasinski JS, Almer JD, Ren Y, Zuo X, Sun Y. Quantitative determination of fragmentation kinetics and thermodynamics of colloidal silver nanowires by in situ high-energy synchrotron X-ray diffraction. Nanoscale. 2014;6(1):365-70.
[37] Toimil-Molares ME, Balogh AG, Cornelius TW, Neumann R, Trautmann C. Fragmentation of nanowires driven by Rayleigh instability. Applied Physics Letters. 2004;85(22):5337-9.
[38] Karim S, Toimil-Molares ME, Balogh AG, Ensinger W, Cornelius TW, Khan EU, et al. Morphological evolution of Au nanowires controlled by Rayleigh instability. Nanotechnology. 2006;17(24):5954-9.
[39] Gurski KF, McFadden GB. The effect of anisotropic surface energy on the Rayleigh instability. Proceedings of the Royal Society a-Mathematical Physical and Engineering Sciences. 2003;459(2038):2575-98.
[40] Gurski KF, McFadden GB, Miksis MJ. The effect of contact lines on the Rayleigh instability with anisotropic surface energy. Siam Journal on Applied Mathematics. 2006;66(4):1163-87.

[41] Muller T, Heinig KH, Schmidt B. Template-directed self-assembly of buried nanowires and the pearling instability. Materials Science & Engineering C-Biomimetic and Supramolecular Systems. 2002;19(1-2):209-13.
[42] Khaligh HH, Goldthorpe IA. Failure of silver nanowire transparent electrodes under current flow. Nanoscale research letters. 2013;8(1):1-6.
[43] Sun Y, Ren Y, Liu Y, Wen J, Okasinski JS, Miller DJ. Ambient-stable tetragonal phase in silver nanostructures. Nature communications. 2012;3:971.
[44] Liu S, Wehmschulte RJ, Lian G, Burba CM. Room temperature synthesis of silver nanowires from tabular silver bromide crystals in the presence of gelatin. Journal of Solid State Chemistry. 2006;179(3):696-701.
[45] Liu CH, Yu X. Silver nanowire-based transparent, flexible, and conductive thin film. Nanoscale Research Letters. 2011;6.
[46] Balberg I. TUNNELING AND NONUNIVERSAL CONDUCTIVITY IN COMPOSITE-MATERIALS. Physical Review Letters. 1987;59(12):1305-8.
[47] Sichel EK, Gittleman JI, Sheng P. TRANSPORT PROPERTIES OF THE COMPOSITE-MATERIAL CARBON-POLY(VINYL CHLORIDE). Physical Review B. 1978;18(10):5712-6.
[48] Steinhogl W, Schindler G, Steinlesberger G, Engelhardt M. Size-dependent resistivity of metallic wires in the mesoscopic range. Physical Review B. 2002;66(7).
[49] Wu W, Brongersma SH, Van Hove M, Maex K. Influence of surface and grain-boundary scattering on the resistivity of copper in reduced dimensions. Applied Physics Letters. 2004;84(15):2838-40.
[50] Chen JY, Wiley BJ, Xia YN. One-dimensional nanostructures of metals: Large-scale synthesis and some potential applications. Langmuir. 2007;23(8):4120-9.
[51] Arjmand M, Mahmoodi M, Park S, Sundararaj U. Impact of foaming on the broadband dielectric properties of multi-walled carbon nanotube/polystyrene composites. Journal of Cellular Plastics. 2014;50(6):551-62.
[52] Arjmand M. Electrical Conductivity, Electromagnetic Interference Shielding and Dielectric Properties of Multi-walled Carbon Nanotube/Polymer Composites. University of Calgary, PhD, 2014.
[53] Shen Y, Lin Y, Li M, Nan CW. High dielectric performance of polymer composite films induced by a percolating interparticle barrier layer. Advanced Materials. 2007;19(10):1418-22.

[54] Raj PM, Balaraman D, Govind V, Wan L, Abothu R, Gerhardt R, et al. High frequency characteristics of nanocomposite thin film" supercapacitors" and their suitability for embedded decoupling. Electronics Packaging Technology Conference, 2004 EPTC 2004 Proceedings of 6th: IEEE; p. 154-61.

[55] Yuan J-K, Yao S-H, Dang Z-M, Sylvestre A, Genestoux M, Bai1 J. Giant dielectric permittivity nanocomposites: realizing true potential of pristine carbon nanotubes in polyvinylidene fluoride matrix through an enhanced interfacial interaction. The Journal of Physical Chemistry C. 2011;115(13):5515-21.

[56] Jiang M-J, Dang Z-M, Bozlar M, Miomandre F, Bai J. Broad-frequency dielectric behaviors in multiwalled carbon nanotube/rubber nanocomposites. Journal of Applied Physics. 2009;106(8):084902.

Chapter 4: Effect of Surface Oxidation on Electromagnetic Interference Shielding of Silver Nanowire

Aref Abbasi Moud, Uttandaraman Sundararaj*

Department of Chemical and Petroleum Engineering, University of Calgary, Calgary, Canada

Keywords: Silver nanowires (AgNWs); Nanocomposites; Electrical conductivity; Electromagnetic interference shielding; Imaginary permittivity; percolation; fragmentation; Corrosion; Nano capacitors

Abstract

Polymer science has been revolutionized recently by introduction of nano inclusions such as MWCNT and metal nanowires. In this study due to amazing properties of metal nanowires compared to other conventional inclusions silver nanowire was singled out for embedding in polymers. Nanowires were produced using electro chemical process. Unfortunately, because of changes in surface chemistry, conductivity of individual AgNWs were reduced and therefore electrical properties were significantly affected. Electrical conductivity experienced a decrease at low volume fractions, whereas at high volume fraction, conductivity stayed relatively constant. This result was expected since conductivity of the sample does not require contribution of all individual AgNWs past a certain point, which in our system is 2.5 vol %. Surprisingly it was also observed that the AgNW/PS nanocomposites were transparent to EM waves at low AgNW loadings, and incorporating AgNW up to about 1.0vol% into the AgNW/PS nanocomposites did not enhance the EMI SE (both the reflection and absorption). However, beyond 1.0vol%, the EMI SE of the AgNW/PS nanocomposites drastically increased. The same trend was observed for EMI SE of the samples after 3 months. For instance, at 2.0 and 2.5vol%, the overall EMI SEs of the AgNW/PS nanocomposites were 22.70 and 31.85dB, respectively, which were slightly higher than

those of their oxidized AgNW/PS counterparts. The clues to understand the strange behavior of the AgNW/PS nanocomposites were sought in the percolation curves. According to the percolation curves, the percolation threshold of the fresh AgNW/PS and the AgNW/PS after 3 months nanocomposites were both 1.20vol%, and beyond these concentrations the number of conductive networks increased. It is believed that EMI shielding does not require filler connectivity; however it increases with filler connectivity. This belief is reinforced due to the fact that EMI shielding efficacy is dependent on the total nomadic charge found in the system. Real and imaginary permittvity also experienced a relative decrease due to oxidization of individual AgNWs.

4.1. Introduction

As usage of computer parts and communication devices in world increases, interference among aforementioned equipment, such as cellphones, laptops and other computer sensitive related devices increases the probability of performance degradation over time. Degradation of sensitive electronic devices is not the only issue arising from EM waves (electromagnetic waves) as EM waves also affect of human health over time. The blockage of electromagnetic radiation is one state of the art technique to mitigate growing concerns associated with electromagnetic irradiation and interference in society. EM waves can be minimized using novel materials including but not limited to metal coated polymers, ICPs (intrinsically conductive polymers) and conductive filler/polymer composites (CPCs). CPCs stand out among the rest as they don't have drawbacks such as delamination of metal, poor adhesion and poor long term stability. CPCs filled with metals are effective materials having wide applicability in shielding industry. Although using metal nanowires, due to metal characteristics, such as accessibility, reproducibility, and easy way of production, are superior to other well-known inclusions such as carbon nanotubes (CNT) and graphene, they are however prone to corrosion, and their performance degrades over course of time even when they are buried deep within the polymer. This problem arises from super active unwanted gas molecules floating around in the ambient low quality air usually found in industrial environments. For example, copper is the main nanowire used for EMI shielding; but it gets readily oxidized even under atmospheric condition. This problem will be mitigated if the exposure time of freshly synthesized nanowires to air is minimized but effects of gradual diffusion of small active gas molecules through polymer cannot be totally stopped. The vulnerability of copper toward active gas molecules put forth the idea of using silver (Ag) nanowires as they have higher electrical

conductivity than copper ($6.3\times10^{+5}$ S·cm^{-1} versus $5.9\times10^{+5}$ S·cm^{-1}) along with greater immunity to oxidation. One should bear in mind that although silver is fairly unreactive as it does not react with oxygen in the air even at high temperature, its surface tarnishes over time due to formation of silver sulfide. Ag is also susceptible to ozone molecules present in the air and it forms silver oxides (AgO and Ag_2O). Ozone is an allotrope of oxygen that is much less stable than the diatomic oxygen, breaking down in the lower atmosphere to diatomic oxygen. Ozone is formed from diatomic oxygen by the action of ultraviolet light and atmospheric electrical discharges, and is present in low concentrations throughout the Earth's atmosphere. In total, ozone makes up only 0.6 ppm of the atmosphere.

Corrosion of Ag with reduced sulfur compounds in the air at atmospheric condition is well-known to be started by sulfur compounds as well as free sulfur. For instance, Elechiguerra et al. [1, 2] found that silver sulfide (Ag_2S) started to form on the surface of the nanowires after three weeks, and corrosion became even worse after six months, leading to the discontinuity of nanowires. Fortunately, none of the sulfur species are abundant in the atmosphere. For the case of ozone, Chen et al. studied the influence of atmospheric corrosion on bare silver. Their result showed that presence of ozone and UV radiation generates reactive atomic oxygen which reacts with Ag rapidly to form Ag_2O. Other silver corrosion by products such as AgCl and Ag_2CO_3 are not formed on the surface of nanowires as their precursors are not abundant in the atmosphere [3].

Although measures were taken in this study to minimize the amount of exposure time to air, the diffusion of gases into polymer affected silver nanowire surface chemically. Both ozone and silver reduced compounds are very small in size and therefore they can diffuse readily through polymers. The problem is exacerbated when one considers that silver oxide and silver sulfide are both semi-conductive and both will affect conductivity and related EMI shielding of nanocomposite made using AgNWs.

Unfortunately, shielding effectiveness (*SE*), i.e. the performance of shields to attenuate EM waves, can be adversely affected by semi-conductive nature of silver oxide and silver sulfide created on the surface of nanowires due to the loss of total charge resulting from the change in silver surface chemistry. Therefore, in future, steps must be taken to make CPCs made of AgNWs robust in terms of ageing (i. e. stable with time). For instance, results published in literature shows that there are

two new methods to address the problem associated with surface chemistry degradation: (1) developing new materials with low permeability to gas (2) encapsulation of the silver nanowires with higher corrosion oxidation-resistant materials. Considering these two methods can mitigate the effects of change in surface chemistry, measures should be taken to improve and keep *SE* level close to 30dB, corresponding to 99.9% attenuation of incident EM waves, which is sufficient for many practical engineering applications.

This paper is aimed at attaining high EMI shielding effectiveness for silver nanowire/polymer nanocomposite and finding a correlation between surface oxidation and EMI shielding efficacy. To the best of our knowledge, no one has studied effect of change in silver surface and subsequent changes in conductivity on EMI shielding effectiveness.

4.2. Experimental

4.2.1. Materials and composites preparation

4.2.1.1. Synthesis of AgNWs

While numerous techniques now exist for making metal nanostructures, the most general method is the so-called soft-template method. In this method, metal ions as result of electrochemical decomposition move into hexagonally packed hollow interiors. For making hexagonally packed pores, aluminum plates with (5cm × 11cm) 1mm thickness were used as primary templates. Aluminium plates were placed in parallel to counter stainless steel electrodes in a large tank filled with 0.3M H_2SO_4 at 2°C prior to implementation of voltage. Firstly, 25.0V were applied for 2hr to create initial hollow interiors and then for making them more uniform though chemical reactions, plates were placed in a 1:1 mixture of 0.2M H_2CrO_4 and 0.6M H_3PO_4 at 60°C for 30min. Secondly, another 8hr immersion in the 0.3M H_2SO_4 solution and continued application of 25.0V voltage lengthened the pores. Thinning the alumina barrier layer is a crucial part of the process since it keeps the end of the porous structure electrically conductive for the electrodeposition process. The voltage was dropped incrementally to reduce the alumina insulative barrier layer at the pore bottom. The protocol for voltage was to reduce 2V/min from 25V to 15V; then followed by 1V/min rate to 9V, and eventually keeping constant at 9V for 5 min, until finally

the voltage was dropped to zero. The result of the carefully designed process was a uniform hexagonally-packed pore structure [4].

Before attempting to electrodeposit Ag into hollow interiors using AC electrodeposition, the edges of the electrodes were insulated by applying nail polish. Square wave voltage pulses were applied between electrodes immersed in the solution of silver sulfate (Ag_2SO_4, 8.5g/L), diammonium hydrogen citrate ($(NH_4)_2HC_6H_5O_7$, 200 g/L), and potassium thiocyanate (KSCN, 105 g/L) to force Ag ions to move into the end of the pores. The voltage pulses were applied at 100Hz frequency and ±8.0V peaks (pulsed every 400ms) for 1.5hr.

Ag nanowires confined in porous alumina were liberated using 1.0M NaOH(aq) at room temperature. NaOH(aq) dissolves the almunia quickly and individual nanowires can be recovered. After liberation, floating detached fragments on the surface were gathered into a 1:1 mixture of 0.1M NaOH(aq) and MeOH, and sonicated for 10min. In order to minimize Ag nanowire exposure time to the surrounding air, immediately collected AgNWs were purified through filter paper (Whatman, with less than 1μm pore size), rinsed with MeOH, and then transferred to a beaker containing 100mL of MeOH. Details on the synthesis of the AgNWs can be found elsewhere [5].

4.2.1.2. AgNW and MWCNT nanocomposites preparation

The nanocomposites with different loadings of AgNWs were mixed through novel miscible solvent mixing and precipitation (MSMP) technique [4]. The essence of this technique is to mix different volumes of 3.3mg/ml AgNW/MeOH suspension with 20mg/ml PS (Styron® 615 APR, Americas Styrenics LLC)/methylene chloride solution. To reach the optimal distribution and dispersion of AgNWs in polymeric matrix each mixture was sonicated in an ultrasound bath for 30min, and then stirred for 10min prior to mixing. Subsequently, the filtered suspension was placed in an evaporation dish for 16h in a fume hood to nearly totally eliminate remaining solvent. The obtained nanocomposite nuggets were further dried in a vacuum oven at 50˚C for 8hr, and then were filled into a rectangular cavity with the dimensions of 22.9×10.2×0.8mm, and molded at 240°C and 38MPa for 15min in a carver compression molder (Wabash, WI). Aging of nanowire inside the nanocomposite happened at ambient pressure and temperature. Reported values was changing during summer in Calgary so average values here will be stated. The average values

during August to September period for temperature was 23°C, for humidity was 40% and finally atmospheric pressure was reported as 101 kPa.

4.2.2. Materials characterization

The TEM analyses of the nanofillers and nanocomposites were carried out on a Tecnai TF20 G2 FEG-TEM (FEI, Hillsboro, Oregon, USA) at 200kV acceleration voltage with a standard single-tilt holder. The images were taken with a Gatan UltraScan 4000 CCD (Gatan, Pleasanton, California, USA) at 2048×2048 pixels. For the TEM analysis of the nanofillers, the droplets of AgNW and MWCNT suspensions were placed on a holey carbon-coated Cu TEM grid, and dried at room conditions. For the TEM analysis of the nanocomposites, the molded nanocomposites were ultramicrotomed to achieve 70nm thick sections.

Both the molded nanocomposites and powdery liberated AgNWs were analyzed by X-ray diffraction (XRD). The XRD analysis was performed using a Rigaku ULTIMA III X-ray diffractometer with Cu K-alpha radiation as the X-ray source. The scan was carried out in the range 2θ=30–90 degrees using a 0.02 degree step and a counting time of 1 degree per minute at 40kV and 44mA to obtain the full diffractogram for the materials.

The electrical conductivity measurements were carried out on the molded rectangular samples. All the samples' surfaces were wiped with ethanol to remove impurities prior to the measurements. For nanocomposites with electrical conductivities more than 10^{-4} S·cm^{-1}, we carried out the measurements according to ASTM 257-75 using a Loresta GP resistivity meter (MCPT610 model, Mitsubishi Chemical Co., Japan). A standard four-pin probe was used to reduce the effect of contact resistance. For an electrical conductivity less than 10^{-4} S·cm^{-1}, a Keithley 6517A electrometer connected to Keithley 8009 test fixture (Keithley Instruments, USA) was used.

The EMI shielding measurements were carried out over the X-band (8.2–12.4GHz) frequency range using an E5071C network analyzer (ENA series 300KHz – 20GHz). The samples under the test were squeezed between two flanges connecting the waveguides of the network analyzer. The network analyzer sent a signal down the waveguide incident to the sample, and then the scattering parameters (S-parameters) of each sample were recorded, and used to calculate *SE*. The dielectric

properties of the generated nanocomposites were also obtained via conversion of the measurements using Reflection/Transmission Mu and Epsilon Nicolson-Ross Model.

4.3. Results and Discussion

4.3.1. Morphology

Morphology of AgNWs before and after processing (sonication and molding) were captured using TEM images. Evidently before sonication, bundles of AgNWs exist (see Figure 4-1(a)), demonstrating the ability of electrochemical process to produce long uniform, silver nanowires similar to copper nanowires previously made in our group. This observation has turned out to be crucial for validation of proposed process with reproducible result and a homogenous growth over entire domain for almost any type of metal. Initial measurements of the length and diameter of over 100 AgNWs demonstrates that pristine AgNWs had average diameter and length of 25 nm and 5.6±1.4 μm, respectively. Surprisingly (see Figure 4-1(b)), after minutes of sonication some of produced AgNWs remained aggregated in the PS matrix. The formation mechanism of the present irreversible aggregates of silver nanowires is complicated. Self-assembly of small metal particles even at room temperature to form larger regular structures or even patterns has attracted considerable attention in the past few years. Many mechanisms in the literature for adherence of metal particle have been proposed, including but not limited to, diffusion-limited aggregation (DLA) and reaction-limited aggregation (RLA). In both mechanisms, minor collisions result in the two particles adhering to each other. On the other hand two main driving forces responsible for adherence are large surface area and huge van der Waals forces between AgNWs which can adversely affect distribution and eventually the electrical properties. Gelves et al. [5] also showed after 30min sonication, scattered irreversible agglomerations still exist in polymer which was ascribed to permanent agglomeration of clean nanowires after liberation.

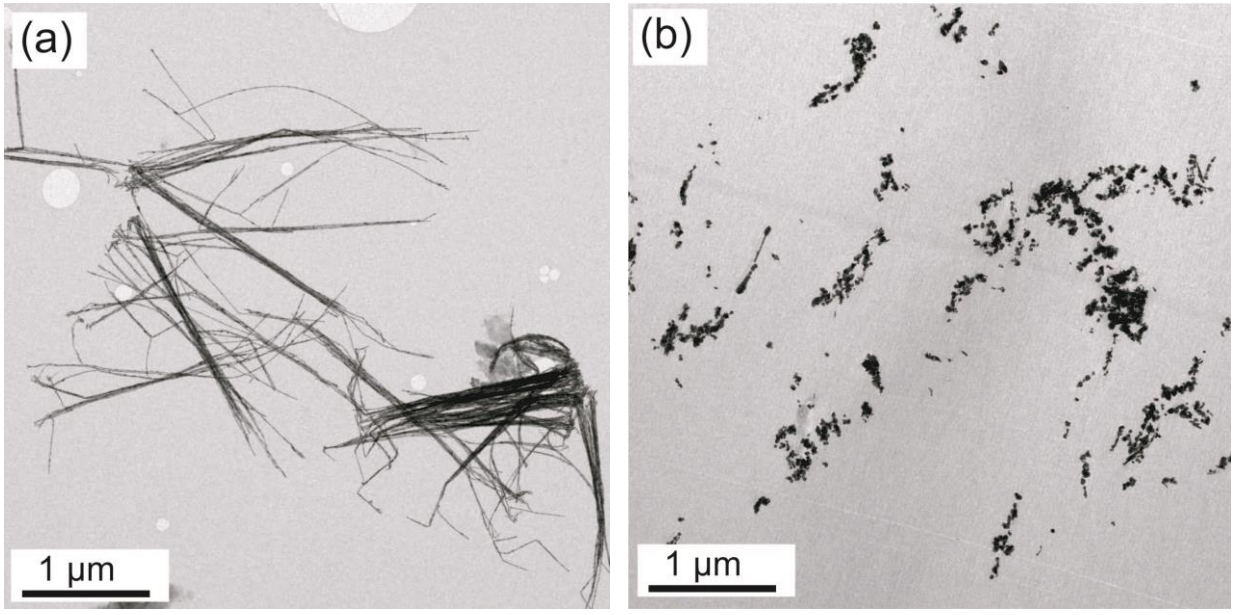

Figure 4-1: (a) TEM micrographs of (a) pristine AgNWs, (b) 1.5vol% AgNW/PS nanocomposite

TEM images of AgNWs embedded in polymer matrix shows discontinuities along the nanowire. Surprisingly, during processing, originally long nanowire has been cut down to very small pseudo spherical particles (Figure 4-1(b)). Transformation of AgNWs during the process at high temperature can be associated to fragmentation phenomenon, which has been reported in the literature [6]. This observation is quite important due to the significant impact of the filler's aspect ratio on the final electrical properties of CPCs. As shown in Figure 4-2, fragmentation impacted aspect ratio of the AgNWs. Discussion about fragmentation is in the previous chapter.

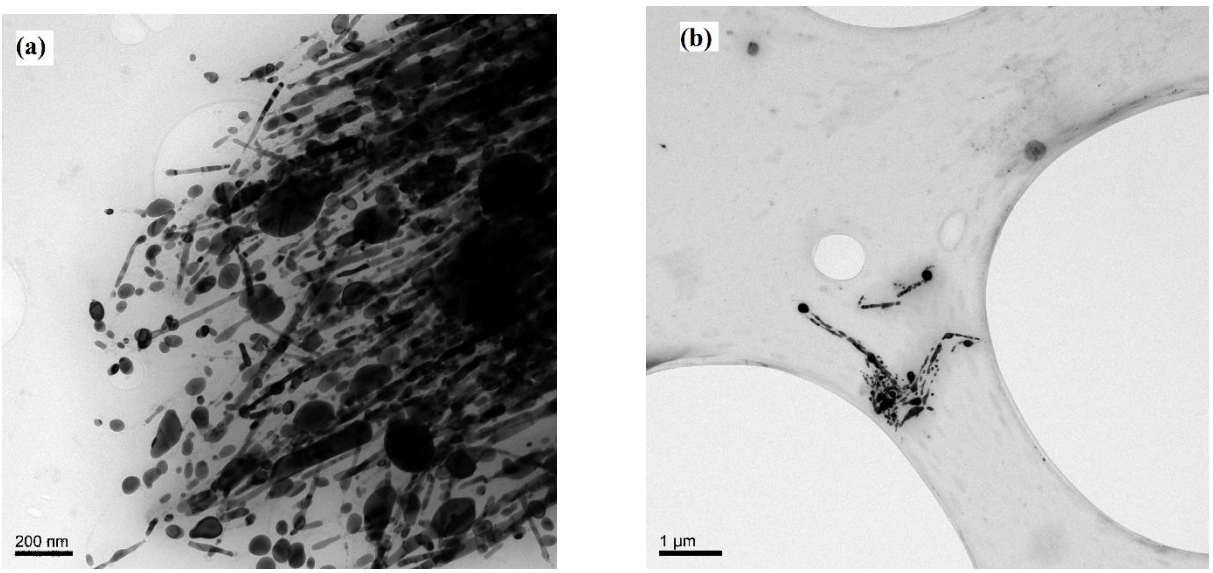

Figure 4-2: Fragmentation in AgNW/PS nanocomposites at two various magnifications. AgNWs were extracted from 2.5vol% AgNW/PS nanocomposites employing CH2Cl2 (a) high magnification (b) low magnification

4.3.2. Effect of ageing (time) on electrical conductivity of AgNW/PS

Technically, polymers are insulating and need to be filled with conductive fillers to create lightweight, electrically conductive materials. The electrical conductivity of polymer nanocomposites is determined by type and concentration of conductive nanoparticles, as well as the dispersion, distribution, alignment, and aspect ratio of the nanoparticles. All of above parameters determine the final relative distance between nano inclusions which is critical for the electrical properties of these advanced materials. The electrical conductivity of CPCs increases nonlinearly beyond a concentration called the percolation threshold. At percolation, the first conductive path forms and transforms CPCs from insulating into conductive. Conduction via physical contact between nanofillers in combination with tunneling and hopping are the main mechanisms for the transfer of electrons in CPCs [7, 8].

We tried to verify changes in surface chemistry via XRD method. The result for 2.5vol% sample before and after ageing is shown if Figure 4.3.

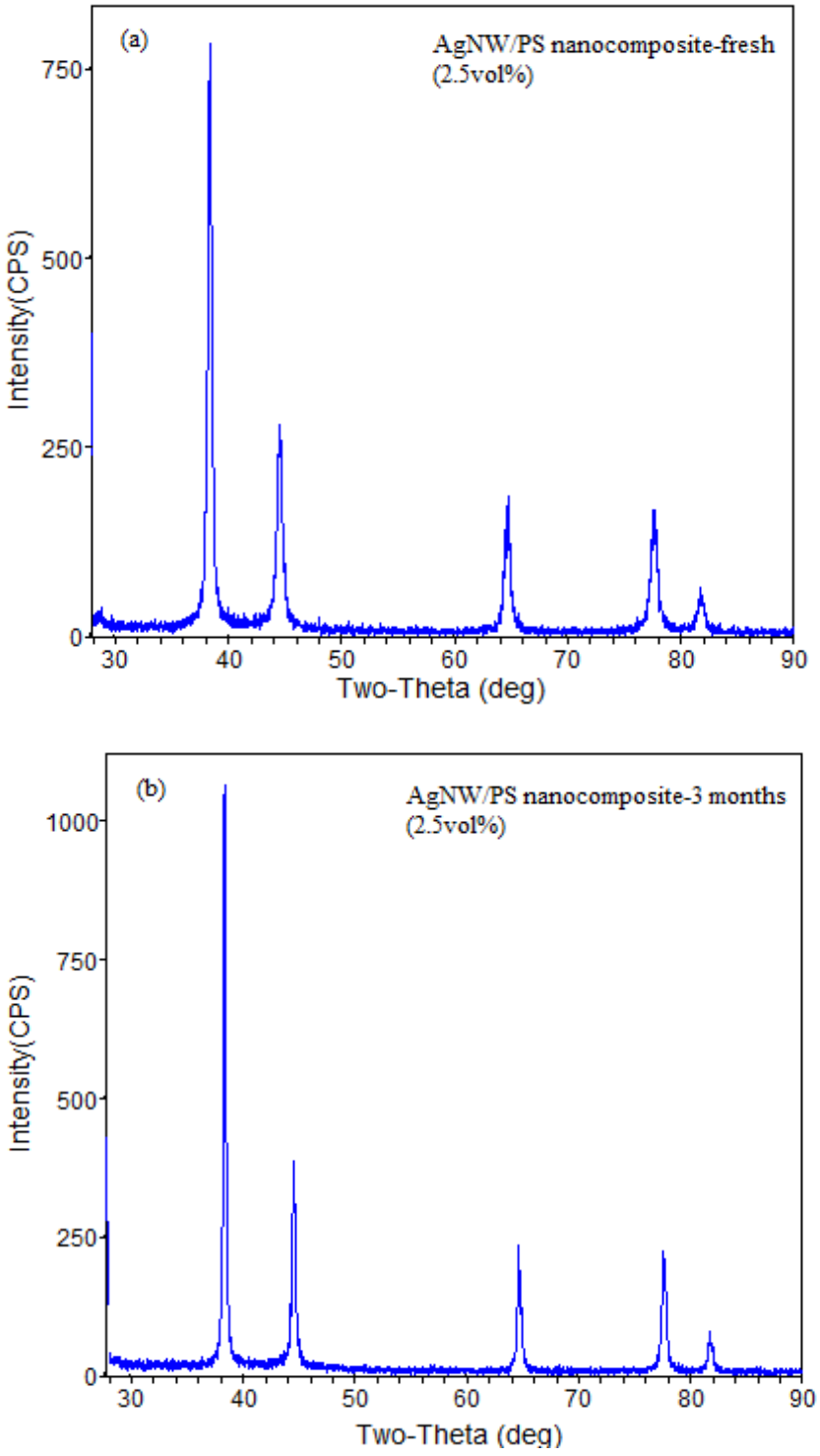

Figure 4-3: XRD pattern of AgNW/PS nanocomposites as a function of nanofiller loading, fresh (a) and oxidized (b).

As it can be clearly seen no traces of changes (i.e. peaks related to silver oxide or silver sulfide were absent) in XRD pattern of nanocomposites were visible. We have conjectured that at this level of surface oxidation, XRD is unable to detect silver oxide or silver sulfide tiny crystals. Considering the conductive nature of silver and semi-conductive nature of silver oxide, the absence of silver oxide will be further verified by high conductivity and shielding of AgNW/polymer nanocomposites.

Figure 4-4 depicts the percolation curves of the AgNW/PS nanocomposites immediately after production and after 3 months. The results showed that regardless of ageing of nanocomposites, adding 2.5vol% conductive nanofiller into the PS matrix led to about 16 orders of magnitude enhancement in the electrical conductivity.

Several factors could account for the relatively high percolation threshold in the AgNW/PS nanocomposites, namely (1) lower aspect ratio of AgNWs, (2) fragmentation phenomenon in AgNWs, and (3) inferior dispersion and distribution of AgNWs. It has been proven both theoretically and experimentally that fillers with higher aspect ratio (higher length and lower diameter) present lower percolation threshold [9]. AgNWs aspect ratio was significantly changed by the fragmentation phenomenon, where AgNWs transformed from cylindrical shapes to linear rows of nanospheres. Furthermore, inferior dispersion and distribution of AgNWs within the PS matrix, as corroborated by the TEM images, could be another reason for the high percolation threshold of the AgNW/PS nanocomposites.

Figure 4-4 indicates that at high filler loadings the electrical resistivity of the AgNW/PS nanocomposites is lower than their oxidized nanocomposites counter-parts. For instance, at 1.5vol%, the electrical resistivity of the AgNW/PS was almost eight orders of magnitude lower than oxidized AgNW/PS nanocomposites. Although electrical resistivity experienced a decrease at low volume fractions but at high volume fraction stayed relatively the same. This result was expected since conductivity of the sample does not require contribution of all individual AgNWs past a certain point which in our system is 2.5 vol %.

At filler loadings far above the percolation threshold, due to the formation of a well-established conductive network, the conductivity of CPCs relies significantly on the innate conductivity of nanofillers [5]. This justifies the higher electrical conductivity seen for the AgNW/PS nanocomposites at high filler loadings.

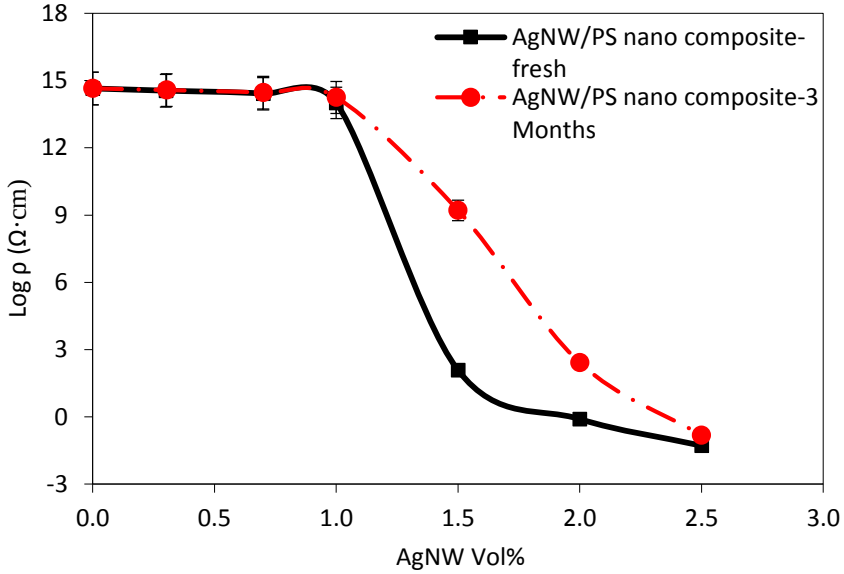

Figure 4-4: Electrical resistivity of AgNW/PS nanocomposites as a function of nanofiller loading, fresh and oxidized.

Figure 4-4 also depicts a huge difference between the maximum obtained electrical conductivity of the AgNW/PS nanocomposite and Ag bulk (19.2 versus $6.25\times10^{+5}S\cdot cm^{-1}$). This dissimilarity can be attributed to junction resistance and possibly the low diameter of AgNWs. Electrical measurements on individual metallic nanowires have shown that as their diameter decreases, their electrical properties deviate from bulk properties [10, 11]. This phenomenon is attributed to the presence of grain boundaries (defects) in the crystalline structure of nanowires, where electrons are scattered (either elastically or inelastically) when they try to go through a grain boundary. Nonetheless, the results of a study by Chen et al. [12] demonstrated that Ag nanowires retain the high conductivity of bulk silver for thicknesses down to ~ 15nm. Sun et al. [13] also measured the conductivity of their in-house synthesized silver nanowire (40nm diameter) by aligning them across two gold probe electrodes, and reported conductivity values close to bulk silver conductivity. Given that 25nm is the average diameter of our synthesized AgNWs, we are uncertain whether or not our synthesized AgNWs suffered from the grain boundary scattering effect. This issue is beyond the scope of the current study.

4.3.3. Effect of changes in surface chemistry of AgNW/PS on EMI shielding

Attenuation is one of the principal indicators for measuring the effectiveness of electromagnetic interference shielding. An EM wave encompasses two components: electric field and magnetic field. These two fields are perpendicular to each other while the EM wave is propagating. The ratio of electric field to magnetic field of a propagating wave is an inherent property of a medium, and named as intrinsic impedance. This ratio is a very significant parameter that defines the level of shielding and prevailing shielding mechanisms in conductive shields. The intrinsic impedance of a medium is defined as follows [2]:

$$\eta = \sqrt{\frac{j\omega\mu}{\sigma + j\omega\epsilon}} \tag{4-1}$$

where η is intrinsic impedance, ω is angular frequency, μ is magnetic permeability, σ is electrical conductivity and ε is real permittivity. The permittivity and permeability of free space are equal to $8.85\times10^{-12}\text{F}\cdot\text{m}^{-1}$ and $4\pi\times10^{-7}\text{H}\cdot\text{m}^{-1}$, respectively. Given the low conductivity of free space, its intrinsic impedance is equal to 377Ω; conductive shields present significantly lower intrinsic impedance [14, 15]. Shield impedance is minimized by using materials with high conductivity and low permeability; as an example steel has much less shielding ability than copper.

Essentially, there are three mechanisms involved in the EMI shielding of CPCs, i.e. reflection, absorption and multiple-reflection. Reflection occurs due to impedance mismatch between two media. That is to say, a highly reflective shield must possess a low magnetic permeability, high electrical conductivity and/or high real permittivity. The portion of the EM wave that is not reflected infiltrates into conductive shields. As the impedance of a conductive shield is much lower than free space, a large portion of the infiltrated electric field is converted to the magnetic field. Thus, it is very important to attenuate both the electric and magnetic fields inside a shield. The attenuation of the EM wave inside a conductive shield is performed through absorption mechanism, which is composed of Ohmic loss and polarization loss (electric polarization and magnetic polarization loss). The Ohmic loss is due to the interaction of propagating EM wave with nomadic charges, is in phase with the EM wave, and is quantified by imaginary permittivity. The polarization loss arises from the energy required to reorient electric/magnetic dipoles in each half cycle of the alternating field [16]. The levels of the electric and magnetic polarizations are expressed by real permittivity and magnetic permeability, respectively.

Multiple-reflection is the third shielding mechanism in CPCs, which occurs due to the existence of huge interfacial area. Theoretically, the first reflection from the second interface of a shield is counted as a part of the reflection mechanism. According to this definition, multiple-reflection adversely impacts the overall EMI shielding due to its augmentation effect on the transmitted waves. It is believed that the multiple-reflection can be ignored if a CPC's thickness is larger than its skin depth or if shielding by absorption is more than 10dB [2]. The skin depth of a conductive shield is defined as the depth inside the shield at which the power of the EM wave drops to 1/e of its incident value. Skin depth is proportional to the root mean square of electrical conductivity and magnetic permeability [14].

Figure 4-5 compares the average EMI shielding (overall, reflection and absorption) of the generated nanocomposites as a function of nanofiller loading over the X-band frequency range. It should be noted that the effect of multiple-reflection is included within the reported values of shielding by reflection and absorption. It was seen that the AgNWs/PS nanocomposites showed a steady ascending trend of EMI SE with increasing conductive filler loading. Surprisingly it was also observed that the AgNW/PS nanocomposites were transparent to EM waves at low AgNW loadings, and incorporating AgNW up to about 1.0vol% into the AgNW/PS nanocomposites did not enhance the EMI SE (both the reflection and absorption). However, beyond 1.0vol%, the EMI SE of the AgNW/PS nanocomposites drastically increased. Same trend observed for EMI SE of the samples after 3 months. For instance, at 2.0 and 2.5vol%, the overall EMI SEs of the AgNW/PS nanocomposites were 22.70 and 31.85dB, respectively, which were slightly higher than those of their oxidized AgNW/PS counterparts. It was noted that EMI SE curve was shifted by approximately 0.5 wt% for the 3 month old sample.

As it pointed out in previous chapter, EMI SE is related to the distribution of the filler inside the polymeric matrix. In fact the distribution of the nano filler determines the void space between filler bundles. The closer the packed array throughout polymeric matrix, like a conducting mesh of nanofiller [17], the better EMI SE efficacy. In our system, fairly good distribution of filler was achieved after sonication and this should have led to better EMI shielding values.

The clues to deciphering the strange behavior of the AgNW/PS nanocomposites are in the percolation curves (Figure 4-4). According to the percolation curves, the percolation threshold of the fresh AgNW/PS and AgNW/PS after 3 months were both 1.20vol%, and beyond these

concentrations, the number of conductive networks increase. In the literature, it is believed that EMI shielding does not require filler connectivity; however it increases with filler connectivity [18]. This could justify the slight difference between the EMI shielding value of the AgNW/PS nanocomposites fresh and after 3 months period. Conductivity of the samples has changed due to slight changes in surface chemistry as result of migration of gases from ambient space. It is worth mentioning that conductivity of the sample has the same value for both nanocomposites fresh and after 3 months for 2.5 vol % of nanofiller. This result was expected since conductivity of the sample does not require contribution of all individual AgNWs past a certain point, which in our system is 2.5 vol %. As a result, changes in EMI SE, which has an indirect relationship with total nomadic charge in the system, can somehow be overshadowed by mere comparison of conductivity. Figure 4-4 denotes that shielding by both reflection and absorption are highly sensitive to the formation of the conductive network.

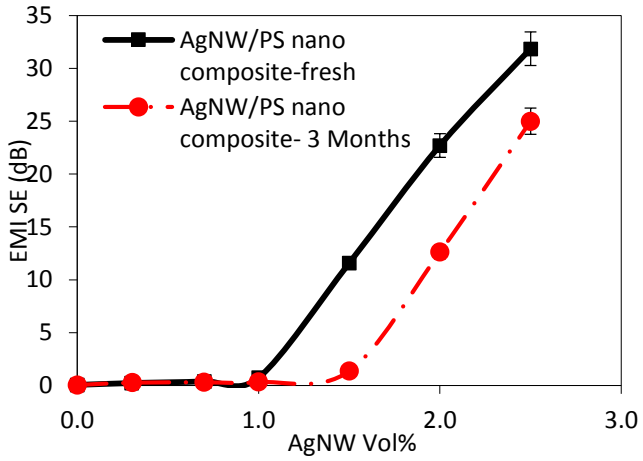

(a)

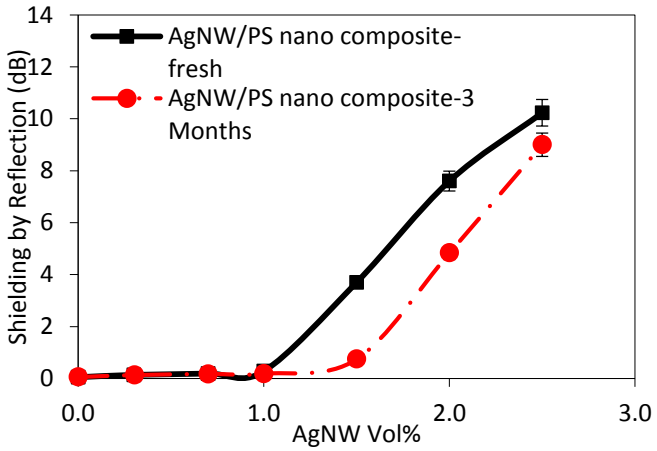

(b)

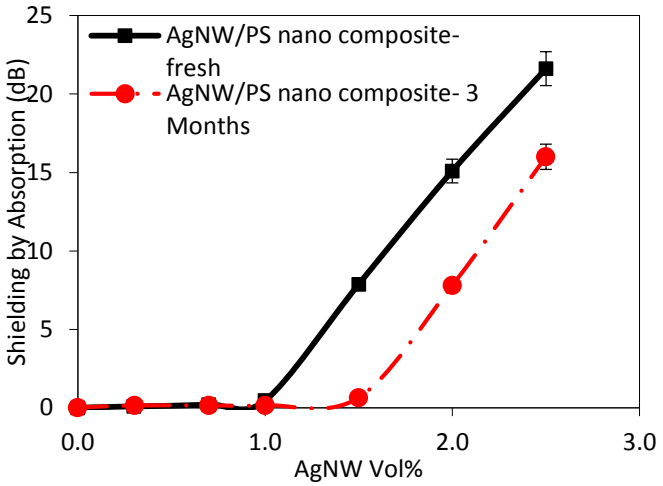

(c)

Figure 4-5: EMI SE ((a) overall, reflection (b) and absorption (c)) of fresh and aged AgNW/PS as a function of nanofiller loading.

In order to validate this, we investigated the imaginary permittivity and real permittivity of the generated nanocomposites (Figure 4-6). It is worth mentioning that all the nanocomposites presented a non-magnetic behavior. Imaginary permittivity signifies the amount of energy dissipated by nomadic charges inside a conductive shield, and is highly sensitive to conductive network formation. It is evident that the imaginary permittivity follows the same trend as EMI SE for the both types of nanocomposites. The imaginary permittivity of the AgNW/PS nanocomposites was close to zero below the percolation threshold, and then it increased pronouncedly above the percolation threshold. Drastic increase in the imaginary permittivity above the percolation threshold stems from the formation of extensive and numerous conductive networks, wherein electrons can find more mean-free-paths to go through in each half cycle of alternating field, and can dissipate more electrical energy.

Figure 4-6 also shows that the imaginary permittivity of the fresh AgNW/PS nanocomposites at high loadings is much greater than AgNW/PS nanocomposites after 3 months. Several factors play a role in determining the imaginary permittivity including the innate conductivity of nanofiller, nanofillers' available surface area and the level of conductive network formation. At low filler loadings, fresh AgNW/PS nanocomposites presented similar imaginary permittivity due to equality of enhancement of conductive network formation (See Figure 4-4) and available surface

area in both fresh and after 3 month nanocomposites. Nevertheless, at high filler contents, the innate conductivity of AgNW overcomes its oxidized counterparts, giving superior electrical properties. Moreover, the comparison of the electrical properties of fresh and oxidized AgNW/PS nanocomposites verifies the dominant role of the total nomadic charge in the system on EMI shielding and imaginary permittivity.

Figure 4-6(b) compares the real permittivities of the generated nanocomposites, which present the same trend as the imaginary permittivity. It is can be seen that the real permittivity of the both nanocomposites shows an ascending trend with filler loading beyond percolation threshold. In general, several polarization mechanisms can occur in CPCs depending on the structure and frequency range, i.e. interfacial, dipolar, atomic and electronic polarization [19]. However, in the current study, due to the nonpolar nature of the PS matrix and high frequency range of the X-band, the electronic polarization of the PS matrix and polarization within the nanofillers are deemed to be the only probable mechanisms in play.

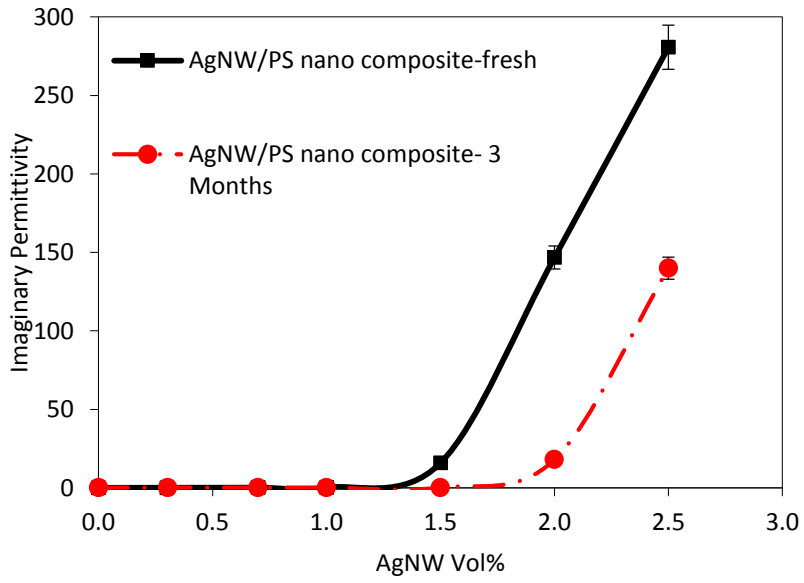

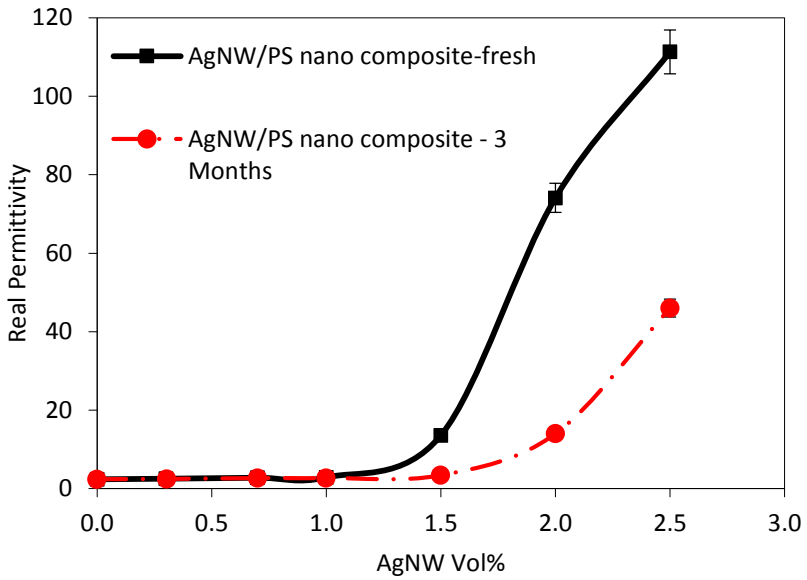

Figure 4-6: (a) Imaginary permittivity, and (b) real permittivity as a function of nanofiller loading.

Electronic polarization in CPCs originates from the concept of nanocapacitors; nanofillers act as nanoelectrodes and the polymer material between them plays the role of nanodielectric [20, 21]. As conductive filler content approaches the percolation threshold, the thickness of nanodielectric decreases, thus the applied electric field within nanodielectric increases, which leads to enhanced electronic polarization. Hence, the enhancement in the real permittivity of the AgNW/PS nanocomposites above the percolation threshold arises from the formation of a large number of nanocapacitor structures. Although the oxidized AgNW/PS nanocomposites forms nanocapacitors at the same loadings, the total nomadic charges are decreased. As formation of nanocapacitors and the ability of these capacitors is directly related to the amount of charge carriers in the system, real permittvity also experienced a relative decrease due to oxidization of AgNWs. The capacitance of a capacitor is defined as following:

$$C = \frac{\varepsilon A}{d} \qquad (4\text{-}2)$$

Where ε is real permittivity, A is surface area and d is thickness of capacitors. Moreover, the capacitance has a direct relationship with the amount of charges stored on the surface of a capacitor. AgNWs, due to their high aspect ratio and conductive network formation ability, possessed large A and low d. However, higher innate electrical conductivity of fresh AgNWs over

oxidized AgNWs led to higher potential charges stored on the surface of nanocapacitors in the fresh AgNW/PS nanocomposites.

The presence of defects in the crystalline structure of both AgNW/PS nanocomposites could result in dipolar polarization and further increase the real permittivity [22, 23].

4.4. Conclusion

Silver nanowires (AgNWs) were synthesized successfully by AC electrodeposition of Ag into porous aluminum oxide templates. AgNWs were embedded into polystyrene via the miscible solvent mixing and precipitation (MSMP) technique. In this study, due to amazing properties of silver nanowires compared to conventional fillers, silver nanowires were singled out for embedding in polymers. Unfortunately because of changes in surface chemistry, conductivity of individual AgNWs were reduced with time and therefore electrical properties were hugely affected. For AgNW/PS nanocomposite electrical conductivity experienced a decrease at low volume fractions, whereas at high volume fraction it stayed relatively the same. This result was expected since conductivity of the sample does not require contribution of all individual AgNWs past a certain point, which in our system was 2.5 vol %. Surprisingly it was also observed that the AgNW/PS nanocomposites were transparent to EM waves at low AgNW loadings, and incorporating AgNW up to about 1.0vol% into the AgNW/PS nanocomposites did not enhance the EMI SE (no enhancement for reflection and absorption). However, beyond 1.0vol%, the EMI SE of the AgNW/PS nanocomposites drastically increased. The same trend was observed for EMI SE of the samples aged for 3 months. For instance, at 2.0 and 2.5vol%, the overall EMI SEs of the AgNW/PS nanocomposites were 22.70 and 31.85dB, respectively, which were slightly higher than those of their aged and oxidized AgNW/PS counterparts. The clues to understand the strange behavior of the AgNW/PS nanocomposites were investigated in the percolation curves. According to the percolation curves, the percolation threshold of the newly made AgNW/PS and AgNW/PS after 3 months nanocomposites were both 1.20vol%, and beyond this concentration, the number of conductive networks increased. Although the oxidized AgNW/PS nanocomposites experienced nanocapacitor formation at the same loadings, at larger filler contents, total nomadic charges decreased. It is believed that EMI shielding does not require filler connectivity; however it

increases with filler connectivity. This belief was found based on the fact that EMI shielding efficacy is dependent on the total nomadic charge found in the system. As formation of nanocapacitors and the ability of these capacitors is directly related to the amount of charge carriers in the system, real permittvity also experienced a relative decrease due to oxidization of individual AgNWs.

4.5 Acknowledgements

Financial support from the Natural Sciences and Engineering Research Council of Canada (NSERC) is highly appreciated.

4.6 References

[1] Elechiguerra JL, Larios-Lopez L, Liu C, Garcia-Gutierrez D, Camacho-Bragado A, Yacaman MJ. Corrosion at the nanoscale: the case of silver nanowires and nanoparticles. Chemistry of Materials. 2005;17(24):6042-52.

[2] Arjmand M, Mahmoodi M, Gelves GA, Park S, Sundararaj U. Electrical and electromagnetic interference shielding properties of flow-induced oriented carbon nanotubes in polycarbonate. Carbon. 2011;49(11):3430-40.

[3] Graedel T. Corrosion mechanisms for silver exposed to the atmosphere. Journal of the Electrochemical Society. 1992;139(7):1963-70.

[4] Gelves GA, Al-Saleh MH, Sundararaj U. Highly electrically conductive and high performance EMI shielding nanowire/polymer nanocomposites by miscible mixing and precipitation. Journal of Materials Chemistry. 2011;21(3):829-36.

[5] Gelves GA, Lin B, Sundararaj U, Haber JA. Low electrical percolation threshold of silver and copper nanowires in polystyrene composites. Advanced Functional Materials. 2006;16(18):2423-30.

[6] Li Z, Okasinski JS, Almer JD, Ren Y, Zuo X, Sun Y. Quantitative determination of fragmentation kinetics and thermodynamics of colloidal silver nanowires by in situ high-energy synchrotron X-ray diffraction. Nanoscale. 2014;6(1):365-70.

[7] Balberg I. TUNNELING AND NONUNIVERSAL CONDUCTIVITY IN COMPOSITE-MATERIALS. Physical Review Letters. 1987;59(12):1305-8.

[8] Sichel EK, Gittleman JI, Sheng P. TRANSPORT PROPERTIES OF THE COMPOSITE-MATERIAL CARBON-POLY(VINYL CHLORIDE). Physical Review B. 1978;18(10):5712-6.

[9] Huang Y, Li N, Ma YF, Feng D, Li FF, He XB, et al. The influence of single-walled carbon nanotube structure on the electromagnetic interference shielding efficiency of its epoxy composites. Carbon. 2007;45(8):1614-21.

[10] Steinhogl W, Schindler G, Steinlesberger G, Engelhardt M. Size-dependent resistivity of metallic wires in the mesoscopic range. Physical Review B. 2002;66(7).

[11] Wu W, Brongersma SH, Van Hove M, Maex K. Influence of surface and grain-boundary scattering on the resistivity of copper in reduced dimensions. Applied Physics Letters. 2004;84(15):2838-40.

[12] Chen JY, Wiley BJ, Xia YN. One-dimensional nanostructures of metals: Large-scale synthesis and some potential applications. Langmuir. 2007;23(8):4120-9.

[13] Sun Y, Yin Y, Mayers BT, Herricks T, Xia Y. Uniform silver nanowires synthesis by reducing AgNO3 with ethylene glycol in the presence of seeds and poly (vinyl pyrrolidone). Chemistry of Materials. 2002;14(11):4736-45.

[14] Kaiser KL. Electromagnetic shielding: CRC Press; 2005.

[15] Chatterton PA, Houlden MA. EMC-Electromagnetic theory to practical design. NASA STI/Recon Technical Report A. 1992;93:17521.

[16] Arjmand M, Mahmoodi M, Park S, Sundararaj U. Impact of foaming on the broadband dielectric properties of multi-walled carbon nanotube/polystyrene composites. Journal of Cellular Plastics. 2014;50(6):551-62.

[17] Mohanraj G, Chaki T, Chakraborty A, Khastgir D. AC impedance analysis and EMI shielding effectiveness of conductive SBR composites. Polymer Engineering & Science. 2006;46(10):1342-9.

[18] Arjmand M, Apperley T, Okoniewski M, Sundararaj U. Comparative study of electromagnetic interference shielding properties of injection molded versus compression molded multi-walled carbon nanotube/polystyrene composites. Carbon. 2012;50(14):5126-34.
[19] Arjmand M. Electrical Conductivity, Electromagnetic Interference Shielding and Dielectric Properties of Multi-walled Carbon Nanotube/Polymer Composites. University of Calgary, PhD, 2014.
[20] Shen Y, Lin Y, Li M, Nan CW. High dielectric performance of polymer composite films induced by a percolating interparticle barrier layer. Advanced Materials. 2007;19(10):1418-22.
[21] Raj PM, Balaraman D, Govind V, Wan L, Abothu R, Gerhardt R, et al. High frequency characteristics of nanocomposite thin film" supercapacitors" and their suitability for embedded decoupling. Electronics Packaging Technology Conference, 2004 EPTC 2004 Proceedings of 6th: IEEE; p. 154-61.
[22] Yuan J-K, Yao S-H, Dang Z-M, Sylvestre A, Genestoux M, Bai1 J. Giant dielectric permittivity nanocomposites: realizing true potential of pristine carbon nanotubes in polyvinylidene fluoride matrix through an enhanced interfacial interaction. The Journal of Physical Chemistry C. 2011;115(13):5515-21.
[23] Jiang M-J, Dang Z-M, Bozlar M, Miomandre F, Bai J. Broad-frequency dielectric behaviors in multiwalled carbon nanotube/rubber nanocomposites. Journal of Applied Physics. 2009;106(8):084902.

Chapter 5: Broadband electrical properties of AgNWs/Ps nanocomposite

Presentation of the study: This article can be divided into two general sections as followings

- ✓ Interpretation of broadband behavior of AgNW/PS composites as functions of filler loading
- ✓ Correlation of properties with microstructure

This work also has been done with the help of Dr. Mohammad Arjmand who has assisted me in interpretation of results.

In this study for dielectric measurements, the broadband dielectric spectroscopy of CPCs was performed with impedance / gain-phase analyzer (Solartron SI 1260) in the frequency range of $10^{-1} - 10^{+6}$ Hz. Holding samples were carried out using 12962A sample holder with electrode diameter of 10 mm. Before measurement commencement, electrode surface were painted with silver paste to minimize resistance between samples and sample holder electrodes. The impedance analyzer applied a voltage over a wide frequency range, and then measured in-phase and out-of phase currents. The obtained data were used to finally calculate impedance and dielectric properties.

The impedance of nanocomposite were obtained via following equations:

$$Z = \frac{V}{I} \tag{5-1}$$

$$I = I_R + I_C \tag{5-2}$$

$$Z = Z' + iZ'' \tag{5-3}$$

$$I_R = \omega C_0 \varepsilon' V \tag{5-4}$$

$$I_C = \omega C_0 \varepsilon' V \quad (5\text{-}5)$$

Where Z is impedance, $V = V_0 . e^{iwt}$ is the AC voltage, C_0 capacitance of free space, ω frequency and I_R and I_C are resistive and capacitive currents, respectively. Substituting I_R and I_C from their respective relationships and then reorganizing them will lead to following final equations:

$$\varepsilon' = \frac{1}{\omega C_0}\left[\frac{-z''}{(z'^2 + z''^2)}\right] \quad (5\text{-}6)$$

$$\varepsilon'' = \frac{1}{\omega C_0}\left[\frac{-z'}{(z'^2 + z''^2)}\right] \quad (5\text{-}7)$$

$$C_0 = \varepsilon_0 \frac{S}{d} \quad (5\text{-}8)$$

Where, ε' is real permittivity, ε'' is imaginary permittivity ε_0 the real permittivity of free space and S and d: the area and thickness of the sample, respectively.

Abstract

This study investigates the dielectric properties of silver nanowire (AgNWs)/polystyrene (PS) composites over a broadband frequency range, i.e., 10^1 to 10^6 Hz. The results showed that the real permittivity and imaginary permittivity increased tremendously with increased AgNWs concentration. For instance, at 100 Hz, the real permittivity and imaginary permittivity of the pristine PS was 2.5 and 0.04, respectively, which increased to 1.2×10^4 and 1.4×10^7 at 2 vol%, respectively. AC conductivity results demonstrated that AC conductivity is highly frequency-dependent in volume fractions far below the percolation threshold. Both real and imaginary permittivity increase astronomically in the vicinity of the percolation threshold. The increase in

real permittivity was conjectured to be related to the formation of a huge number of nanocapacitors (AgNWs as nanoelectrodes and PS as nanodielectrics). For instance, in defective CNTs with defects, real permittivity increases dramatically. Watts et al. [1, 2] performed a systematic study on the effect of defects on electrical properties and reported dramatic increase in real permittivity with an increase in the number of defects. An increase in imaginary permittivity was also shown to be rooted in : (1) an increased number of total present nomadic charges in the system (2) a more advanced network of AgNWs (3) an increase in polarization loss. The descending trend of real permittivity and imaginary permittivity after the percolation threshold was attributed to failure in full reorientation of induced electrons, and an inability of the nomadic charges to fully make use of the conductive path, respectively.

5.1 Introduction

Polymers filled with novel inclusions with high dielectric permittivity have shown great potential to store electrical energy. Therefore there is the potential for them to be used in a wide range of high tech applications, such as radio wave communicating devices, robots moving organs, etc [3-5]. Traditionally, manufacturers incorporated ceramic powders into the polymer matrix to increase their permittivity to large values [6]. However, their great permittivity came with loss of flexibility and poor mechanical strength due to the large amount of ceramic powder needed to fill the polymer matrix. An abrupt shift in using ceramic powder occurred when conductive nano-sized inclusions were discovered. Technically, adding nanosized inclusions impacts the dielectric properties more than conventional microsized inclusions, as they create a higher interfacial contact area between them and the polymer matrix.

Strategically, researchers produced nanocomposites with high permittivity using conductive or semi-conductive nano-inclusion with a high aspect ratio. In these nanocomposites, nearing the percolation threshold would produce an abrupt increase in dielectric permittivity [7, 8], while problems associated with ceramic powders would not arise, as volume fraction in these new nanocomposites would be relatively low. Getting closer to the percolation threshold in these systems forces the nanoparticles to be separated only by a thin layer of polymer matrix, forming nanocapacitors (conductive nanoparticle as the nanoelectrode and polymer matrix as the

nanodielectric) [8, 9]. One should bear in mind that the high dielectric permittivity in CPCs is not due to the innate nature of the filler, but is due to the huge increase in interfacial polarization. However, nanoinclusions above the percolation threshold get connected physically and therefore lead to high dissipation factor.

So far, many studies' main focus have been on developing CPCs with low dissipation factors. The main focus has been on developing CPCs with low dissipation factors. For instance, some strategies have been developed to stop the direct contact between the conductive particles, such as wrapping an insulating thin layer around the nano inclusion [10, 11], intentionally oxidizing surfaces of metals [12, 13], and increasing the alignment of nanofiller [14, 15]. For instance Liu et al have used copper oxide as a separating thin layer between copper and carbon to produce a coaxial single nanocapacitor [16]. In this study, we present a novel silver nanowire/polystyrene (AgNW/PS) nanocomposite with high dielectric permittivity and relatively low dissipation factor.

5.2 AC conductivity

The real part of the AC conductivity is directly related to the dielectric loss and occurs due to the flow of electrons within the dielectric material [13]. The imaginary part of AC conductivity accounts for charge polarized and are lined against each other in the dielectric materials, which is called dielectric dispersion. Dielectric dispersion in physics is defined as the dependence of the permittivity of a dielectric material on the frequency of an applied electric field. Because there is always a delay between application of field, charge migration and the final charge accumulation in certain zones, the resulting permittivity of the dielectric is a complex function of electric field frequency.

Dielectric dispersion, on molecular structure of the filler, filler chemical integrity, surface-imposed charges, stemming from interfacial, dipolar and electronic polarization in CPCs, can be dependent polymer polar nature and final morphology of filler inside the matrix [17]. For instance, knitting a mesh with precise mesh size of nanoinclusion can effectively impact EMI shielding and dielectric properties of CPCs. Generally, when the frequency becomes really high: (1) dipolar polarization cannot cope with the pace of frequency change in the microwave region, which is around 10^{10} Hz; (2) ionic polarization and molecular distortion polarization can no longer track the electric field past the infrared or far-infrared region, which is around 10^{13} Hz, ; and (3) electronic polarization

cannot cope with the pace of frequency change in the ultraviolet region, around 10^{15} Hz [18]. In frequencies above ultraviolet, permittivity values approach the permittivity value of free space. Given the frequency range focused on in this study, i.e., 10^{1} to 10^{6} Hz, interfacial polarization played the main role in developing the dielectric properties of the AgNW/PS nanocomposites. Interfacial polarization, the local accumulation of charges inside the dielectric material, can easily take place in CPCs. Additionally, since they are made of materials with different conductivities or dielectric permittivities, it normally occurs due to a buildup of charges at the surface of phases with dissimilar conductivity of permittivities. As interfacial polarization requires charges to migrate from deep layers to the conflict zone, it usually takes a while. As it has to be done in longer periods of time compared to other simpler types of polarizations, it can usually be observed at much lower frequencies[8]. In other words, when the frequency gets really high, such as X-band regime, relating this type of polarization toward changes in dielectric properties is nonsensical. Fig. 5-1 presents the AC conductivity of the AgNW/PS nanocomposites.

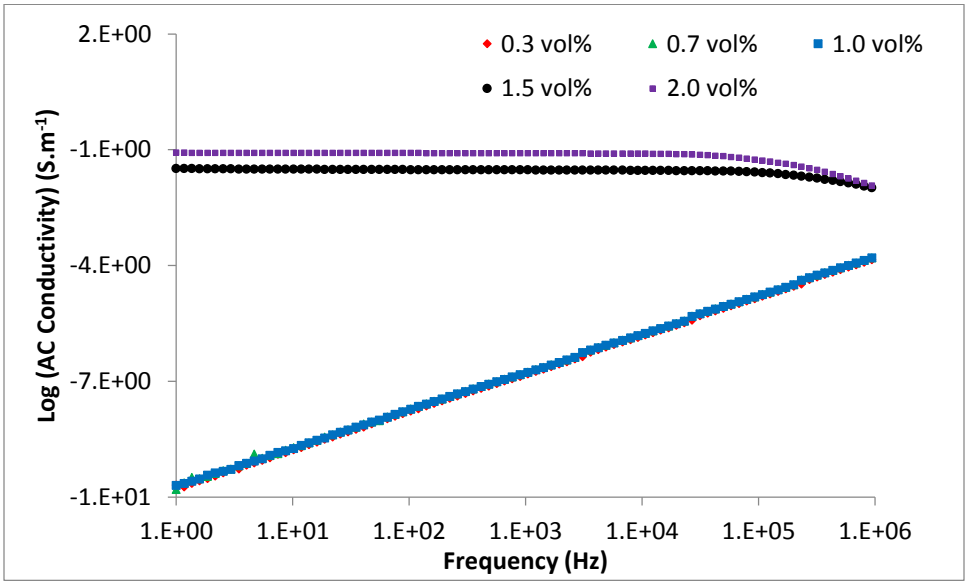

Figure 5-1: AC conductivity of the AgNW/ PS nanocomposites as a function of frequency

As is obvious in Figure 5-1, the percolation threshold in our system has occurred somewhere between 1.0 vol% and 1.5 vol %. This result can be related to lower aspect ratio of AgNWs as result of fragmentation, which reduces the probability of AgNWs contacting each other, i.e., lower percolation threshold. AC conductivity, as can be seen, exhibits a relatively continuous increase

with addition of filler, which shows underlying microstructure evolution in the system. Also, relative increase can also be attributed to increase in polarization centers and consequent interfacial polarization. Unfilled polymer and nanocomposites with low filler volume fractions displayed AC conductivity is hugely dependent on frequency, indicating an insulating behavior. Also, at low volume fractions of filler, because of large distance between adjacent nanoparticles, low frequency part of AC conductivity is very low. However, as the filler content was increased, the AC conductivity became independent of frequency, indicating the formation of a connected conductive network. As frequency increases, the role of dielectric dispersion discussed earlier is heightened due to increased interfacial polarization; therefore, AC conductivity experiences an ascending trend. Evidently, at higher volume fractions, the AC conductivity of the AgNWs/PS nanocomposite was independent of frequency, showing the dominant role of Ohmic conduction and well-established conductive network formation.

5.3 Mechanisms for charge polarization in AgNW/PS nanocomposites

In general, charge polarization in AgNWs/polymer (nonpolar) composites originates from three sources, namely (1) interfacial polarization, (2) AgNWs polarization, and (3) electronic polarization of polymer. Electronic polarization is omnipresent, as all of the material in this universe contains atoms [19]. AgNWs polarization happens as a result of the presence of chemical impurities and defects on or within individual nanowires. Interfacial (Maxwell–Wagner–Sillars) polarization is usually observed in heterogeneous systems, with phases with different conductivities, such as AgNWs/polymer composites [32–34]. At the cross-section of two materials with dissimilar electrical properties, free charges that are mobile throughout either of the materials migrate to the interface and intensify the charge polarization. Interfacial polarization, as the mechanism behind it also fully implies, has a long relaxation time which makes it possible only at the very low frequencies. It should be noted that Maxwell–Wagner polarization model may not be valid in many cases for single-phase ceramics and single crystals; however, in multiphase composites, the Maxwell–Wagner polarization may dominate [20]. Although crystallographic defects in AgNWs weakens inclusion mechanically and deteriorates their outstanding electrical properties, they are polarized in a broad band frequency range. For instance, it was reported by

Watts et al that localized defects may not significantly alter electronic properties but they act as polarization centers, which display higher ε' compared to defect-free CNTs [1].

Similar evidence has been found for MWCNTs [14, 35]. These types of polarizations are referred to as the polarization within AgNWs, as they are particularly effective at higher frequencies. In another example, a crystallographic defect in the armchair-type CNT (conductive type) can cause the surrounding carbonic regions to act as a semiconducting material. Consequently, at the molecular level there might be two neighboring domains with different levels of conductivity that can interact and induce charge polarization on the molecular scale. Generally, properties of materials with defects such as chemical reactivity, mechanical strength, optical absorption, and electronic transport all vary with defect concentration. Last but not least, electronic polarization of matrix can also contribute to total polarization in AgNW/polymer composites. The electric field between adjacent nanoparticles goes toward infinity as they approach each other very closely [36, 37]. Buildup of a massive electric field will hugely polarize the polymer chains and, as a result, total permittivity increases at high frequencies [19]. For instance, Arjmand and Sundararaj [21] proved through experiments that $BaTiO_3$ can act as an insulative layer between MWCNTs and decrease the dielectric permittivity and loss in the nanocomposite.

Arjmand and Sundararaj [22] claimed in their paper that contribution to real permittivity from three mentioned mechanisms has the following order. At interfacial polarization sites, the charges are often separated over a larger distance (compared to the atomic and molecular sizes), and the contribution to dielectric loss can therefore be orders of magnitude larger than the dielectric response due to molecular fluctuations. They also explained that, with increase in frequency, the slow mechanisms will fail, and faster ones will contribute to total real permittivity.

5.4 The Broadband Behavior of Real Permittivity

Figure 5-2 demonstrates the real permittivity of the composites with different AgNWs loading levels over the broadband frequency range. The results showed that the real permittivity and imaginary permittivity increased astronomically with increased AgNWs concentration. For instance, at 100 Hz, the real permittivity and imaginary permittivity of the pristine PS was 2.5 and

0.04, respectively, which increased to 1.2×10^4 and 1.4×10^7 at 2 vol%, respectively. After the addition of a small amount of AgNWs to the PS matrix, initial nanostructures were formed, which led to an increase in real permittivity compared to unfilled PS. Additionally, charge polarization within AgNWs themselves also contributed hugely to very high real permittivity at higher AgNWs loadings. Interestingly enough, when volume fraction went above the percolation threshold, an abrupt growth in the real permittivity was observed. Arjmand and Sundararaj [22] also observed a similar trend in their MWCNT/PVDF nanocomposite. This interesting behavior can be attributed to the formation of the large number of nanocapacitors. To explain this behavior fully, the concept of nanoelectrodes at volume fractions close to the percolation threshold should be described. As volume fraction nears the percolation threshold, there will be an increase in the number of nanoelectrodes, as well as a decrease thickness of the insulative gap between nanoelectrodes. These two effects intertwine and manifest as a huge increase in real permittivity. After the percolation threshold, despite completion of a conductive network of AgNWs, the real permittivity kept on increasing as a result of the remaining AgNWs still wrapped with polymer chain molecules. Poorer network formation generally aids in better charge preservation as it also means a shorter mean free path for electrons in each half cycle of AC field.

Based on Fig. 5-2 it can be claimed that real permittivity stays relatively the same despite changes in frequency for volume fractions below the percolation threshold, while it can be varied within the conductive domain. For instance, the real permittivity of insulative nanocomposites was frequency independent; however, at higher volume fractions, the real permittivity demonstrated a descending trend in the low frequency range, then was constant, and finally showed another descending trend.

Generally, at a low filler content, the number of nanocapacitors is limited so real permittivity, which is hugely dependent on these structures, stays relatively the same. However, at high filler loadings, the abundance of nanostructure formation increases the probability of charge preservation and, therefore, real permittivity increases.

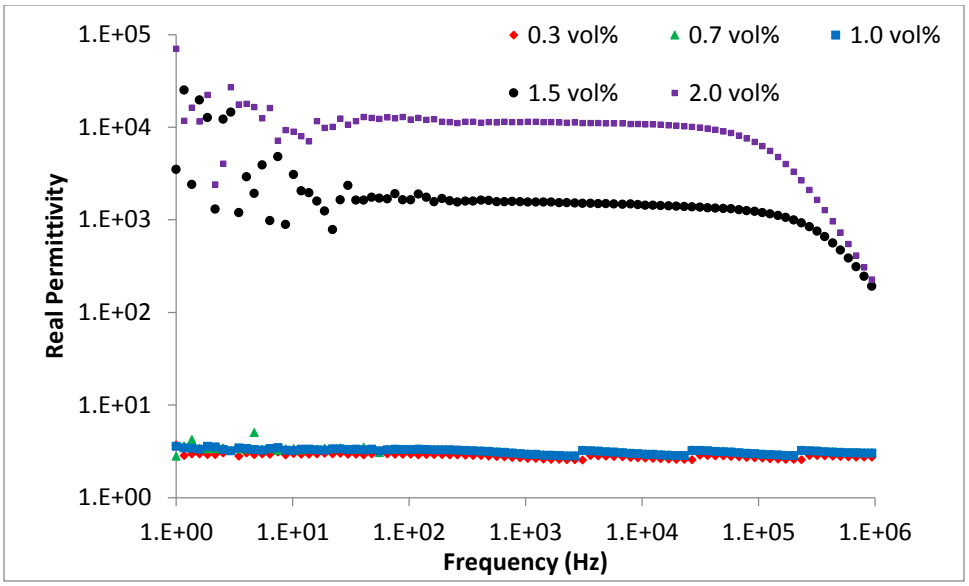

Figure 5-2: Real permittivity of the AgNW/ PS nanocomposites as a function of frequency

5.5 The Broadband Behavior of Imaginary Permittivity

The larger the imaginary permittivity, the more energy is being lost through electrons and atomic motion, and less energy is available to propagate past the induced dipoles. CPCs designed for charge storage application need to show a low imaginary permittivity. Ohmic loss is directly related to the amount of mobile charge carriers, and polarization loss is also related to the number of nanocapacitors. Polarization loss comes from changes in orientation of induced electric dipoles in an AC field. As shown in Fig. 5-3, the imaginary permittivity was at its lowest where concentration was not large enough to reach the percolation threshold; however, as the concentration approached the percolation threshold, imaginary permittivity also increased. Increasing the AgNWs content in a polymeric matrix increases the total nomadic charges inside the system and also makes the network of AgNWs more advanced. More advanced networks contribute to higher imaginary permittivity, as it provides a longer mean free path for electrons to travel, and consequently wastes higher amount of energy [2]. Moreover, defects and the points with greater resistance, such as contact points between nanowires, dissipate more energy as electrons try to pass these obstacles.

Polarization loss that comes from interfacial polarization is dependent on filler content, as the generated electric field gets stronger as fillers near each other, particularly at the percolation threshold. It is worth mentioning that imaginary permittivity at concentrations above the percolation threshold has a strong dependency on frequency. The descending trend can be explained based on the mechanism behind imaginary permittivity in a CPC. As the frequency increases, nomadic charges have less time to go from one end of the conductive path to the other; ergo, they dissipate less energy during each half cycle of the AC field. Polarization loss is also affected, as some of the polarized electrons fail to fully reorient themselves at high frequencies.

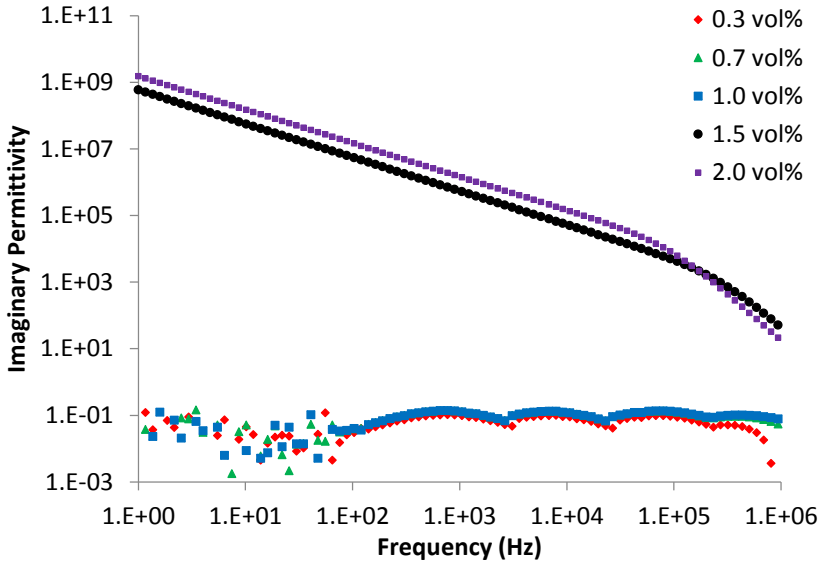

Figure 5-3: Imaginary permittivity of the AgNW/ PS nanocomposites as a function of frequency

The combined effect of dielectric permittivity and dielectric loss can be sought in a term named dissipation factor, which is of great importance in assessing the overall potential of a CPC. The dissipation factor is simply ratio of imaginary permittivity over real permittivity. Electrical energy is dissipated in all dielectric materials, usually in form of heat. The amount of heat generated inside the nanocomposite becomes important as excessive heat generation can sabotage the function of the nanocomposite. As a rule of thumb, in industry the lower dissipation factors a CPC has, the better charge storage ability it can offer. Although the dissipation factor that our generated system offers doesn't show outstanding results, it is comparable to the results usually obtained from MWCNTs. For instance, in a study by da Silva et al. [13], trends and values reported for

MWCNT/PVDF system is comparable to our AgNWs/PS system. In another study, Arjmand et al [23] investigated the effect of foaming on the percolation threshold and reported that foaming broadens the insulator-conductor transition span; ergo, reducing the dissipation factor of the MWCNT/PS nanocomposites. Generally, in poorer conductive networks, electrons have less mean free path to move in each half cycle of the AC field and thus less electrical energy will be wasted.

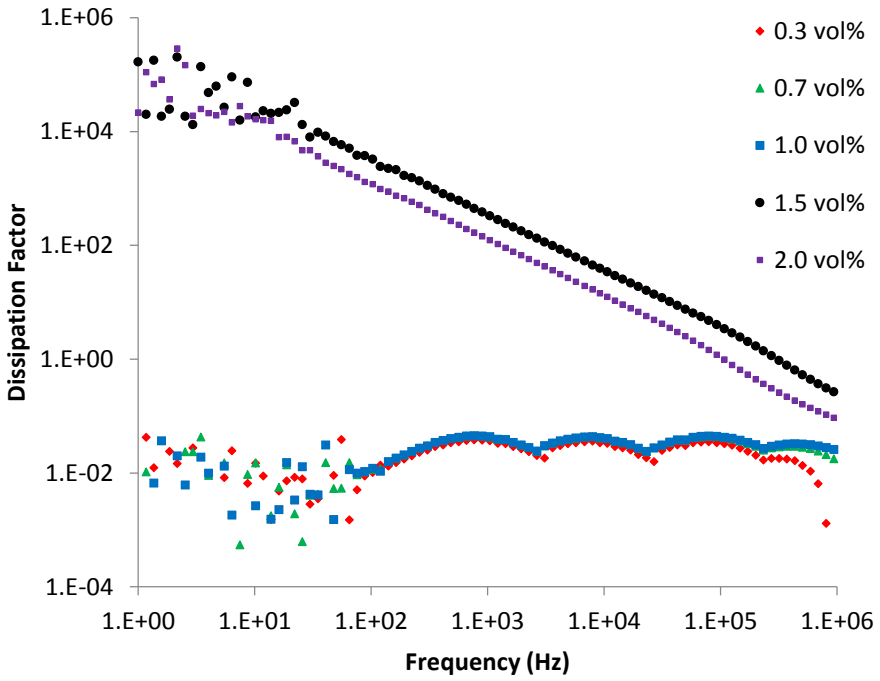

Figure 5-4: Dissipation factor of the AgNW/ PS nanocomposites as a function of frequency

5.6 Conclusion

Preparation of AgNW/PS nanocomposite through the MSMP method was carried out, and the resulting nanocomposite exhibits outstanding electrical results. AC conductivities results demonstrated that AC conductivity is highly frequency-dependent for volume fractions far below the percolation threshold. Both real and imaginary permittivity increases dramatically in the vicinity of the percolation threshold. The increase in real permittivity was conjectured to be related to the formation of a huge number of nanocapacitors (AgNWs as nanoelectrodes and PS as nanodielectrics). For instance, in CNTs with many defects, real permittivity increases dramatically. Watts et al. [1] performed a systematic study on the effect of defects on electrical properties and

reported a dramatic increase in real permittivity with an increase in the number of defects. An increase in imaginary permittivity was also shown to be rooted in (1) an increased number of total present nomadic charges in the system, (2) a more advanced network of AgNWs and (3) an increase in polarization loss. The descending trend of real permittivity, and imaginary permittivity, after the percolation threshold was attributed to failure in full reorientation of induced electrons and an inability of the nomadic charges to fully make use of the conductive path, respectively.

5.7 References

[1] Watts PC, Hsu WK, Barnes A, Chambers B. High Permittivity from Defective Multiwalled Carbon Nanotubes in the X-Band. Advanced Materials. 2003;15(7-8):600-3.

[2] Arjmand M, Apperley T, Okoniewski M, Sundararaj U. Comparative study of electromagnetic interference shielding properties of injection molded versus compression molded multi-walled carbon nanotube/polystyrene composites. Carbon. 2012;50(14):5126-34.

[3] Dang Z-M, Yuan J-K, Zha J-W, Zhou T, Li S-T, Hu G-H. Fundamentals, processes and applications of high-permittivity polymer–matrix composites. Progress in Materials Science. 2012;57(4):660-723.

[4] Popielarz R, Chiang C, Nozaki R, Obrzut J. Dielectric properties of polymer/ferroelectric ceramic composites from 100 Hz to 10 GHz. Macromolecules. 2001;34(17):5910-5.

[5] Barber P, Balasubramanian S, Anguchamy Y, Gong S, Wibowo A, Gao H, et al. Polymer composite and nanocomposite dielectric materials for pulse power energy storage. Materials. 2009;2(4):1697-733.

[6] Cho S-D, Lee S-Y, Hyun J-G, Paik K-W. Comparison of theoretical predictions and experimental values of the dielectric constant of epoxy/BaTiO3 composite embedded capacitor films. Journal of Materials Science: Materials in Electronics. 2005;16(2):77-84.

[7] Bao S, Liang G, Tjong SC. Effect of mechanical stretching on electrical conductivity and positive temperature coefficient characteristics of poly (vinylidene fluoride)/carbon nanofiber composites prepared by non-solvent precipitation. Carbon. 2011;49(5):1758-68.

[8] Lu J, Wong C. Recent advances in high-k nanocomposite materials for embedded capacitor applications. Dielectrics and Electrical Insulation, IEEE Transactions on. 2008;15(5):1322-8.

[9] Jiang M-J, Dang Z-M, Bozlar M, Miomandre F, Bai J. Broad-frequency dielectric behaviors in multiwalled carbon nanotube/rubber nanocomposites. Journal of Applied Physics. 2009;106(8):084902.

[10] Yuan J-K, Yao S-H, Dang Z-M, Sylvestre A, Genestoux M, Bai1 J. Giant dielectric permittivity nanocomposites: realizing true potential of pristine carbon nanotubes in polyvinylidene fluoride matrix through an enhanced interfacial interaction. The Journal of Physical Chemistry C. 2011;115(13):5515-21.

[11] Dang Z-M, Yao S-H, Yuan J-K, Bai J. Tailored dielectric properties based on microstructure change in BaTiO3-carbon nanotube/polyvinylidene fluoride three-phase nanocomposites. The Journal of Physical Chemistry C. 2010;114(31):13204-9.

[12] Lu J, Moon K-S, Xu J, Wong C. Synthesis and dielectric properties of novel high-K polymer composites containing in-situ formed silver nanoparticles for embedded capacitor applications. Journal of Materials Chemistry. 2006;16(16):1543-8.

[13] da Silva AB, Arjmand M, Sundararaj U, Bretas RES. Novel composites of Copper nanowire/PVDF with superior dielectric properties. Polymer. 2014;55(1):226-34.

[14] Arjmand M, Mahmoodi M, Park S, Sundararaj U. An innovative method to reduce the energy loss of conductive filler/polymer composites for charge storage applications. Composites Science and Technology. 2013;78:24-9.

[15] Arjmand M, Mahmoodi M, Gelves GA, Park S, Sundararaj U. Electrical and electromagnetic interference shielding properties of flow-induced oriented carbon nanotubes in polycarbonate. Carbon. 2011;49(11):3430-40.
[16] Liu Z, Zhan Y, Shi G, Moldovan S, Gharbi M, Song L, et al. Anomalous high capacitance in a coaxial single nanowire capacitor. Nature communications. 2012;3:879.
[17] Steeman P, Van Turnhout J. Dielectric properties of inhomogeneous media. Broadband Dielectric Spectroscopy: Springer 2003, p. 495-522.
[18] MEHTA N. Textbook of engineering physics: PHI Learning Pvt. Ltd.; 2008.
[19] Askeland DR, Phulé PP. The science and engineering of materials. 2003.
[20] Yu Z, Ang C. Maxwell–Wagner polarization in ceramic composites BaTiO 3–(Ni 0.3 Zn 0.7) Fe 2.1 O 4. Journal of applied physics. 2002;91(2):794-7.
[21] Arjmand M, Sundararaj U. Impact of BaTiO3 as insulative ferroelectric barrier on the broadband dielectric properties of MWCNT/PVDF nanocomposites. Polymer Composites. 2014.
[22] Arjmand M, Sundararaj U. Broadband dielectric properties of multiwalled carbon nanotube/polystyrene composites. Polymer Engineering & Science. 2015;55(1):173-9.
[23] Arjmand M, Mahmoodi M, Park S, Sundararaj U. Impact of foaming on the broadband dielectric properties of multi-walled carbon nanotube/polystyrene composites. Journal of Cellular Plastics. 2014;50(6):551-62.

Chapter 6: CONCLUSIONS AND FUTURE WORK

Silver nanowires, due to their unique properties, are poised to replace traditional nanoinclusions such as metals and ITO in both electrical and optical devices. It was shown experimentally in our study that AgNWs can offer better electrical properties compared to commercial CNTs. Therefore, related devices currently being employed in military and other applications can be replaced effectively using novel made AgNWs/polymer nanocomposite. Interestingly enough, AgNWs also have several other advantageous characteristics, including low sheet resistance and high optical transparency. An excellent example of ongoing research on AgNWs, attempts to find a replacement for ITO in optical devices can be mentioned. ITO is still the most applicable material for transparent electrodes; however, there is a demand for manufacturing a new generation of transparent electrode materials which can outperform ITO in terms of cost and ductility [1]. In other words, endeavors are being aimed at manufacturing devices with sufficient flexibility. Long AgNWs, with their high electrical conductivity, seem to be a huge step toward realization of this dream. Although many studies reported promising success stories regarding AgNWs, the need for some improvement is present.

The aim of this study was to synthesize silver nanowire and utilize it in CPCs through the Miscible Solution Mixing and Precipitation (MSMP) method, and to assess electrical conductivity and EMI shielding of compression molded composites. In our study, comprehensive characterization techniques like scanning electron microscopy (SEM) and transmission electron microscopy (TEM) were carried out to track the morphological and structural variations of Ag nanowires. Results demonstrated that AgNWs with an average diameter of 25 nm and an average length of 2.5 µm were synthesized successfully via AC electrodeposition into a porous aluminum oxide (PAO) template. Observed synthesized AgNWs underline that, using our proposed manufacturing method, AgNWs with manageable final morphology and uniform size can be prepared readily and rapidly.

A comparative study of AgNW/PS and CNT/PS composites was carried out using identical processing conditions, and EMI shielding properties were measured and compared. XRD showed silver FCC crystal structure peaks, but no trace of crystalline silver oxide or silver sulfide before

or after processing were visible. The absence of silver oxide peaks was related to the natural resistance of silver towards oxidation. Peaks related to silver sulfide were also not observed, as AgNWs exposure time to sulfur components in the air was minimal.

TEM analysis verified successful synthesis of AgNWs with an average diameter and length of 25nm and 5.6±1.4 μm, respectively. TEM images also revealed that an AgNW at high temperature transformed into a chain of nanospheres by fragmentation phenomenon. Crystalline phase transition might be the main driving force for the fragmentation, but other factors such as corrosion with sulfur gases in the air might also come into play to break up the nanowires. The latter was ruled out since no noticeable peak related to corrosion was observed in XRD patterns. Moreover, TEM images demonstrated that fragmentation was at its early stages and a good level of distribution, and dispersion was achieved by sonication.

Electrical resistivity measurements indicate that the percolation thresholds, obtained from the percolation theory, for the MWCNT/PS nanocomposites was 0.04vol%, while the AgNW/PS nanocomposites presented a percolation threshold noticeably higher, equal to 1.2vol%. Several factors could explain the higher percolation threshold in the AgNW/PS nanocomposites, namely (1) a lower aspect ratio of AgNWs, (2) the fragmentation phenomenon in AgNWs, and (3) inferior dispersion and distribution of AgNWs. EMI SE, like electrical conductivity, reduced due to adverse effect of fragmentation in delaying the network formation. Despite negative effect of fragmentation on EMI shielding, EMI SE of AgNW/PS were 31.84 dB, ~10 dB higher than MWCNT/PS at 2.5vol % loading. It seems that at high filler loadings, where a conductive network was well established for both types of nanocomposites, a higher innate conductivity of AgNWs played a dominant role.

The imaginary permittivity of the AgNW/PS nanocomposites at high loadings is much greater than MWCNT/PS nanocomposites. At low filler loading, the MWCNT/PS nanocomposites presented a higher imaginary permittivity due to an enhanced conductive network formation and larger available surface area, but at high filler contents, the innate conductivity of AgNW dominated over the effect of the lower aspect ratio. Real permittivity experienced the trend as imaginary permittivity. There is an ascending trend for real permittivity of MWCNT/PS nanocomposites from any low concentrations, while there is a jump in real permittivity of AgNW/PS nanocomposites at 1.2 vol %. The enhancement in the real permittivity of the

AgNW/PS nanocomposites above the percolation threshold originates from the formation of a great number of nanocapacitors, i.e. starting at 0.04vol% for MWCNT/PS nanocomposites and 1.2vol % for AgNW/PS nanocomposites. Additionally, defects in the crystalline structure of both MWCNT and AgNW could result in dipolar polarization and further enhancement of the real permittivity.

6.1 Future Work

1. The synthesis process caused some irreversible agglomeration, as was discovered in different silver nanowire/polymer composites. Even allowing sufficient sonication time did not resolve the issue, as scattered bundles of silver nanowire were visible infrequently throughout the TEM images. Prolonging the sonication deteriorated properties of the nanocomposite, as it further lowered the original high aspect ratio of silver nanowires. Thus, chemical modifications should be carried out at or during the liberation phase to minimize initial agglomerations. AgNWs oxidation overtime was another issue that should be addressed since it directly affects good electrical properties of AgNWs. Myriad methods could tested, including but not limited to (1) adding anti-oxidants into the non-solvent where the AgNWs are dispersed (2) performing production and molding of AgNWs made CPCs inside an inert medium (3) artificially increasing AgNWs stability. For instance, Ramasamy et al. coated AgNWs with TiO_2. Although TiO_2 increased the thermal stability of AgNWs, because of the low conductivity of TiO_2 overall, conductivity was hugely negatively affected. In another study, Ahn et al. utilized graphene oxide to increase resistance of AgNWs against diffusing gas molecules. Although theoretically, the selected approach seemed promising, experimental results were not ideal. Coated graphene oxide only slowed the increase rate of sheet resistance of AgNWs electrodes when exposed to harsh conditions.

   Due to the mentioned problems, it is suggested that future work on AgNWs/polymer nanocomposites revolve around solving these problems. All in all, novel aspects such as coating, electrode sheet resistance, and nanowire diameter need to be studied carefully

before reaping benefits of AgNWs electrodes, as their properties deteriorate over time and under certain harsh conditions.

2. Another interesting future work is to mix nickel nanowires with silver nanowires. The dependence of shielding effectiveness on magnetic permeability and conductivity demonstrates that better absorption values can be obtained for materials with higher conductivity and magnetization. Therefore, it can be concluded that the incorporation of magnetic and dielectric fillers in the polymer matrix lead to better absorbing material, which makes them futuristic novel EMI shielding materials. For instance, nickel filaments of a diameter of 0.4 μm, made by electroplating 0.1 μm diameter nickel upon carbon filaments, have been shown to be extremely effective materials for EMI shielding [2-4]. A shielding effectiveness of 87 dB at 1 GHz has been attained in a polymer-matrix composite containing just 0.7 vol. % nickel filaments. Nickel is more beneficial in the long run than copper, due to its superior oxidation resistance. The oxide film demonstrates lower conductivities than pure metal and increases the overall resistance in the system. Last but not least, mixing a magnetic nanofiller like nickel with a highly electrically conductive nanofiller like AgNWs will produce highly efficient shields.

3. Another useful project would be to compare the EMI shielding and dielectric properties of CPCs containing MWCNTs and CuNWs over the X-band. This investigation can further validate information obtained in our current study regarding the mechanisms behind the relationship between intrinsic conductivity of filler and EMI shielding for high-frequency applications.

4. Probing the level of changes in AgNW surface chemistry (in terms of sulfurization and oxidation) on the electrical properties of AgNW/polymer composites.

5. Studying the effects of foaming on dielectric properties and its impact on delaying the conductive network formation [17] is another worthy endeavor. Foaming, like alignment,

is a novel way to improve dielectric properties and widens the typically narrow concentration window used to manipulate the dielectric properties

6. We can also utilize traditional yet effective methods of processing such as injection to take advantage of the influence of changes in surface chemistry of AgNWs together with AgNW alignment on the dielectric properties.

7. We should investigate the rheological properties of AgNWs before and after fragmentation. This will provide more information on the effects of AgNWs fragmentation on viscosity and shear rate, which can be an important factor of aspect ratio loss and developed morphology in fragmented samples. Studying this novel way of assessing fragmentation status is important due to its significant impact on AgNWs aspect ratio and subsequently on electrical properties. (MWCNT aspect ratio is decreased by more severe processing.)

8. Measurements using atomic force microscopy (AFM) should be done on individual AgNWs. This process can be highly beneficial in determining the effect of surface chemistry changes in individual wires. For instance, changing and probing surface chemistry along with measurement of conductivity would hugely revolutionize understanding of AgNW-conductivity correlations.

6.2. References

[1] Van De Lagemaat J, Barnes TM, Rumbles G, Shaheen SE, Coutts TJ, Weeks C, et al. Organic solar cells with carbon nanotubes replacing In2O3: Sn as the transparent electrode. Applied Physics Letters. 2006;88(23):233503.
[2] Shui X, Chung D. 0.4 μm diameter nickel-filament silicone-matrix resilient composites for electromagnetic interference shielding. Journal of Electronic Packaging. 1997;119(4):236-8.
[3] Shui X, Chung D. Nickel filament polymer-matrix composites with low surface impedance and high electromagnetic interference shielding effectiveness. Journal of electronic materials. 1997;26(8):928-34.
[4] Chiou J-M, Zheng Q, Chung D. Electromagnetic interference shielding by carbon fibre reinforced cement. Composites. 1989;20(4):379-81.